

Human RPA Activates BLM's Bidirectional DNA Unwinding from a Nick

Zhenheng Qin^{1,2,3†}, Lulu Bi^{1†}, Xi-Miao Hou⁴, Siqi Zhang^{1,2,3}, Xia Zhang¹,
Ying Lu⁵, Ming Li^{3,5}, Mauro Modesti⁶, Xu-Guang Xi^{7*}, and Bo Sun^{1*}

¹School of Life Science and Technology, ShanghaiTech University, Shanghai, 201210, China; ²Shanghai Institute of Biochemistry and Cell Biology, Chinese Academy of Sciences, Shanghai, 200031, China; ³University of Chinese Academy of Sciences, Beijing, 100049, China; ⁴College of Life Sciences, Northwest A&F University, Yangling, 712100, China; ⁵Institute of Physics, Chinese Academy of Sciences, Beijing, 100190, China; ⁶Cancer Research Center of Marseille, CNRS UMR7258, Inserm U1068, Institut Paoli-Calmettes, Aix-Marseille Université, 13273 Marseille, France; ⁷LBPA, IDA, ENS de Cachan, CNRS, Université Paris-Saclay, Cachan, F-94235, France.

*To whom correspondence should be addressed. Emails: sunbo@shanghaitech.edu.cn, and xxi01@ens-cachan.fr

†These authors contributed equally to this work.

Abstract

BLM is a multifunctional helicase that plays critical roles in maintaining genome stability. It processes distinct DNA substrates, but not nicked DNA, during many steps in DNA replication and repair. However, how BLM prepares itself for diverse functions remains elusive. Here, using a combined single-molecule approach, we find that a high abundance of BLMs can indeed unidirectionally unwind dsDNA from a nick when an external destabilizing force is applied. Strikingly, human replication protein A (hRPA) not only ensures that limited quantities of BLMs processively unwind nicked dsDNA under a reduced force but also permits the translocation of BLMs on both intact and nicked ssDNAs, resulting in a bidirectional unwinding mode. This activation necessitates BLM targeting on the nick and the presence of free hRPAs in solution whereas direct interactions between them are dispensable. Our findings present novel DNA unwinding activities of BLM that potentially facilitate its function switching in DNA repair.

30 **Introduction**

31 DNA helicases are ubiquitous motor proteins that couple the hydrolysis of nucleoside
32 triphosphates (NTPs) to the unwinding of double-stranded DNA (dsDNA), providing the
33 single-stranded DNA (ssDNA) required for many biological processes, including DNA replication,
34 repair and recombination (Singleton, Dillingham, & Wigley, 2007). Among these DNA helicases,
35 the RecQ family helicases have been highly conserved during evolution from prokaryotes to
36 humans and play critical roles in genome maintenance and stability (Bernstein, Gangloff, &
37 Rothstein, 2010; Croteau, Popuri, Opresko, & Bohr, 2014). Defects in three of the five human RecQ
38 members (BLM, WRN and RECQ4) give rise to distinct heritable human disease syndromes
39 (Bloom's, Werner's and Rothmund-Thomson syndromes, respectively), characterized by genomic
40 instability and an increased incidence of cancers (Ellis et al., 1995; Kitao, Lindor, Shiratori,
41 Furuichi, & Shimamoto, 1999; Yu et al., 1996). These genetic linkages underscore the importance
42 of the RecQ family helicases in cellular homeostasis. Thus, an in-depth understanding of their
43 unwinding mechanisms at the molecular level may inform potential therapeutic strategies.

44

45 Bloom syndrome protein (BLM) is one of the five RecQ family helicases that unwind DNA in a
46 3'-5' direction (Croteau et al., 2014; Karow, Chakraverty, & Hickson, 1997). It is involved in many
47 aspects of genome maintenance, including DNA end resection (Kowalczykowski, 2015),
48 displacement-loop (D-loop) processing (Bugreev, Yu, Egelman, & Mazin, 2007), rescuing stalled or
49 collapsed replication forks (Davies, North, & Hickson, 2007), and resolution of Holliday junction
50 (Bizard & Hickson, 2014). BLM's diverse functions are realized by its remarkable unwinding
51 capabilities of many unique DNA structures, such as G-quadruplex (Chatterjee et al., 2014). In
52 particular, BLM has been verified to participate in many steps in repairing DNA double-strand
53 breaks (DSBs) via homologous recombination (HR) (Nimonkar et al., 2011; Nimonkar, Ozsoy,
54 Genschel, Modrich, & Kowalczykowski, 2008; Sturzenegger et al., 2014; Woglar & Villeneuve,

2018). It has been demonstrated to be recruited to the DSB ends and facilitate resection of the 5' termini to generate 3' end protruding ssDNAs in the first step of HR (Gravel, Chapman, Magill, & Jackson, 2008). BLM either unwinds dsDNA to provide ssDNA for exonuclease resection by EXO1 or DNA2 or directly stimulates their nucleolytic activities (Nimonkar et al., 2008; Sturzenegger et al., 2014). Paradoxically, even though BLM is distinctive in preferentially unwinding unique substrates (Mohaghegh, Karow, Brosh, Bohr, & Hickson, 2001), an in vitro ensemble study has demonstrated that this helicase alone is unable to initiate dsDNA unwinding from a nick which is a prevalent and essential DNA intermediate during HR (Maizels & Davis, 2018; Mohaghegh et al., 2001). These contradictory findings may be reconciled by BLM's varying unwinding activities, which are often regulated by other *in vivo* factors (Croteau et al., 2014).

It has been widely appreciated that the BLM helicase interacts and collaborates with many protein partners to aid in cellular responses to replication stress and DNA damage in vivo (Croteau et al., 2014). These interactions and collaborations dictate BLM's specialized functions in genome maintenance. A key partner of BLM is the single-stranded DNA-binding (SSB) protein, replication protein A (RPA), a heterotrimeric protein complex consisting of the RPA70, RPA32 and RPA14 subunits, which is also essential in DNA repair and recombination (Fanning, Klimovich, & Nager, 2006; Wold, 1997). A recent in vivo study directly demonstrated that RPA co-localizes with BLM at the foci of DNA damage, suggesting that these two proteins coordinate and function together in DNA repair (Woglar & Villeneuve, 2018). In addition, biochemical, structural and single-molecule studies have revealed that RPA not only physically interacts with BLM but also stimulates its unwinding activity by increasing its processivity or improving its unwinding initiation (Brosh et al., 2000; Doherty et al., 2005; Soniat, Myler, Kuo, Paull, & Finkelstein, 2019). The poor ability of a heterologous SSB protein to stimulate BLM's unwinding further suggests that this stimulation is specific (Brosh et al., 2000). These findings, coupled with the inability of BLM alone to unwind a

nicked DNA in vitro, suggest that RPA might also promote BLM in unwinding nicked dsDNA to facilitate efficient end resection in HR. A thorough understanding of how BLM-mediated DNA unwinding is regulated by RPA would advance our knowledge in its diverse roles and functions in genome maintenance.

In this study, by combining optical tweezer with confocal fluorescence microscopy, we examined BLM unwinding activities under various conditions at the single-molecule level. We found that, in the absence of hRPA, BLM at high concentrations can unwind dsDNA from a nick unidirectionally with a requirement of an external destabilizing force on the DNA template. Surprisingly, the presence of hRPA permits BLM's unwinding in two opposite directions from a nick at low and zero forces. This stimulation demands free hRPAs in solution, suggesting that the coating of hRPA on the newly generated ssDNA is essential for enhancing BLM unwinding activity. These findings reveal a distinct SSB-enabled helicase unwinding mode that might facilitate the generation of the 3' ssDNA tail in HR. Additionally, this study demonstrates various DNA unwinding activities by BLM that are regulated by tension on DNA, the concentration of BLM, and the presence of RPA, which provide a molecular insight into how BLM realizes its diverse biological functions.

Results

Force assists BLM's unidirectional unwinding from a nick

We combined dual-optical traps with confocal microscopy to monitor unwinding of a single DNA molecule by wild type (WT) *Gallus gallus* BLM (gBLM). gBLM (hereafter referred to as BLM) has two similar RPA binding domains to the human BLM (hBLM) and the sequence of its helicase-core domain (core-gBLM) has an 80% identity with the one from hBLM. Figure 1A shows a schematic of our experimental configuration in which a λ phage DNA molecule is suspended between one fixed

trap and one steered trap via two streptavidin-coated microspheres, while a confocal laser repeatedly scanned along the plane of the DNA template (Figure 1A). A high-frequency feedback system on the steered trap was employed to ensure the force on the DNA template remained constant, while BLM unwound the DNA template. The difference in extension between ssDNA and dsDNA under tension would result in a change in DNA length once the BLM helicase started unwinding (Bustamante, Bryant, & Smith, 2003), thus allowing for monitoring of its unwinding activity. In addition, the fluorescent binding agent Sytox was used as a dsDNA probe, and its immediate dissociation led by converting dsDNA to ssDNA by BLM served as an additional signal for dsDNA unwinding. This combined single-molecule technique allowed us not only to record the change of DNA length induced by BLM-catalyzed dsDNA unwinding but also to directly visualize individual unwinding events and DNA intermediates along the DNA template.

We started the unwinding experiment at a force of 10 pN for ~ 1 min and increased it by 10 pN each time until dsDNA unwinding was detected. In the presence of 20 nM BLM, apparent dsDNA unwinding was not observed over a broad force range from 10 pN to 40 pN (Figure 1B). In contrast, at a high BLM concentration of 200 nM, one or few unwinding events on a single DNA molecule were recorded once the force was increased to a range of 10 - 40 pN in all examined traces ($n = 30$) (Figure 1-figure supplement 1). Figure 1C shows a kymograph of a DNA molecule and the force and DNA length as a function of time in the presence of 200 nM BLM: DNA length and fluorescence signals did not change under 10 or 20 pN; however, the DNA length displayed a continuous increase while a dark region in the middle of the fluorescent dsDNA appeared and subsequently expanded just after the force was increased to 30 pN. Omitting ATP did not result in changes in either fluorescence or DNA length signal in this experimental condition, confirming that our observations were a result of BLM-catalyzed dsDNA unwinding (Figure 1-figure supplement 2A). Control experiments without Sytox exhibited similar DNA length increases in the presence of BLM,

suggesting that the fluorescent dye does not affect BLM's unwinding activities (Figure 1-figure supplement 2B).

As nicks can be accidentally generated along the long λ phage DNA template used in these assays, the observed dsDNA unwinding by BLM could be initiated either from a nick or from an intact duplex region melted internally, leading to distinct DNA intermediates during unwinding (Rad, Forget, Baskin, & Kowalczykowski, 2015). To differentiate between these two possibilities, we analyzed the fluorescence signal of each individual unwinding event. In all 49 examined events from 33 traces, the unwinding progressed in one direction only, as reflected by the progression of the dark region of the fluorescence signal as well as the biased disappearance of its adjacent dsDNA (Figure 1D). This finding is not consistent with the possibility that the observed dsDNA unwinding was initiated by melting dsDNA internally where bidirectional progression of the unwinding fork movement was expected. Thus, we attributed these events to dsDNA unwinding initiated from a nick and the appearance and subsequent growth of the dark regions along the DNA track represented ssDNA. The rate of each unwinding fork movement was determined from the increase in ssDNA length revealed by the fluorescence signal and was converted to unwound base pair per second based on the elasticity of ssDNA (Figure 1-figure supplement 3). This yielded an unwinding rate of 60 ± 9 bp/s (mean \pm SD) under 30 pN (Figure 1E and Figure 1-source data 1).

In conclusion, the BLM helicase at a high concentration is indeed able to perform unidirectional unwinding from a nick, but this requires exerting an external destabilizing force (tens of pN) on the DNA template.

BLM translocates on intact ssDNA during unidirectional unwinding

Our data suggest that the BLM helicase unwinds dsDNA unidirectionally from a nick. This generates one intact strand under tension and one relaxed coiled strand in our experimental configuration. Since BLM unwinds by translocating on ssDNA in a 3' to 5' manner, we next sought to determine on which strand BLM prefers to translocate when initiating unwinding from a nick. This strand preference directly determines BLM's unwinding polarity from a single nick (Figure 2A). Thus, we designed a 6.4 kbp dsDNA harboring a single nick at 2.2 kbp and 4.2 kbp away from the 5' and the 3' ends, respectively (Figures 2B and Figure 2-figure supplement 1). BLM unwinds a 4.2 kbp dsDNA region if it translocates on the tensioned strand during unwinding or a 2.2 kbp dsDNA region if it translocates on the relaxed strand. To ensure the occurrence of DNA unwinding, we conducted the unwinding assay with this nicked DNA template under 30 pN. We found that 25 traces out of 29 examined DNA molecules showed continuous DNA unwinding from the nick. The 4.2 kbp dsDNA segments in these 25 traces were always unwound while the 2.2 kbp dsDNA segments remained intact, independent of the orientation of the suspended nicked DNA (Figure 2B). These findings suggest that BLM exclusively employed the intact ssDNA under tension as the track strand to unwind dsDNA. In addition, the inability of BLM to unwind the 2.2 kbp dsDNA segment reinforced our conclusion that BLM alone unwinds unidirectionally from a nick.

RPA stimulates DNA unwinding by limited BLMs at low forces

Since RPA is a major protein partner that physically and functionally interacts with BLM, we next aimed to address how the human RPA (hRPA, hereafter referred to as RPA) regulates dsDNA unwinding by BLM. We first examined whether the presence of RPA could enhance BLM unwinding activity by reducing the required destabilizing force on the DNA template. To do so, we monitored helicase unwinding on the λ phage DNA in the presence of BLM and RPA while discretely increasing the external force (5, 10, 20 and 30 pN) until DNA unwinding was detected. Control experiments confirmed that RPA alone was incapable of unwinding dsDNA under these

external forces (Figure 3-figure supplement 1). In the presence of 200 nM BLM and RPA at various concentrations, DNA unwinding events initiated from the middle of the DNA template and the blunt-ended termini were observed. With the increase of RPA concentration, the required force to monitor DNA unwinding indeed significantly reduced (Figure 3A and Figure 3-source data 1). Moreover, we demonstrated that BLM/RPA-mediated DNA unwinding can even take place in the absence of any externally applied force (Figure 1-figure supplement 2).

Next, we asked whether a high abundance of BLMs are necessary for dsDNA unwinding when RPA is present. We assayed DNA unwinding of BLM at a concentration of 20 nM with various concentrations of RPA. In contrast to the observations with 20 nM BLM alone where no DNA unwinding was monitored from 10 to 40 pN at all (Figures 1B and 3C), the presence of RPA can indeed stimulate BLM-mediated DNA unwinding in these conditions and the required force was consistently decreased with the increase of RPA concentration (Figure 3C and and Figure 3-source data 1). It is noteworthy that with the presence of 200 nM RPA and 20 nM BLM, half of examined traces exhibited continuous DNA unwinding at a low force of 5 pN (Figure 3C and 3D).

Collectively, we conclude that RPA stimulates DNA unwinding of limited BLMs by lowering the required force on the DNA template.

RPA activates BLM's bidirectional unwinding from a nick

We next sought to examine individual unwinding events in the presence of 50 nM RPA and 200 nM BLM and compare to those with 200 nM BLM alone. On average, there were 3.4 independent unwinding events monitored on a single DNA molecule, slightly higher than that without RPA (Figure 1-figure supplement 1D). Strikingly, careful analyses of fluorescence images on the λ phage DNA under a force of 30 pN revealed that, in addition to the expected unidirectional

unwinding events, 53% of them ($n = 40$) showed bidirectional progression of dsDNA unwinding (Figure 4A). In line with these observations, 26 out of 27 traces from the experiments with the 6.4 kbp nicked DNA showed DNA unwinding in the presence of BLM and RPA and 35% of them also exhibited BLM's bidirectional unwinding initiated from the single nick on the template (Figure 4-figure supplement 1).

This RPA-activated bidirectional unwinding by BLM could be initiated from either internally melted dsDNA or a nick. To determine that, we labeled the RPA with enhanced green fluorescent protein (eGFP) and repeated the unwinding experiments. This eGFP-RPA allowed for the direct visualization of the unwinding intermediates of ssDNA instead of dsDNA (King et al., 2013). If dsDNA unwinding is initiated from melted regions of dsDNA, two continuous ssDNA strands under tension would be expected, and no frayed relaxed ssDNA exists. However, in most examined unwinding events (90%, $n = 95$), we observed at least one bright spot locating at the end of the newly generated tensioned ssDNA under 30 pN (Figure 4B). These spots increased in intensity as the unwinding fork progressed, and are thus attributed to unwound coiled ssDNA coated by RPA. These observations support the interpretation that the RPA-stimulated DNA unwinding by BLM is initiated from a nick instead of internally melted dsDNA regions. Moreover, 23 unwinding events were marked with two spots on both ends of an ssDNA, progressing in opposite directions (Figure 4B). These observations can be interpreted as BLM helicases unwind two opposite DNA forks by translocating on tensioned ssDNA in one direction and on relaxed ssDNA in the other, further strengthening our conclusion that that RPA activates BLM's bidirectional unwinding. Intriguingly, both Sytox and eGFP signals indicated that the bidirectional unwinding only initiates from a nick instead of starting an opposite unwinding direction in the middle of an ongoing unidirectional unwinding. The average bidirectional unwinding rate (117 ± 25 bp/s, mean \pm SD) was 1.6-fold higher than that of the unidirectional unwinding (72 ± 24 bp/s, mean \pm SD) which is slightly faster than that with BLM alone (60 ± 9 bp/s, mean \pm SD) (Figure 4C and Figure 4-source data 1). These

findings indicate that the unwinding rates for both directions might be a little different. As the opposite DNA unwinding forks differ in that BLMs translocate on relaxed and tensioned ssDNAs, we reasoned that the tension on the ssDNA might modulate BLM unwinding activity a bit. Notably, bidirectional DNA unwinding events were also observable under low and zero external forces (Figure 3-figure supplement 2 and Figure 4-figure supplement 2).

To rule out that the observed bidirectional DNA unwinding was due to the heterologous combination of gBLM and hRPA, we also conducted the DNA unwinding experiments by using hBLM. When testing the homologous pair of hBLM and hRPA, results similar to the heterologous combination were obtained: hBLM alone initiates unidirectional unwinding from a nick and hRPA activates its bidirectional unwinding (Figure 4-figure supplement 3).

RPA can also activate core-BLM's bidirectional unwinding

To examine whether BLM's RPA-activated bidirectional unwinding is due to the interactions between them, we utilized a core fragment of *Gallus gallus* BLM that lacks major interaction domains with RPA (hereafter referred to as core-BLM) (Figure 5A) (Doherty et al., 2005; Kang et al., 2018). The WT BLM helicase was replaced with core-BLM mutant in the helicase unwinding assay with the λ DNA. Control experiments verified that core-BLM alone also unidirectionally unwinds dsDNA from a nick with a relatively slower rate compared with WT BLM (Figure 5-figure supplement 1A-C). When RPA was present, both the unidirectional (58%) and bidirectional (42%) unwinding events ($n = 45$) by this mutant were recorded (Figure 5B). These observations were further substantiated by experiments using eGFP-RPA (Figure 5C) and the 6.4 kbp DNA template (32%, $n = 37$) (Figure 5-figure supplement 1D). The rate of the bidirectional unwinding is 1.7-fold higher than that of the unidirectional unwinding, in agreement with the results with WT BLM (Figure 4C and 5D and Figure 5-source data 1). These findings resemble the observations with WT BLM,

reflecting that BLM's RPA-activated bidirectional unwinding possibly does not rely on the interactions between them.

Free RPAs in solution permits BLM's continuous unwinding

Having demonstrated that RPA activates BLM's bidirectional unwinding, we next aimed to gain mechanistic insights into this activation. A few potential mechanisms have been proposed to explain how RPA stimulates helicase unwinding of long duplex dsDNA (Awate & Brosh, 2017). RPA may enhance BLM-catalyzed DNA unwinding by coating the unwound ssDNAs and relieving the pressure from their reannealing to prolong BLM tethering at the ssDNA/dsDNA junction during unwinding of relatively long duplexes. Alternatively, RPA coated onto ssDNA at the fork junction may help recruit additional BLM helicases from solution to aid in duplex unwinding. To examine these possibilities, we conducted a BLM unwinding experiment in a microfluidic system which allows for the rapid switching of experimental conditions (Figure 6-figure supplement 1). In one channel, we first started the dsDNA unwinding by using 20 nM BLM and 50 nM RPA at 30 pN to ensure the initiation of dsDNA unwinding from a nick. Following that, we depleted the free proteins in solution by rapidly transporting the DNA tether to an ATP-containing reaction buffer channel. We found that, in the buffer channel, the DNA length slowly decreased and the dark region along the DNA template gradually disappeared, indicating the reannealing of the unwound ssDNA ($n = 30$, Figure 6A). This transition from DNA unwinding to rewinding is a result of the dissociation of ssDNA coated RPA and is possibly due to BLM strand switching and/or dissociation. This observation suggests that either free RPAs or BLMs are indispensable for the processive unwinding. To further determine that, we transported BLM/RPA-initiated DNA unwinding template to a channel containing either BLM or RPA. In these experiments, we observed that up to 75% of traces ($n = 53$) in the following RPA channel continued DNA unwinding, and yet only 16% of traces showed continuous unwinding in the BLM channel ($n = 38$) (Figure 6B and 6C). We thus conclude that free RPAs in solution are indispensable for promoting continuous dsDNA unwinding by BLM.

Finding that only free RPA is necessary for BLM-mediated dsDNA unwinding once initiated raises a possibility that BLM might be needed to recognize a nick and bind to it. To test this hypothesis, we started the experiment by first placing the dsDNA tether in a buffer containing 20 nM BLM only where no dsDNA unwinding occurred (Figure 6D). Sequentially, the DNA tether was rapidly switched to a channel containing 50 nM RPA. In this channel, we immediately observed continued unwinding from both DNA length and fluorescence signals in 21 out of 32 traces, resembling the unwinding traces observed when both proteins were present at the same time (Figure 6D). Depleting ATP in the RPA channel abolished the unwinding, confirming that these observations relied on BLM unwinding activity (Figure 6-figure supplement 1B). In addition, 17% of the unwinding events ($n = 12$) were also observed to progress bidirectionally in this experiment, further supporting that this observed unwinding was due to the presence of both BLM and RPA. Since the BLM helicase has poor binding ability to intact dsDNA (Shi, Liu, Yang, & Xi, 2017), the immediate unwinding observed in the RPA channel suggest that limited BLMs recognize and bind to nicks along the DNA template in the BLM channel, and they are stimulated by RPA to unwind a substantial distance without dissociation. To further examine whether DNA-bound RPA could recruit BLM to the DNA template, we transported RPA-coated DNA template to the BLM and RPA channel. Only 17% of unwinding events ($n = 33$) showed continued unwinding in this channel (Figure 6-figure supplement 2), in disagreement with the recruitment model.

In summary, we conclude that once BLM recognizes a nick and initiates unwinding with RPA, only free RPAs are indispensable for its processive unwinding. These findings favor the model that ssDNA generated by BLM was immediately coated by free RPA, preventing the separated ssDNAs from reannealing.

Discussion

There are several lines of evidence supporting that unwinding activities of the RecQ family helicases can be regulated by the presence of SSB proteins (Awate & Brosh, 2017; Bagchi et al., 2018; Cui et al., 2004; Mills et al., 2017; Shen, Gray, Oshima, & Loeb, 1998; Xue, Daley, et al., 2019). Herein, our experimental approach combining optical tweezers with fluorescence microscopy has shed new light on the effect of RPA on BLM's ability to catalyze dsDNA unwinding. This combined technique allows for the direct monitoring of individual unwinding events by BLM along tensioned dsDNA in real time, leading to the discovery of a distinct unwinding mode. In this mode, RPA activates BLM's bidirectional unwinding from a nick where BLMs can translocate on both relaxed and tensioned ssDNAs during unwinding. This is the first observation, to our knowledge, of helicase bidirectional unwinding from a nick. Previous studies of replicative and DNA repair helicases have reported bidirectional unwinding attributable to helicase melting dsDNA internally, which differs from our observed results (Rad et al., 2015; Yardimci et al., 2012).

In the absence of RPA, BLM alone can only initiate unidirectional dsDNA unwinding from a nick where it translocates on the ssDNA with the assistance of an external destabilizing force on DNA (Figure 1D, Figure 4-figure supplement 3, and Figure 5-figure supplement 1). Since the physical barriers presented by dsDNA on both directions from a nick are similar, the inability of BLM to unwind in the opposite direction is mostly likely due to the lack of tension on the relaxed ssDNA which might possibly promote the unwinding activity of BLM. This unidirectional unwinding on nicked dsDNA by BLM alone occurred with the high protein concentrations. The core-BLM lacking the oligomerization domain also exhibited unidirectional unwinding from a nick in the absence of RPA (Figure 5-figure supplement 1) (Karow, Newman, Freemont, & Hickson, 1999; Shi, Chen, et al., 2017), leading us to exclude the possibility that processive unwinding could depend on oligomerization of the protein. Instead, proteins at high concentrations might ensure sufficient

binding of the enzyme to the ssDNA generated during an unwinding event, allowing for successive rounds of unwinding and preventing the unwound strands against reannealing.

A distinct feature of the bidirectional dsDNA unwinding by BLM and RPA is that the unwinding directionality is determined initially at a nick (Figure 4). The sequential protein incubation assays demonstrated that, once preloaded with BLM, only free RPAs are indispensable for activating the bidirectional dsDNA unwinding, suggesting that only limited BLMs are required to first recognize and load on the nicked dsDNA (Figure 6C and 6D). Thus, we reasoned that the bidirectional unwinding necessitates the preloading of more than one helicase at the nick and subsequent binding of RPA on the newly generated ssDNA prolongs the binding and unwinding of BLM at the fork. The unidirectional unwinding probably results from only one BLM helicase preloading at the nick and the inability of BLM to associate with RPA-coated ssDNA (Xue, Daley, et al., 2019). This speculation could also explain a recent single-molecule observation that only unidirectional DNA unwinding by BLM and RPA was detected wherein low concentrations of BLM were used (Xue, Daley, et al., 2019).

Our study also provided insights into the mechanisms by which BLM and RPA cooperate to facilitate end resection in HR. Recent studies support a model that the long-range end resection in HR initiates from a nick generated by the MRN/X complex once the DSB ends are coated by DNA adducts (Cannavo & Cejka, 2014). This demands that the helicase and the nuclease unwind and resect bidirectionally from a nick. It is highly likely that the abilities of BLM to recognize and preload on the nick would help identify the locations of DSB and possibly play a role in recruiting other required proteins for the resection. Although it needs to be further validated, the inherent ability of BLM and RPA to unwind bidirectionally from a nick would facilitate the resection by DNA adduct coated DSB ends which provides ssDNA for the DNA2/EXO1 nucleases to degrade from 5' to 3'

and the MRN complex to degrade from 3' to 5' (Symington, 2016). Interestingly, inhibition of MRN exonuclease activity only confers a relatively lower resection defect compared with the inhibition of its endonuclease activity, suggesting that other proteins might also participate in the initial short ssDNA generation (Shibata et al., 2014). In support of this notion, the complete unwinding of the short dsDNA between the nick and the DSB end may serve as an additional pathway in generating the short stretches of ssDNA.

The finding that the SSB proteins promote helicase-catalyzed dsDNA unwinding from a nick might be conserved among the RecQ-like helicases. For example, the RecQ helicase from *E. coli* is also able to promote dsDNA unwinding in both directions in the presence of *E. coli* SSB (Rad et al., 2015). However, its bidirectional unwinding was initiated by melting dsDNA internally instead of a nick, which resembles replicative helicases in DNA replication initiation (Mott & Berger, 2007). In fact, the unwinding by RecQ progresses unidirectionally if initiated from a nick. In addition, the Sgs1 helicase, the *Saccharomyces cerevisiae* homologue of BLM, was also found to unwind dsDNA from blunt-ended termini or a nick with RPA (Wang et al., 2018; Xue, Wang, et al., 2019), but its unwinding directionality when initiated from a nick has not been determined. A previous single-molecule FRET study revealed that BLM could not unwind more than 34 bp even in the presence of RPA (Yodh, Stevens, Kanagaraj, Janscak, & Ha, 2009). This difference may be due to the fact that the action of applied force on the DNA template can lower the energy required to melt the DNA and prevent reannealing of the separated strands, thus stimulating BLM's unwinding activity. Given the fact that hRPA can activate hBLM's, gBLM's and core-gBLM's bidirectional unwinding from a nick (Figures 4 and 5 and Figure 4-figure supplement 3), this activation might be a conserved feature for the SSB proteins and the RecQ helicases and does not require a homologous system or physical interactions between them.

Key Resources Table				
Reagent type (species) or resource	Designation	Source or reference	Identifiers	Additional information
Gene (<i>Gallus gallus</i>)	<i>gBLM</i>	NCBI	RRID: SCR:006472	NP_001007088.2
Gene (<i>Homo sapiens</i>)	<i>hBLM</i>	NCBI	RRID: SCR:006472	NP_000048.1
Strain, strain background (<i>Escherichia coli</i>)	2566	This paper		Competent cell
Strain, strain background (<i>Escherichia coli</i>)	BL21(DE3)	This Paper		Competent cell
Recombinant DNA reagent	Lambda DNA	Thermo Fisher Scientific	SD0021	
Recombinant DNA reagent	pBR322 (plasmid)	Takara	RRID: Addgene_10877	
Recombinant DNA reagent	pTWIN1 (plasmid)	New England BioLabs	N6951S	Expression of <i>core BLM</i> in <i>E. coli</i>
Recombinant DNA reagent	pET21a-sumo (plasmid)	This paper		Expression of BLM in <i>E. coli</i>

Recombinant DNA reagent	p11d-tRPA (plasmid)	Vector Builder	Addgene:102613	Expression of <i>human RPA</i> in <i>E. coli</i>
Peptide, recombinant protein	T4 DNA ligase	New England BioLabs	M0202L	
Peptide, recombinant protein	Klenow Fragment, exo-	Thermo Fisher Scientific	EP0421	
Peptide, recombinant protein	Nde I	New England BioLabs	R0111S	
Peptide, recombinant protein	Sal I	New England BioLabs	R3138S	
Peptide, recombinant protein	BstX I	New England BioLabs	R0113L	
Chemical compound, drug	Biotin-dATP	Invitrogen	Invitrogen: 19524016	
Chemical compound, drug	Biotin-dCTP	Invitrogen	Invitrogen: 19518018	
Chemical compound, drug	IPTG	Thermo Fisher Scientific	15529019	
Commercial assay, kit	Streptavidin Coated Polystyrene Particles (1.76 μ m)	Spherotech	AG02	

Commercial assay, kit	Streptavidin Coated Polystyrene Particles (4.42 µm)	Spherotech	AL01	
Commercial assay, kit	DNA Purification	Sangon Biotech	B518141	
Commercial assay, kit	SP Sepharose Fast Flow	GE Healthcare	17072904	
Commercial assay, kit	Q Sepharose Fast Flow	GE Healthcare	17051004	
Commercial assay, kit	Sytox orange Nucleic Acid Stain	Thermo Fisher Scientific	S11368	5 mM
Software, algorithm	MATLAB, Data analysis	MathWorks	RRID: SCR:001622	

Preparation of DNA templates

The λ phage DNA template was constructed as described elsewhere (Gross, Farge, Peterman, & Wuite, 2010). Briefly, biotinylated λ phage DNA was made through 3'-end labeling by fill-in of 5'-overhangs with an exo- Klenow Fragment. The reaction was conducted by incubating 330 nM λ phage DNA, 600 µM dGTP/dATP/dTTP, 400 µM biotin-14-dCTP, and 5U Klenow in 1X Klenow reaction buffer at 37 °C for 1 h. The mixture was purified by Column DNA Purification Kit.

389 The 6.4 kbp DNA template containing a single nick consisted of two DNA segments connected
390 by an adaptor (Figure 2-figure supplement 1). The two 2.2 kbp and 4.2 kbp DNA segments were
391 PCR amplified from the plasmid pBR322 using a biotin-labeled primer. The resulting DNA
392 fragments were digested with BstXI to create an overhang. The adaptor was produced by
393 annealing three oligonucleotides where a nick was automatically generated because the 5'
394 phosphate of one oligonucleotide was absent (Figure 2-figure supplement 1). The final product was
395 produced by ligating the two DNA segments with the adaptor at 1:1:1 ratio using T4 ligase.
396

397 **Protein purification**

398 **BLM.** The wild type *Gallus gallus* bloom syndrome protein (gBLM, referred to as WT BLM) and its
399 helicase core mutant (BLM⁶¹⁰⁻¹²⁵⁸, referred to as core-BLM) were used in our experiments. Both
400 WT BLM and core-BLM were expressed and purified as previously described (Shi, Chen, et al.,
401 2017). In brief, the BLM gene was amplified and constructed into the pET21a-sumo vector. The
402 N-terminal-domain-truncated core-BLM was constructed into pTWIN1 by using Nde I and Sal I
403 restriction sites, and transformed into BL21 (DE3). Expression was induced in the T7 expressing *E.*
404 coli strain 2566 by 0.3 mM isopropyl 1-thio-D-galactopyranoside at 18 °C for 16 h. Protein was
405 homogenously purified sequentially by affinity chromatography with a complete His tag purification
406 resin column and ion exchange chromatography on SP Sepharose Fast Flow and Q-Sepharose
407 Fast Flow respectively. hBLM was purified as described previously (Karow, Chakraverty, &
408 Hickson, 1997).
409

410 **hRPA.** The human RPA plasmid was a gift from Dr. Marc Wold. The *E. coli* strain BL21 (DE3) was
411 transformed with the plasmid p11d-tRPA, permitting the co-expression of RPA70, RPA32, and
412 RPA14. RPA was then purified over Affi-Gel Blue, Hydroxyapatite (Biorad), and Q-Sepharose
413 chromatography columns as described previously (Henricksen, Umbricht, & Wold, 1994). The

purified protein was eluted in phosphate buffer containing 300 mM KCl (pH 7.5). To obtain fluorescent human RPA, a DNA fragment encoding a variant of the enhanced GFP (eGFP) with a polyhistidine tag was inserted in frame at the 3' end of the cDNA encoding the large subunit of RPA in the expression plasmid p11d-tRNA. eGFP-RPA purification was performed as previously described (van Mameren et al., 2009).

Single-molecule experiments

Single-molecule experiments were performed at 25 °C on an instrument combining three-color confocal fluorescence microscopy with dual optical traps (LUMICKS, C-trap). In brief, a 1,064-nm fiber laser and a water-immersion objective were used to create two orthogonally polarized optical traps. The trap separation was controlled using a piezo mirror for beam-steering one trap. Force measurements were performed by back-focal plane interferometry of the condenser top lens using a position-sensitive detector. A computer-controlled stage enabled rapid movement of the optical traps within a multiple-channel flow cell (Figure 6-figure supplement 1). This flow cell allowed for the rapid in situ construction and characterization of dumbbell constructs, and facilitated the swift and complete transfer of the tethered DNA between different flow channels.

As described previously (Gross et al., 2010), DNA molecules were captured between two streptavidin-coated polystyrene beads (1.76 μm for 6.4 kbp DNA and 4.5 μm for λ phage DNA) using the multichannel laminar flow cell and tensioned by increasing the distance between the optical traps (Figure 6-figure supplement 1). A single DNA was verified by its inherent mechanical force-extension curve. The trap was then moved to protein channels as described for each assay. Unless stated otherwise, all experiments were carried out in a reaction buffer containing 25 mM Tris-HCl pH 7.5, 100 mM NaCl, 1 mM MgCl_2 , 0.1 mg/ml BSA, 2 mM ATP, 3 mM DTT and 50 nM Sytox Orange.

Fluorescence microscopy was achieved by imaging the stained DNA on an EMCCD camera. Here, a 488-nm excitation laser and a 532-nm excitation laser were used for imaging eGFP-hRPA and Sytox Orange respectively. Kymographs were generated via a confocal line scan through the center of the two beads.

Data acquisition and analysis.

Single-molecule force and fluorescence data were analyzed using custom software provided by LUMICKS (available at <http://www.nat.vu.nl/~iheller/download.html>). Force and DNA extension data were taken at 50 kHz and filtered to 30 Hz. The kymograph was used to track the edge of the unwinding forks. The edges were marked manually by examining each pixel image and comparing to a set threshold value. Elasticity parameters of ssDNA were obtained from the DNA force-extension measurements for data conversion. The force-extension relation of ssDNA in our experimental condition was described as an extensible freely jointed-chain model (Figure 1-figure supplement 3A) (Smith, Cui, & Bustamante, 1996). The unwinding rate was obtained from fitting to the linear region of the increase of the unwinding fork versus time (Figure 1-figure supplement 3B). The unwinding rates were reported as the mean \pm S.D. from the indicated number of events.

Competing interests

The authors declare that no competing interests exist.

Acknowledgments

This research was supported by the National Key R&D Program of China (2016YFA0500902 and 2017YFA0106700), the Natural Science Foundation of Shanghai (19ZR1434100), the French

463 National Cancer Institute (PLBIO2017-167), and French National League Against Cancer
464 (EL2028.LNCC/MaM).

465

References

- Awate, S., & Brosh, R. M., Jr. (2017). Interactive Roles of DNA Helicases and Translocases with the Single-Stranded DNA Binding Protein RPA in Nucleic Acid Metabolism. *Int J Mol Sci*, 18(6). doi:10.3390/ijms18061233
- Bagchi, D., Manosas, M., Zhang, W., Manthei, K. A., Hodeib, S., Ducos, B., . . . Croquette, V. (2018). Single molecule kinetics uncover roles for E. coli RecQ DNA helicase domains and interaction with SSB. *Nucleic Acids Res*, 46(16), 8500-8515. doi:10.1093/nar/gky647
- Bernstein, K. A., Gangloff, S., & Rothstein, R. (2010). The RecQ DNA helicases in DNA repair. *Annu Rev Genet*, 44, 393-417. doi:10.1146/annurev-genet-102209-163602
- Bizard, A. H., & Hickson, I. D. (2014). The dissolution of double Holliday junctions. *Cold Spring Harb Perspect Biol*, 6(7), a016477. doi:10.1101/cshperspect.a016477
- Brosh, R. M., Jr., Li, J. L., Kenny, M. K., Karow, J. K., Cooper, M. P., Kureekattil, R. P., . . . Bohr, V. A. (2000). Replication protein A physically interacts with the Bloom's syndrome protein and stimulates its helicase activity. *J Biol Chem*, 275(31), 23500-23508. doi:10.1074/jbc.M001557200
- Bugreev, D. V., Yu, X., Egelman, E. H., & Mazin, A. V. (2007). Novel pro- and anti-recombination activities of the Bloom's syndrome helicase. *Genes Dev*, 21(23), 3085-3094. doi:10.1101/gad.1609007
- Bustamante, C., Bryant, Z., & Smith, S. B. (2003). Ten years of tension: single-molecule DNA mechanics. *Nature*, 421(6921), 423-427. doi:10.1038/nature01405
- Cannavo, E., & Cejka, P. (2014). Sae2 promotes dsDNA endonuclease activity within Mre11-Rad50-Xrs2 to resect DNA breaks. *Nature*, 514(7520), 122-125. doi:10.1038/nature13771
- Chatterjee, S., Zagelbaum, J., Savitsky, P., Sturzenegger, A., Huttner, D., Janscak, P., . . . Rothenberg, E. (2014). Mechanistic insight into the interaction of BLM helicase with intra-strand G-quadruplex structures. *Nat Commun*, 5, 5556. doi:10.1038/ncomms6556
- Croteau, D. L., Popuri, V., Opresko, P. L., & Bohr, V. A. (2014). Human RecQ Helicases in DNA Repair, Recombination, and Replication. *Annual Review of Biochemistry*, Vol 83, 83, 519-552. doi:10.1146/annurev-biochem-060713-035428
- Cui, S., Arosio, D., Doherty, K. M., Brosh, R. M., Falaschi, A., & Vindigni, A. (2004). Analysis of the unwinding activity of the dimeric RECQ1 helicase in the presence of human replication protein A. *Nucleic Acids Research*, 32(7), 2158-2170. doi:10.1093/nar/gkh540
- Davies, S. L., North, P. S., & Hickson, I. D. (2007). Role for BLM in replication-fork restart and suppression of origin firing after replicative stress. *Nat Struct Mol Biol*, 14(7), 677-679. doi:10.1038/nsmb1267
- Doherty, K. M., Sommers, J. A., Gray, M. D., Lee, J. W., von Kobbe, C., Thoma, N. H., . . . Brosh, R. M., Jr. (2005). Physical and functional mapping of the replication protein a interaction domain of the werner and bloom syndrome helicases. *J Biol Chem*, 280(33), 29494-29505. doi:10.1074/jbc.M500653200

505 Ellis, N. A., Groden, J., Ye, T. Z., Straughen, J., Lennon, D. J., Ciocchi, S., . . . German, J. (1995).
506 The Bloom's syndrome gene product is homologous to RecQ helicases. *Cell*, 83(4),
507 655-666.

508 Fanning, E., Klimovich, V., & Nager, A. R. (2006). A dynamic model for replication protein A (RPA)
509 function in DNA processing pathways. *Nucleic Acids Res*, 34(15), 4126-4137.
510 doi:10.1093/nar/gkl550

511 Gravel, S., Chapman, J. R., Magill, C., & Jackson, S. P. (2008). DNA helicases Sgs1 and BLM
512 promote DNA double-strand break resection. *Genes & Development*, 22(20), 2767-2772.
513 doi:10.1101/gad.503108

514 Gross, P., Farge, G., Peterman, E. J., & Wuite, G. J. (2010). Combining optical tweezers,
515 single-molecule fluorescence microscopy, and microfluidics for studies of DNA-protein
516 interactions. *Methods Enzymol*, 475, 427-453. doi:10.1016/S0076-6879(10)75017-5

517 Henricksen, L. A., Umbricht, C. B., & Wold, M. S. (1994). Recombinant Replication Protein-a -
518 Expression, Complex-Formation, and Functional-Characterization (Vol 269, Pg 11121,
519 1994). *Journal of Biological Chemistry*, 269(23), 16519-16519.

520 Kang, D., Lee, S., Ryu, K. S., Cheong, H. K., Kim, E. H., & Park, C. J. (2018). Interaction of
521 replication protein A with two acidic peptides from human Bloom syndrome protein. *FEBS*
522 *Lett*, 592(4), 547-558. doi:10.1002/1873-3468.12992

523 Karow, J. K., Chakraverty, R. K., & Hickson, I. D. (1997). The Bloom's syndrome gene product is a
524 3'-5' DNA helicase. *J Biol Chem*, 272(49), 30611-30614.

525 Karow, J. K., Newman, R. H., Freemont, P. S., & Hickson, I. D. (1999). Oligomeric ring structure of
526 the Bloom's syndrome helicase. *Curr Biol*, 9(11), 597-600.

527 King, G. A., Gross, P., Bockelmann, U., Modesti, M., Wuite, G. J., & Peterman, E. J. (2013).
528 Revealing the competition between peeled ssDNA, melting bubbles, and S-DNA during
529 DNA overstretching using fluorescence microscopy. *Proc Natl Acad Sci U S A*, 110(10),
530 3859-3864. doi:10.1073/pnas.1213676110

531 Kitao, S., Lindor, N. M., Shiratori, M., Furuichi, Y., & Shimamoto, A. (1999). Rothmund-thomson
532 syndrome responsible gene, RECQL4: genomic structure and products. *Genomics*, 61(3),
533 268-276. doi:10.1006/geno.1999.5959

534 Kowalczykowski, S. C. (2015). An Overview of the Molecular Mechanisms of Recombinational
535 DNA Repair. *Cold Spring Harb Perspect Biol*, 7(11). doi:10.1101/cshperspect.a016410

536 Maizels, N., & Davis, L. (2018). Initiation of homologous recombination at DNA nicks. *Nucleic*
537 *Acids Research*, 46(14), 6962-6973. doi:10.1093/nar/gky588

538 Mills, M., Harami, G. M., Seol, Y., Gyimesi, M., Martina, M., Kovacs, Z. J., . . . Neuman, K. C.
539 (2017). RecQ helicase triggers a binding mode change in the SSB-DNA complex to
540 efficiently initiate DNA unwinding. *Nucleic Acids Res*, 45(20), 11878-11890.
541 doi:10.1093/nar/gkx939

542 Mohaghegh, P., Karow, J. K., Brosh, R. M., Bohr, V. A., & Hickson, I. D. (2001). The Bloom's and
 543 Werner's syndrome proteins are DNA structure-specific helicases. *Nucleic Acids Research*,
 544 29(13), 2843-2849. doi:DOI 10.1093/nar/29.13.2843

545 Mott, M. L., & Berger, J. M. (2007). DNA replication initiation: mechanisms and regulation in
 546 bacteria. *Nat Rev Microbiol*, 5(5), 343-354. doi:10.1038/nrmicro1640

547 Nimonkar, A. V., Genschel, J., Kinoshita, E., Polaczek, P., Campbell, J. L., Wyman, C., . . .
 548 Kowalczykowski, S. C. (2011). BLM-DNA2-RPA-MRN and EXO1-BLM-RPA-MRN
 549 constitute two DNA end resection machineries for human DNA break repair. *Genes Dev*,
 550 25(4), 350-362. doi:10.1101/gad.2003811

551 Nimonkar, A. V., Ozsoy, A. Z., Genschel, J., Modrich, P., & Kowalczykowski, S. C. (2008). Human
 552 exonuclease 1 and BLM helicase interact to resect DNA and initiate DNA repair.
 553 *Proceedings of the National Academy of Sciences of the United States of America*,
 554 105(44), 16906-16911. doi:10.1073/pnas.0809380105

555 Rad, B., Forget, A. L., Baskin, R. J., & Kowalczykowski, S. C. (2015). Single-molecule
 556 visualization of RecQ helicase reveals DNA melting, nucleation, and assembly are required
 557 for processive DNA unwinding. *Proc Natl Acad Sci U S A*, 112(50), E6852-6861.
 558 doi:10.1073/pnas.1518028112

559 Shen, J. C., Gray, M. D., Oshima, J., & Loeb, L. A. (1998). Characterization of Werner syndrome
 560 protein DNA helicase activity: directionality, substrate dependence and stimulation by
 561 replication protein A. *Nucleic Acids Res*, 26(12), 2879-2885.

562 Shi, J., Chen, W. F., Zhang, B., Fan, S. H., Ai, X., Liu, N. N., . . . Xi, X. G. (2017). A helical bundle
 563 in the N-terminal domain of the BLM helicase mediates dimer and potentially hexamer
 564 formation. *Journal of Biological Chemistry*, 292(14), 5909-5920.
 565 doi:10.1074/jbc.M116.761510

566 Shi, J., Liu, N. N., Yang, Y. T., & Xi, X. G. (2017). Purification and enzymatic characterization of
 567 Gallus gallus BLM helicase. *J Biochem*, 162(3), 183-191. doi:10.1093/jb/mvx013

568 Shibata, A., Moiani, D., Arvai, A. S., Perry, J., Harding, S. M., Genois, M. M., . . . Tainer, J. A.
 569 (2014). DNA double-strand break repair pathway choice is directed by distinct MRE11
 570 nuclease activities. *Mol Cell*, 53(1), 7-18. doi:10.1016/j.molcel.2013.11.003

571 Singleton, M. R., Dillingham, M. S., & Wigley, D. B. (2007). Structure and mechanism of helicases
 572 and nucleic acid translocases. *Annu Rev Biochem*, 76, 23-50.
 573 doi:10.1146/annurev.biochem.76.052305.115300

574 Smith, S. B., Cui, Y. J., & Bustamante, C. (1996). Overstretching B-DNA: The elastic response of
 575 individual double-stranded and single-stranded DNA molecules. *Science*, 271(5250),
 576 795-799. doi:DOI 10.1126/science.271.5250.795

577 Soniat, M. M., Myler, L. R., Kuo, H. C., Paull, T. T., & Finkelstein, I. J. (2019). RPA
 578 Phosphorylation Inhibits DNA Resection. *Mol Cell*, 75(1), 145-153 e145.
 579 doi:10.1016/j.molcel.2019.05.005

580 Sturzenegger, A., Burdova, K., Kanagaraj, R., Levikova, M., Pinto, C., Cejka, P., & Janscak, P.
 581 (2014). DNA2 Cooperates with the WRN and BLM RecQ Helicases to Mediate Long-range

DNA End Resection in Human Cells. *Journal of Biological Chemistry*, 289(39), 27314-27326. doi:10.1074/jbc.M114.578823

Symington, L. S. (2016). Mechanism and regulation of DNA end resection in eukaryotes. *Crit Rev Biochem Mol Biol*, 51(3), 195-212. doi:10.3109/10409238.2016.1172552

van Mameren, J., Gross, P., Farge, G., Hooijman, P., Modesti, M., Falkenberg, M., . . . Peterman, E. J. G. (2009). Unraveling the structure of DNA during overstretching by using multicolor, single-molecule fluorescence imaging. *Proceedings of the National Academy of Sciences of the United States of America*, 106(43), 18231-18236. doi:10.1073/pnas.0904322106

Wang, W., Daley, J. M., Kwon, Y., Xue, X., Krasner, D. S., Miller, A. S., . . . Sung, P. (2018). A DNA nick at Ku-blocked double-strand break ends serves as an entry site for exonuclease 1 (Exo1) or Sgs1-Dna2 in long-range DNA end resection. *J Biol Chem*, 293(44), 17061-17069. doi:10.1074/jbc.RA118.004769

Woglar, A., & Villeneuve, A. M. (2018). Dynamic Architecture of DNA Repair Complexes and the Synaptonemal Complex at Sites of Meiotic Recombination. *Cell*, 173(7), 1678-1691. doi:ARTN 1691.e1610.1016/j.cell.2018.03.066

Wold, M. S. (1997). Replication protein A: A heterotrimeric, single-stranded DNA-binding protein required for eukaryotic DNA metabolism. *Annual Review of Biochemistry*, 66, 61-92. doi:DOI 10.1146/annurev.biochem.66.1.61

Xue, C., Daley, J. M., Xue, X., Steinfeld, J., Kwon, Y., Sung, P., & Greene, E. C. (2019). Single-molecule visualization of human BLM helicase as it acts upon double- and single-stranded DNA substrates. *Nucleic Acids Research*. doi:10.1093/nar/gkz810

Xue, C., Wang, W., Crickard, J. B., Moevus, C. J., Kwon, Y., Sung, P., & Greene, E. C. (2019). Regulatory control of Sgs1 and Dna2 during eukaryotic DNA end resection. *Proc Natl Acad Sci U S A*. doi:10.1073/pnas.1819276116

Yardimci, H., Wang, X., Loveland, A. B., Tappin, I., Rudner, D. Z., Hurwitz, J., . . . Walter, J. C. (2012). Bypass of a protein barrier by a replicative DNA helicase. *Nature*, 492(7428), 205-209. doi:10.1038/nature11730

Yodh, J. G., Stevens, B. C., Kanagaraj, R., Janscak, P., & Ha, T. (2009). BLM helicase measures DNA unwound before switching strands and hRPA promotes unwinding reinitiation. *EMBO J*, 28(4), 405-416. doi:10.1038/emboj.2008.298

Yu, C. E., Oshima, J., Fu, Y. H., Wijsman, E. M., Hisama, F., Alisch, R., . . . Schellenberg, G. D. (1996). Positional cloning of the Werner's syndrome gene. *Science*, 272(5259), 258-262.

Figure legends

Figure 1. BLM unwinds dsDNA unidirectionally from a nick. (A) A Schematic of the experimental configuration. Biotinylated λ phage DNA was suspended by two streptavidin coated beads manipulated by two optical traps. Meanwhile, confocal lasers repeatedly scanned along the DNA template. DNA length was expected to increase under a constant force when dsDNA was converted to ssDNA by BLM. (B, C) A representative kymograph of a tethered λ DNA as well as its corresponding force and DNA length as a function of time in the presence of 20 nM (B) or 200 nM (C) BLM. (D) Kymograph of an individual unwinding event showing the unidirectional DNA unwinding. The arrow indicates the direction of the unwinding fork movement. (E) Distributions of the dsDNA unwinding rates in the presence of 200 nM BLM under 30 pN.

Figure 1-source data 1. The dsDNA unwinding rates of 200 nM BLM under 30 pN.

Figure 1-figure supplement 1. DNA unwinding in the presence of 200 nM BLM. (A, B) Representative traces of BLM unwinding λ DNA in the presence of 200 nM BLM. Three individual unwinding events were detected once the force was increased to 30 pN in A, and two were monitored under 20 pN in B. (C) The forces required to monitor DNA unwinding by BLM range from 10 pN to 40 pN. (D) Number of unwinding events on a single λ DNA with or without RPA.

Figure 1-figure supplement 2. Control experiments verified BLM's unwinding activity. (A) To confirm that the observed unwinding was a result of BLM's helicase activity, we conducted the unwinding experiment in the absence of ATP. In the presence of 200 nM BLM, we started the experiment at 10 pN force for ~1 min and increased it by 10 pN each time. There was no change of either fluorescent or DNA length signal under 10 - 40 pN ($n = 13$), indicating that the unwinding signals we observed were indeed due to BLM's helicase activity. (B) BLM-mediated DNA length

increases were comparable in the presence and absence of Sytox, indicating that the fluorescence dye does not affect BLM's unwinding activity.

Figure 1-figure supplement 3. Elasticity parameters of ssDNA and DNA unwinding rate calculation. (A) Elasticity parameters of ssDNA were necessary for data conversion. They were obtained from the DNA force-extension measurements. Force-extension curve of this ssDNA (8,358 nt) in reaction buffer containing 50 nM Sytox was shown in black. The force-extension relation of ssDNA was described as extensible freely jointed-chain (FJC) model. The fitting result was shown in red. The contour length was 4.07 ± 0.12 nm and stretch module was 297.6 ± 11.8 pN ($n = 6$). (B) Kymographs were used to calculate DNA unwinding rate by BLM from a nick. It was obtained from fitting to the linear region of the increase of the unwinding fork versus time. The velocity in nm/s was further converted to bp/s based on the elasticity parameters.

Figure 2. BLM unwinds DNA template containing a single nick. (A) Two models of BLM unwinding dsDNA from a nick. BLM initiates unidirectional dsDNA unwinding from a nick by translocating either on the tensioned ssDNA or on the relaxed ssDNA. The unwinding polarities are opposite in these two scenarios. (B) The 6.4 kbp dsDNA template unwinding in the presence of 200 nM BLM. The 6.4 kbp dsDNA contains a nick located at 2.2 kbp and 4.2 kbp from the 5' and 3' termini, respectively. Representative kymographs and DNA length signals showed the 4.2 kbp dsDNA segments were always unwound under 30 pN. The arrows indicate the directions of the unwinding fork movement.

Figure 2-figure supplement 1. Construction of the 6.4 kbp DNA template. The 6.4 kbp nicked DNA template containing a single nick consists of two DNA segments (2.2 kbp and 4.2 kbp) connected by an adaptor. The two DNA segments were PCR amplified from the plasmid pBR322

using a biotin-labeled primer. The resulting DNA fragments were digested with BstXI to create an overhang. The adaptor was a product by annealing three oligonucleotides where a nick was automatically generated due to the missing of the 5' phosphate of one oligonucleotide. The final product was produced by ligating the two DNA segments with the adaptor at 1:1:1 ratio using T4 ligase.

Figure 3. BLM unwinds dsDNA in the presence of RPA. (A, C) Distributions of the required forces to monitor DNA unwinding in the presence of 200 nM (A) or 20 nM (C) BLM and RPA with indicated concentrations. N.U. represents no unwinding. (B, D) Kymographs of tethered λ phage DNA showing DNA unwinding in the presence of 50 nM RPA and 200 nM BLM (B) or 200 nM RPA and 20 nM (D) BLM under 5 pN.

Figure 3-source data 1. The required forces for BLM/RPA-mediated DNA unwinding.

Figure 3-figure supplement 1. RPA alone was incapable of unwinding DNA. To confirm that the observed unwinding in the presence of BLM and RPA was a result of BLM's helicase activity, we conducted the unwinding experiment in the absence of ATP. In the presence of 200 nM BLM and 200 nM RPA, we started the experiment at 10 pN force for ~1 min and increased to 10/20/30 pN orderly. There was no change of either fluorescent or DNA length signal ($n = 10$), indicating that the unwinding signals we observed were indeed due to BLM's helicase activity.

Figure 3-figure supplement 2. BLM and RPA unwind nicked DNA in the absence of external force. To determine whether BLM and RPA can unwind nicked DNA in the absence of force, we designed a new DNA unwinding assay. We first incubated a relaxed λ DNA tether (under zero force) in a channel containing 200 nM WT BLM and 400 nM eGFP-RPA for ~10 s. The relaxed DNA

tether was then transported to a buffer channel wherein DNA unwinding could not occur due to the absence of BLM, RPA and ATP. In this channel, we stretched the DNA tether to 10 pN and examined the fluorescence signal along the DNA template before RPA dissociates. As shown above, the bidirectional unwinding DNA intermediates were detected ($n = 10$), indicating RPA and BLM can indeed unwind nicked DNA in the first channel in which no external force exists.

Figure 4. BLM's RPA-activated bidirectional unwinding from a nick. (A) Kymographs of individual unwinding events of a tethered λ phage DNA in the presence of 200 nM BLM and 50 nM RPA under 30 pN showing unidirectional and bidirectional DNA unwinding. The arrows indicate unwinding directions. (B) Representative kymographs of unidirectional (up) and bidirectional (down) DNA unwinding in the presence of 200 nM WT BLM and 50 nM eGFP-RPA. To illustrate the coiled ssDNAs, confocal laser scanned a rectangle area instead of only the DNA template track. The arrows indicate the directions of the unwinding fork movement. (C) Distributions of the uni- and bi- directional dsDNA unwinding rates in the presence of 200 nM BLM and 50 nM RPA under 30 pN. p -value < 0.01 calculated by Student's t test. These rate distributions were compared with that in the presence of 200 nM BLM alone (black).

Figure 4-source data 1. The uni- and bi- directional dsDNA unwinding rates.

Figure 4-figure supplement 1. RPA supports BLM's bidirectional unwinding on the 6.4 kbp nicked DNA template. A kymograph of an individual unwinding event on the 6.4 kbp nicked DNA template shows bidirectional DNA unwinding (50 nM RPA and 200 nM WT BLM). The red arrows indicate the directions of the unwinding fork movement.

Figure 4-figure supplement 2. RPA supports BLM's bidirectional unwinding under low forces. Under 5 pN, bidirectional unwinding events were also observable when RPA and BLM were present. We showed representative kymographs of bidirectional DNA unwinding events at 5 pN under different conditions. The red arrows indicate the directions of the unwinding fork movement.

Figure 4-figure supplement 3. hBLM unwinds dsDNA in the presence and absence of hRPA.

(A) Kymographs of individual unwinding events showing the unidirectional unwinding (left) and bidirectional unwinding (right) in the presence of 200 nM hBLM and 100 nM hRPA under 30 pN. The arrow indicates the direction of the unwinding fork movement. In this experimental condition, 18 out of 48 unwinding events showed bidirectional DNA unwinding and the rest showed unidirectional DNA unwinding. **(B)** Kymograph of an individual unwinding event showing the unidirectional unwinding in the presence of 200 nM hBLM alone under 30 pN. Only unidirectional DNA unwinding was detected with hBLM alone ($n = 15$). **(C)** Kymograph of bidirectional DNA unwinding in the presence of 200 nM hBLM and 100nM eGFP-hRPA. To illustrate the coiled ssDNAs, confocal laser scanned a rectangle area instead of only the DNA template track. The arrows indicate the directions of the unwinding fork movement. **(D)** Distributions of the uni- and bi-directional dsDNA unwinding rates in the presence of 200 nM hBLM and 100 nM hRPA under 30 pN. p -value < 0.01 calculated from Student's t test.

Figure 5. RPA supports core-BLM's bidirectional unwinding from a nick. **(A)** Schematic representations of WT BLM and core-BLM. Helicase, RQC and HRDC domains are shown in different colors. **(B)** Kymograph of an individual unwinding event in the presence of 20 nM core-BLM and 50 nM RPA under 35 pN showing unidirectional (up) and bidirectional (down) DNA unwinding. The arrows indicate the directions of the unwinding fork movement. **(C)** A

representative kymograph of a single DNA tether unwound in the presence of 20 nM core-BLM and 50 nM eGFP-RPA. To demonstrate the coiled ssDNAs, confocal laser scanned a rectangle area instead of the DNA template track only. **(D)** Distributions of the uni- and bi- directional dsDNA unwinding rates in the presence of 20 nM BLM and 50 nM RPA under 35 pN. p -value < 0.01 calculated by Student's t test.

Figure 5-source data 1. The uni- and bi- directional dsDNA unwinding rates.

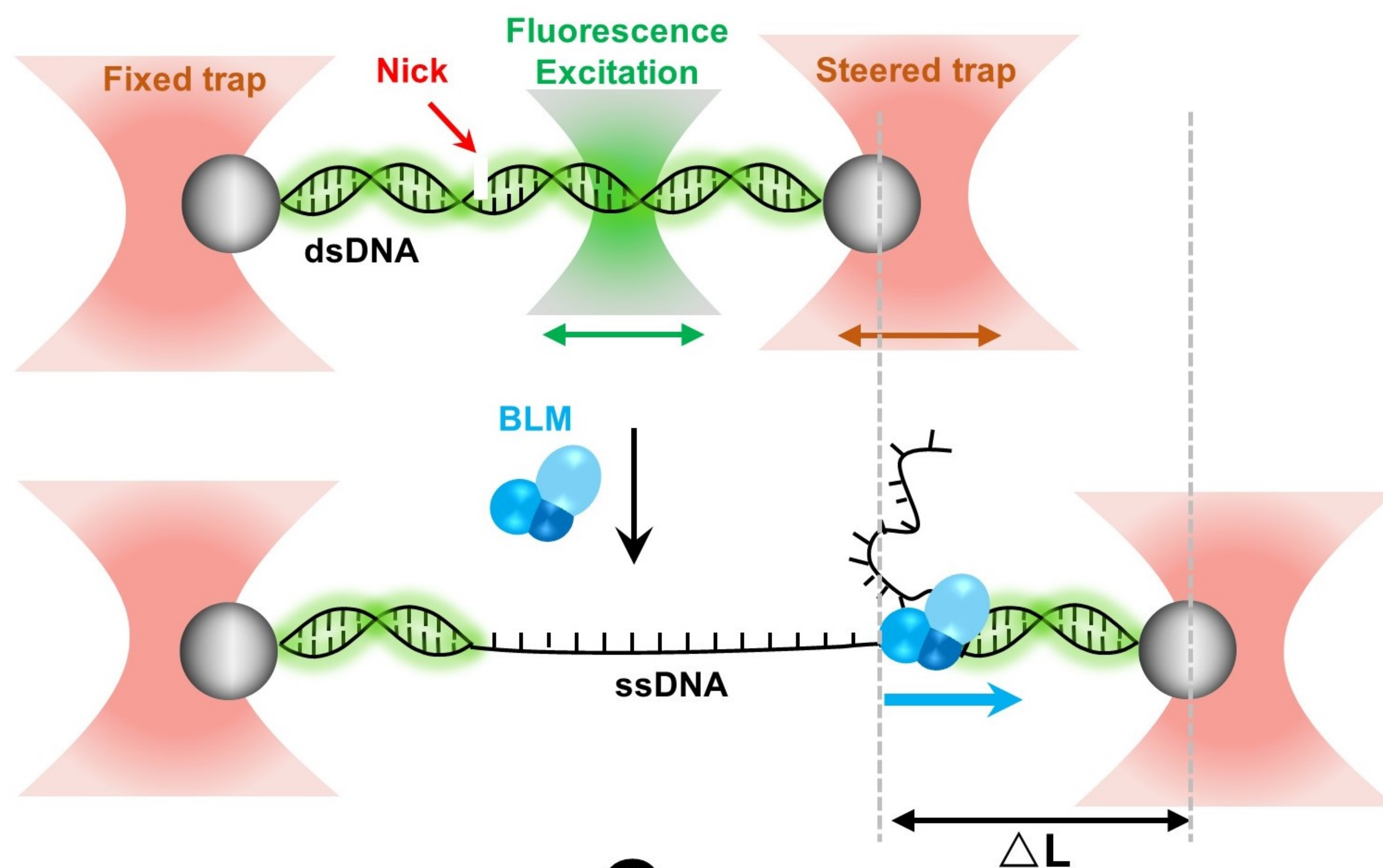
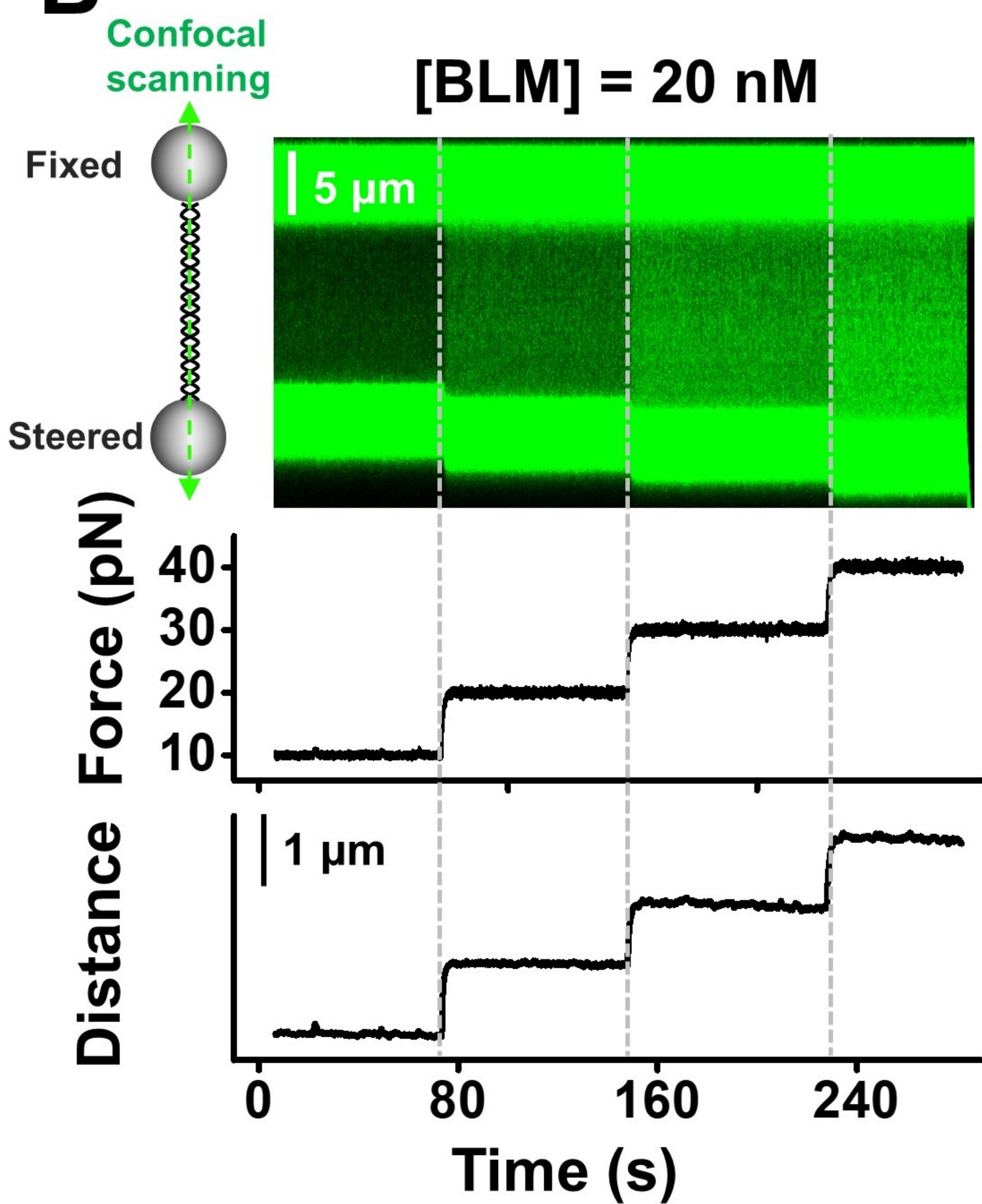
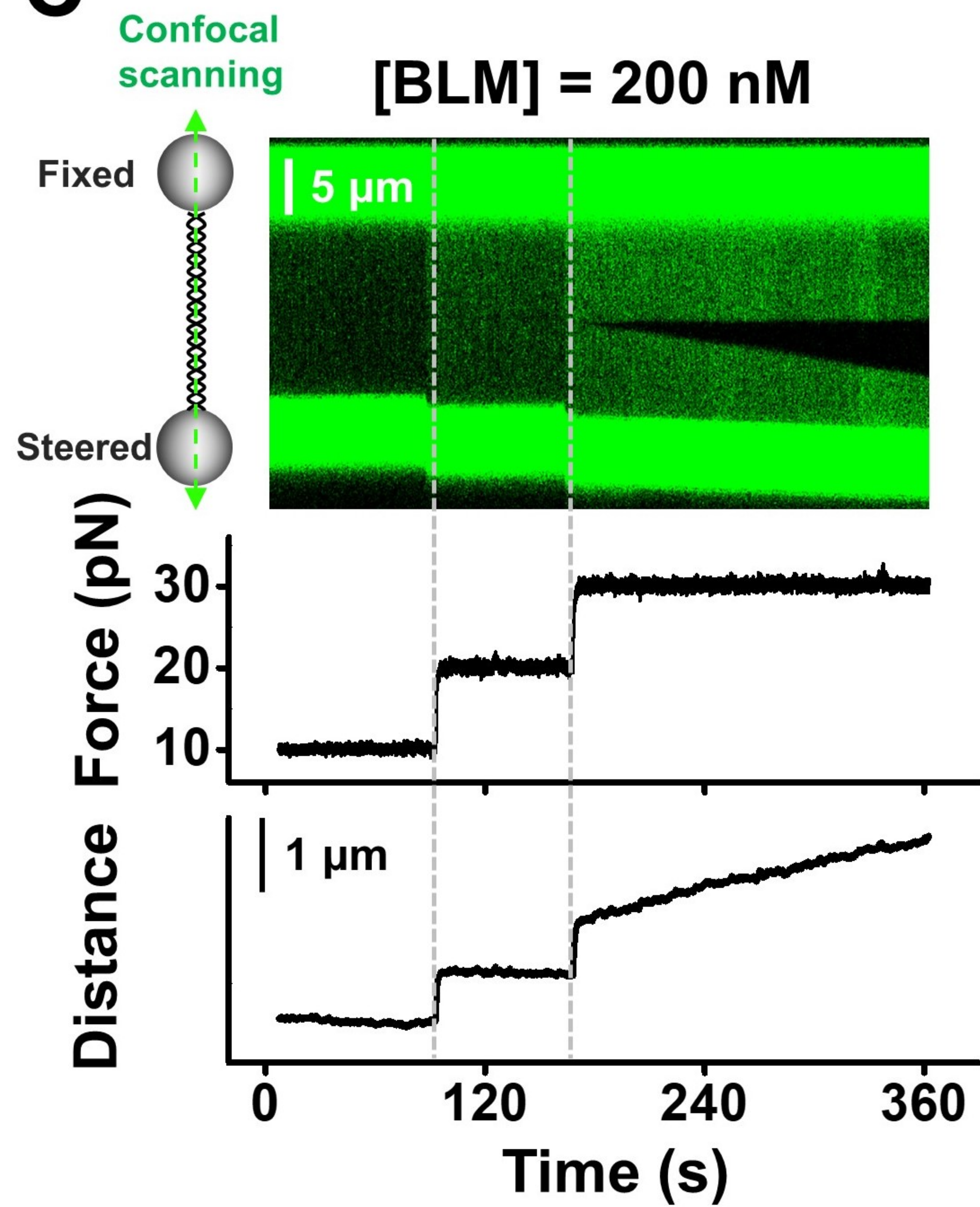
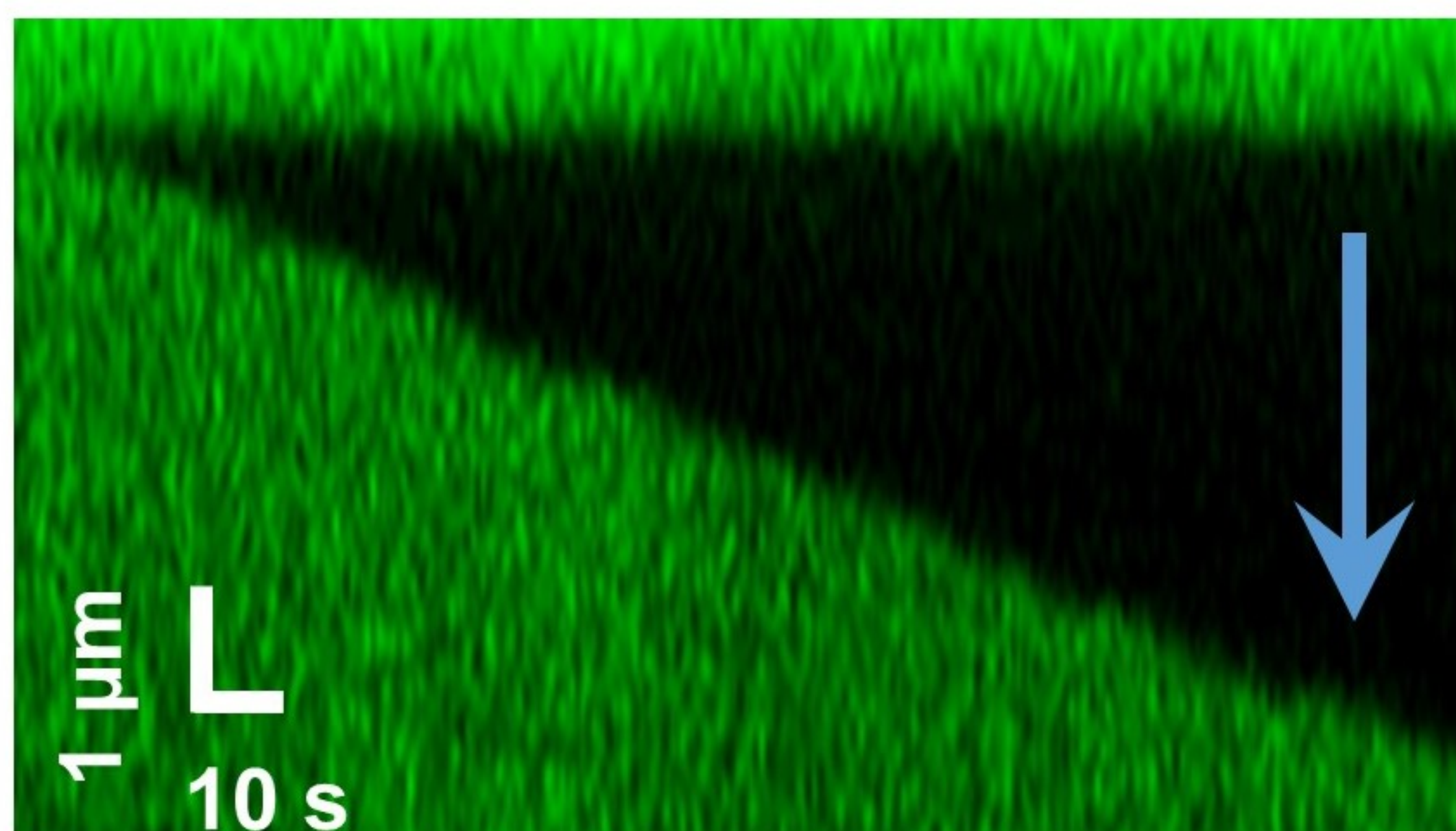
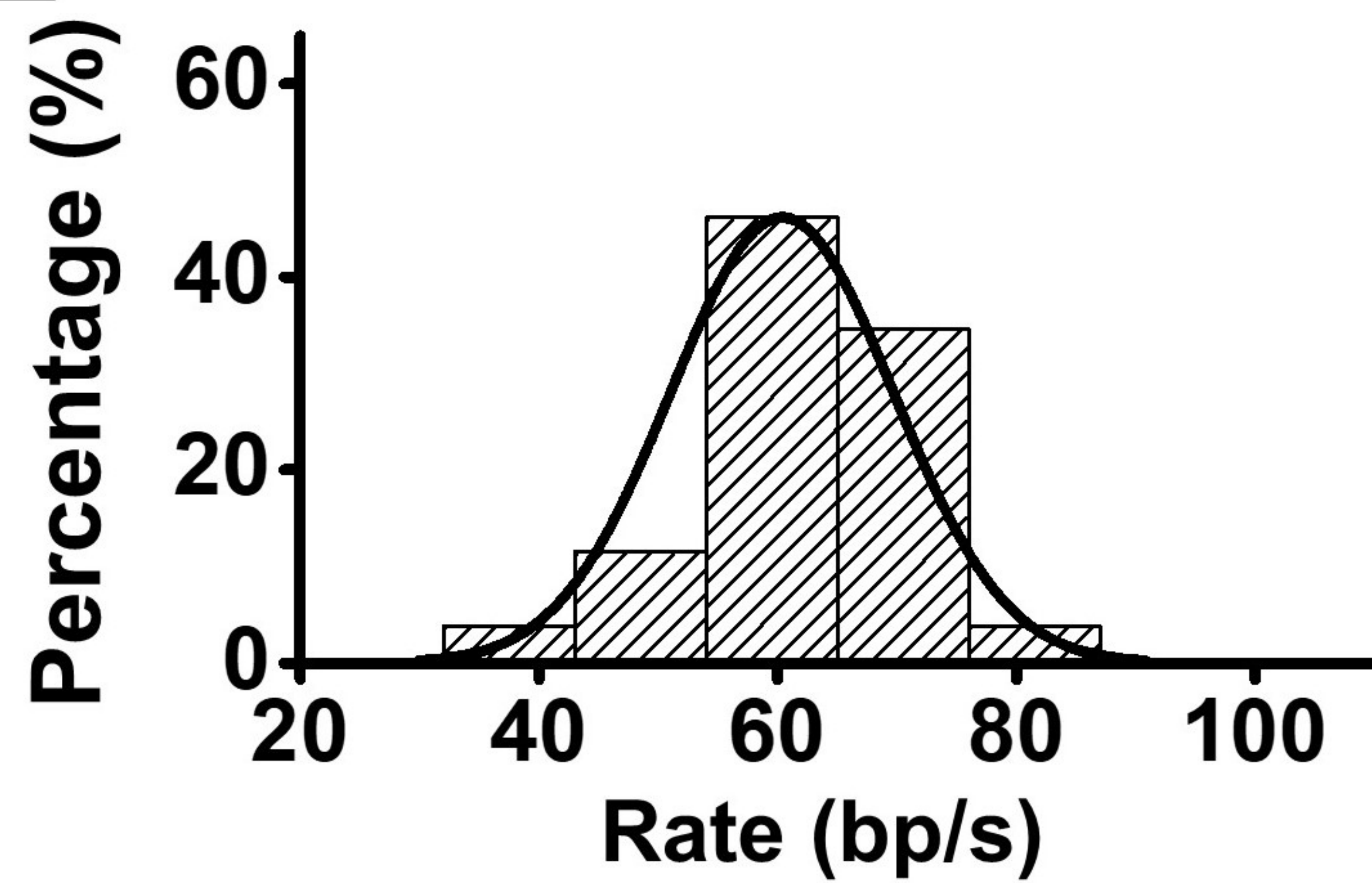
Figure 5-figure supplement 1. Core-BLM unwinds dsDNA in the presence and absence of RPA. (A) Kymograph of an individual unwinding event showing the unidirectional unwinding in the presence of 200 nM core-BLM under 30 pN. The arrow indicates the direction of the unwinding fork movement. In all examined unwinding events ($n = 48$), DNA unwinding occurred unidirectionally. **(B)** Distribution of the dsDNA unwinding rates in the presence of 200 nM core-BLM under 30 pN. **(C)** The 6.4 kbp dsDNA template unwinding in the presence of 200 nM core-BLM. A representative kymograph and DNA length signal showed the 4.2 kbp dsDNA segment was unwound under 35 pN. In all examined traces ($n = 27$), only the 4.2 kbp dsDNA segment was unwound, indicating that core-BLM unwinds unidirectionally by translocating on the tensioned ssDNA. **(D)** A kymograph of an individual unwinding event in the presence of 50 nM RPA and 200 nM core-BLM showing bidirectional unwinding. The arrows indicate the directions of the unwinding fork movement.

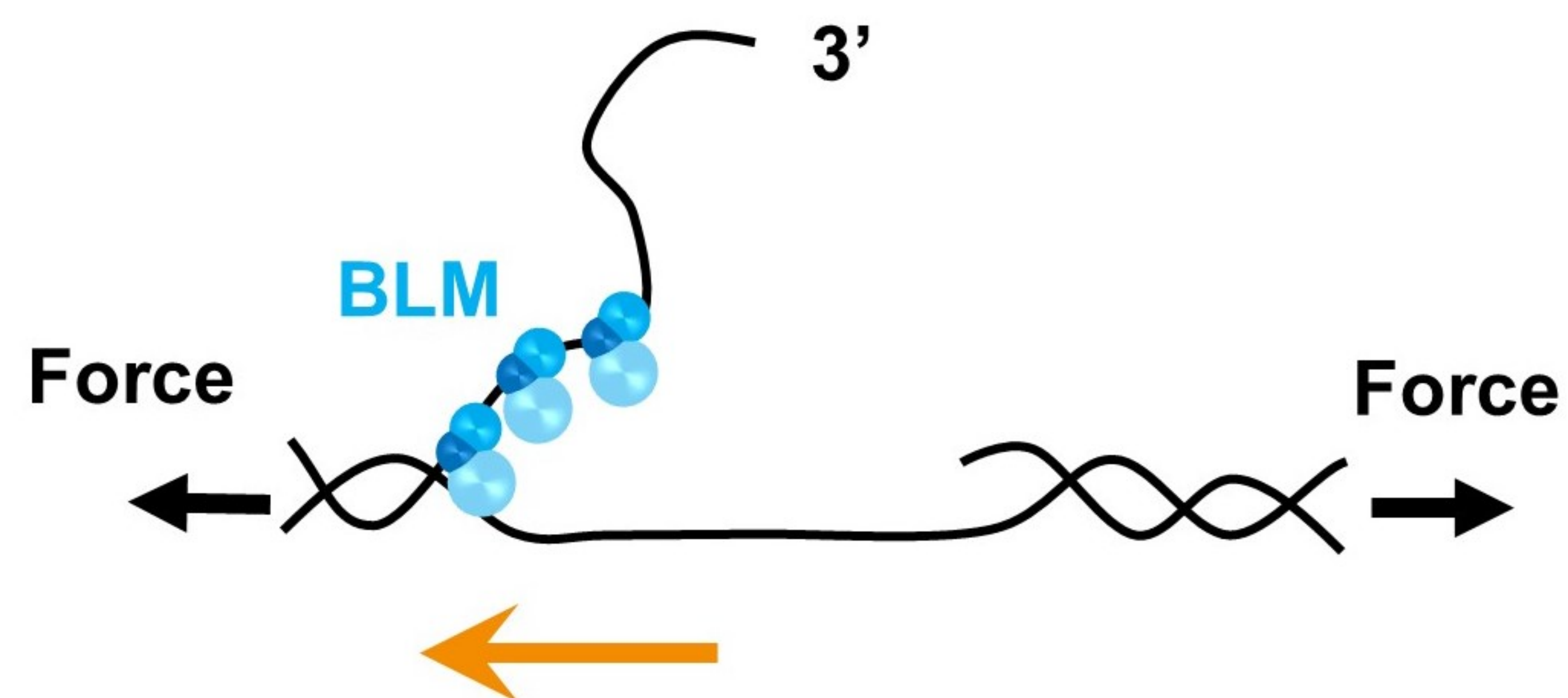
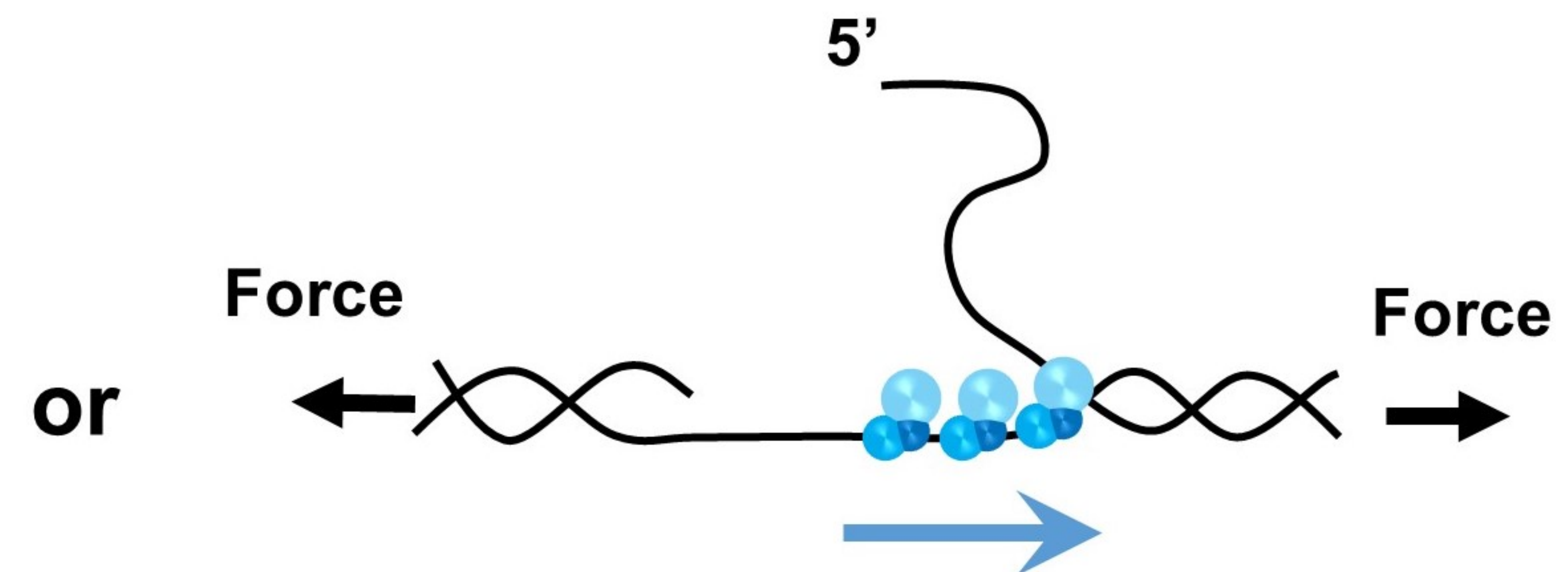
Figure 6. Free RPAs are indispensable for stimulating BLM-mediated DNA unwinding. (A-C) Kymographs and DNA length vs. time traces of DNA tethers showing dsDNA unwinding initiating in a channel containing 20 nM BLM and 50 nM RPA under 30 pN, followed by quickly transporting to a channel containing ATP reaction buffer **(A)**, 20 nM BLM **(B)** or 50 nM RPA **(C)** only. Red arrows indicate bidirectional DNA unwinding. **(D)** Kymograph and DNA length vs. time of a DNA tether

showing the DNA template incubated in a channel containing 20 nM BLM under 30 pN, followed by transporting to a channel containing 50 nM RPA. Red arrows indicate bidirectional DNA unwinding.

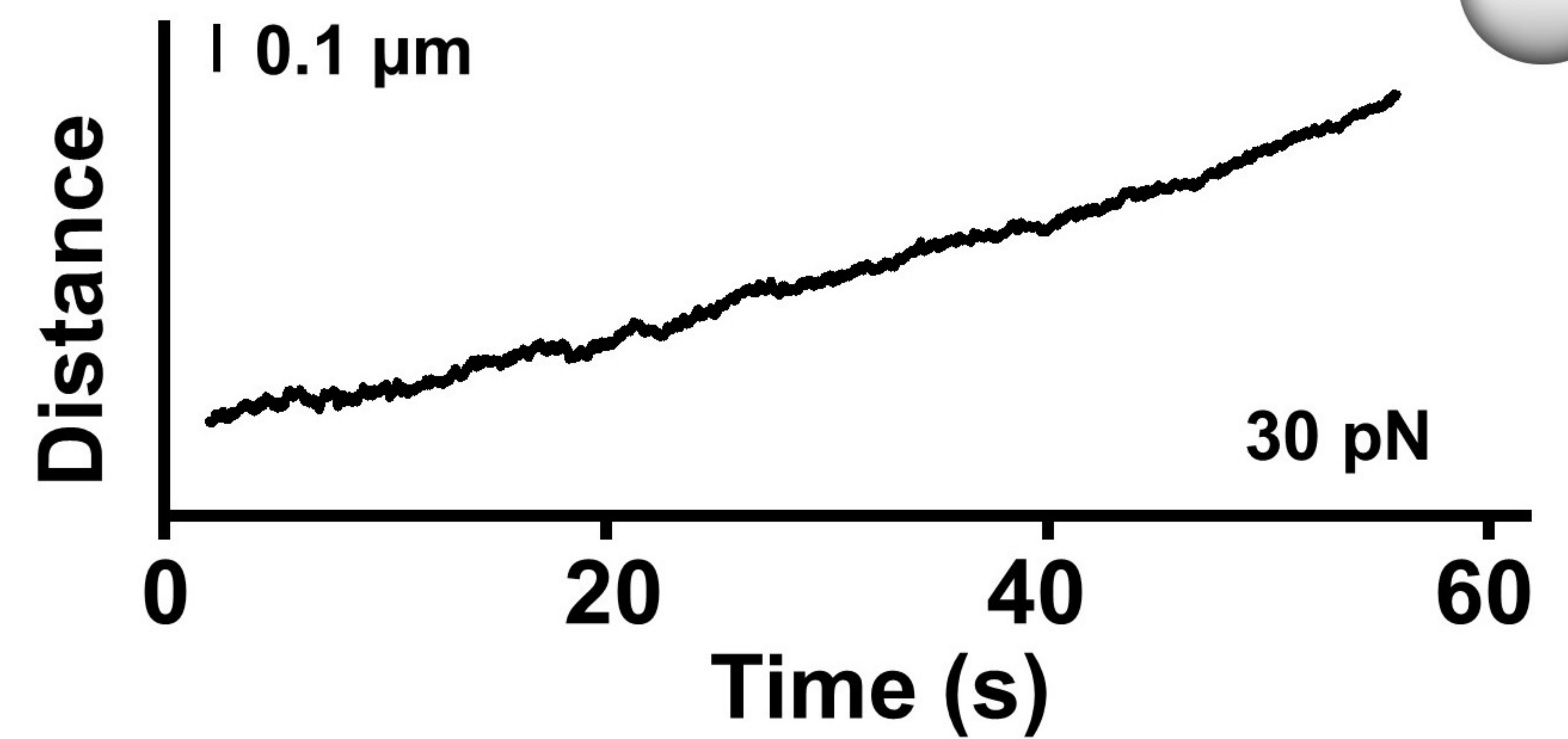
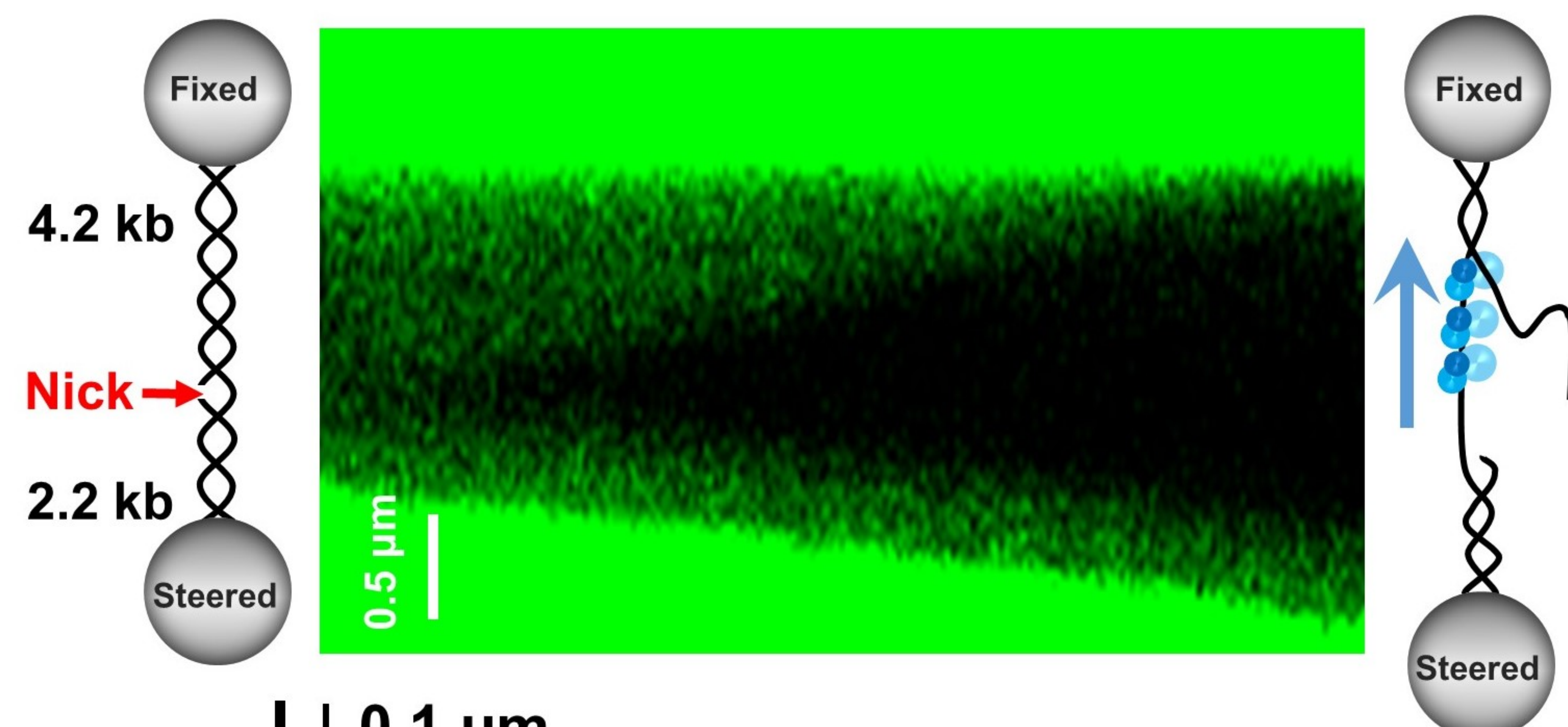
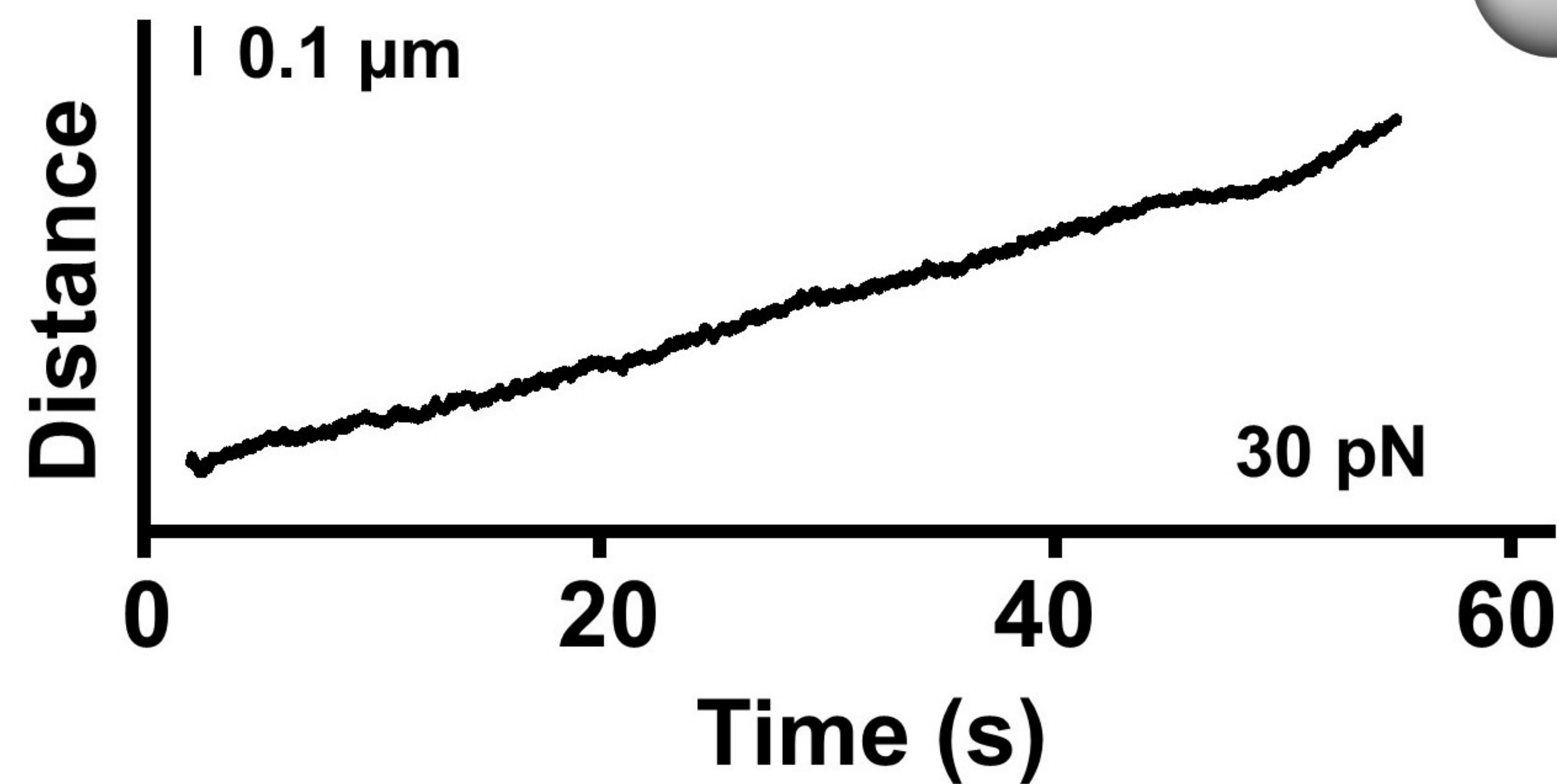
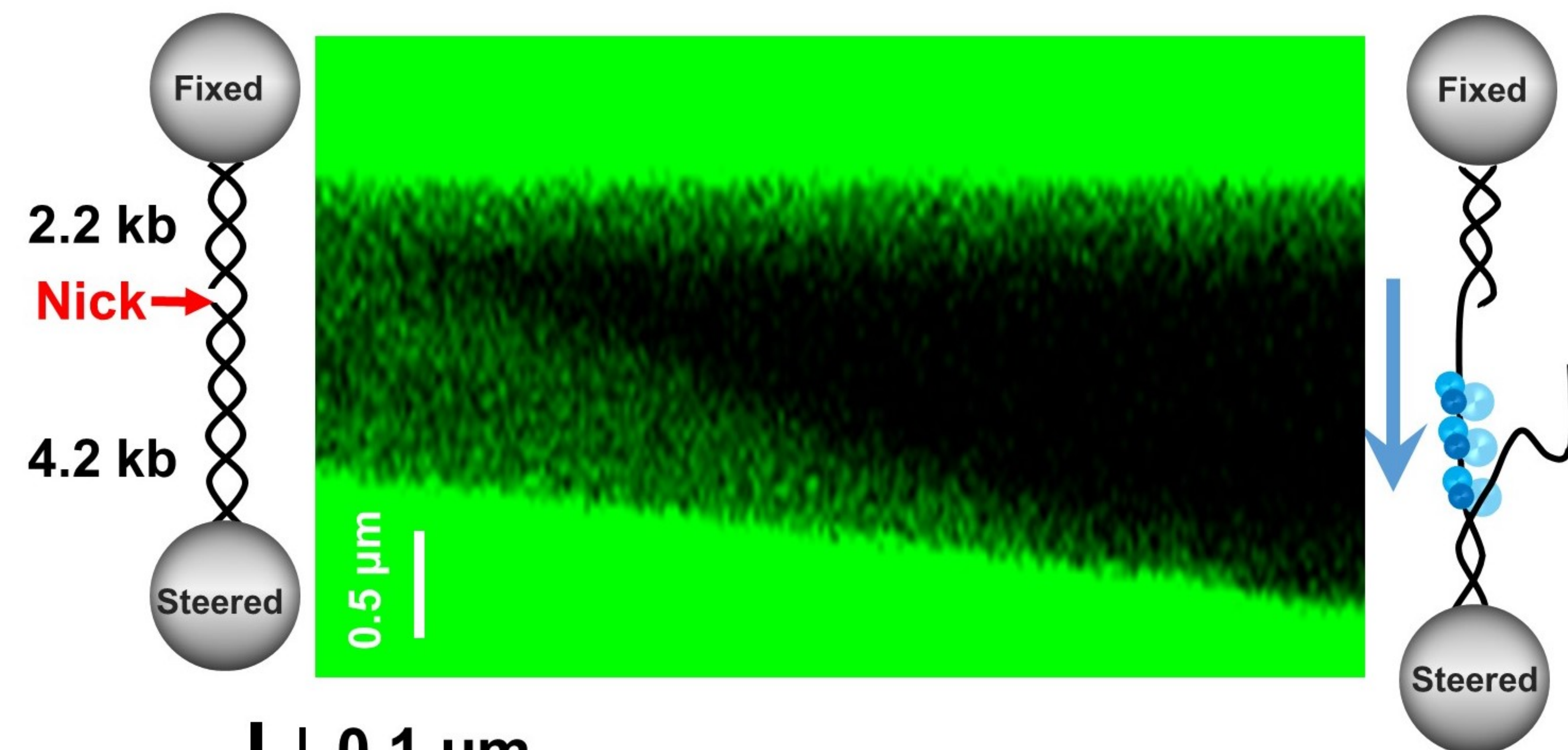
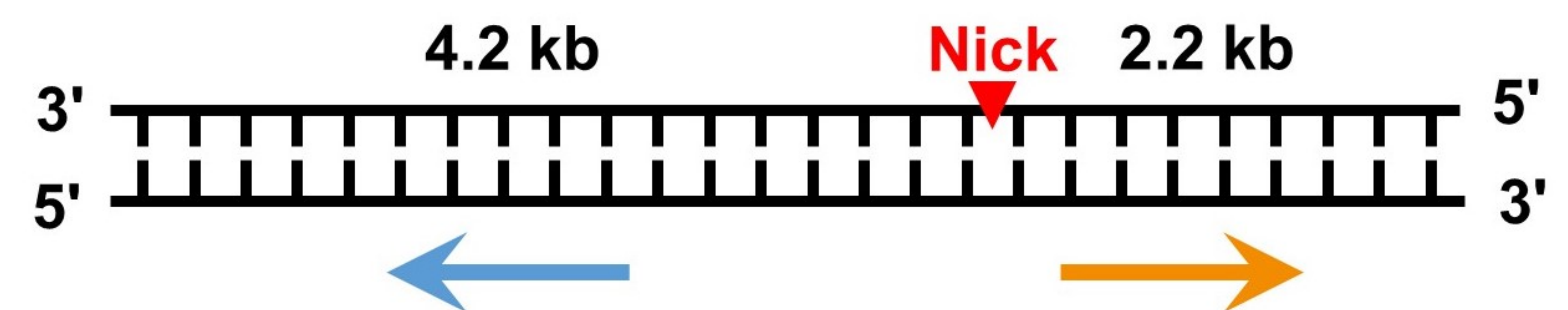
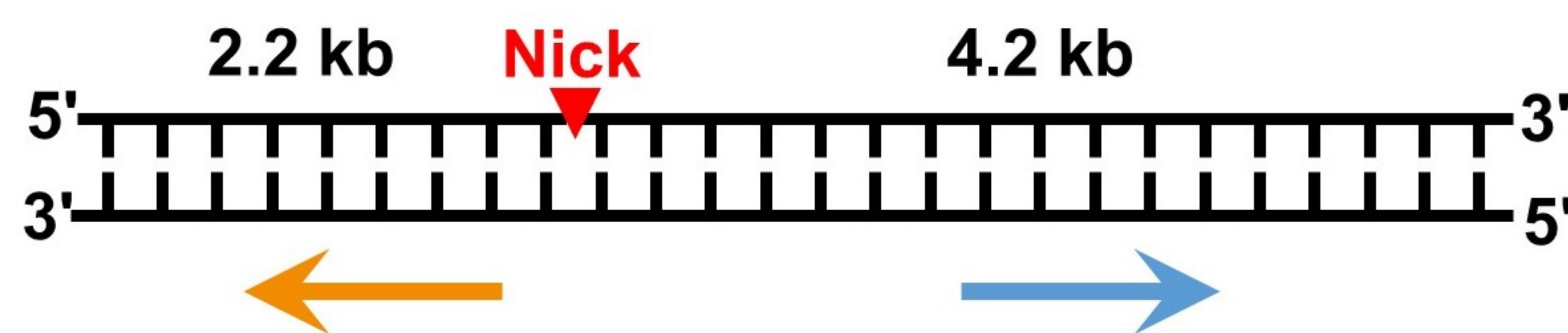
Figure 6-figure supplement 1. The micro-flow cell assay confirmed the observe DNA unwinding requires BLM's unwinding activity. (A) Schematic of the 4-channel micro-flow cell. Two beads were optically trapped in channel 1. A single DNA molecule was caught between the two beads and a DNA tether was formed in channel 2. The DNA molecule was incubated with the studied proteins in channels 3 and 4 and the unwinding activity was monitored. The buffer conditions as well as proteins in channels 3 and 4 were specified in the main text for each experiment. (B) Kymograph and DNA length vs. time trace of DNA tether showing dsDNA unwinding initiating in a channel containing 20 nM BLM and 50 nM RPA under 35 pN, followed by transporting to a channel containing 50 nM RPA and 0 mM ATP. In the following RPA channel, DNA unwinding was immediately terminated for all examined traces (n = 8).

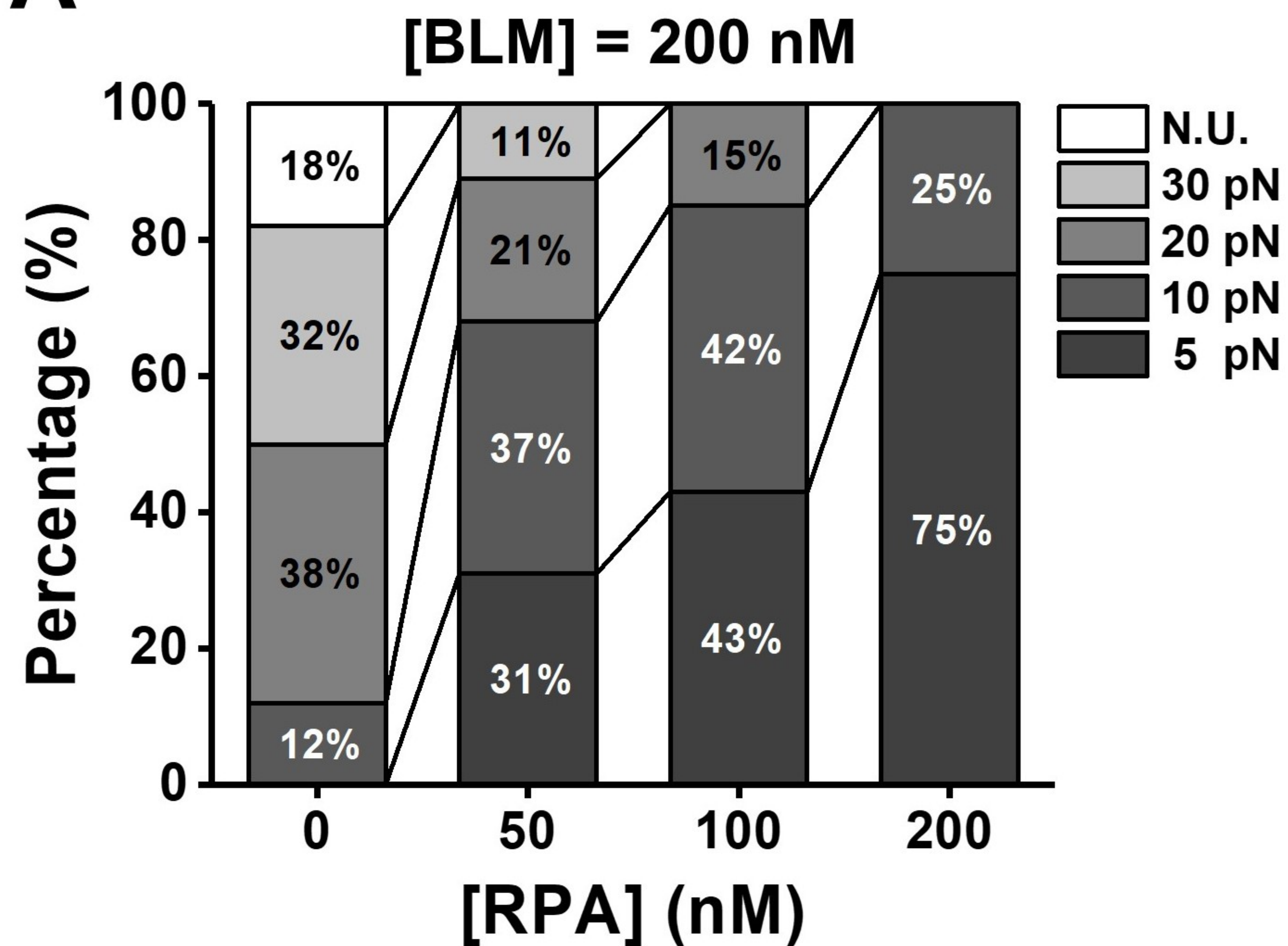
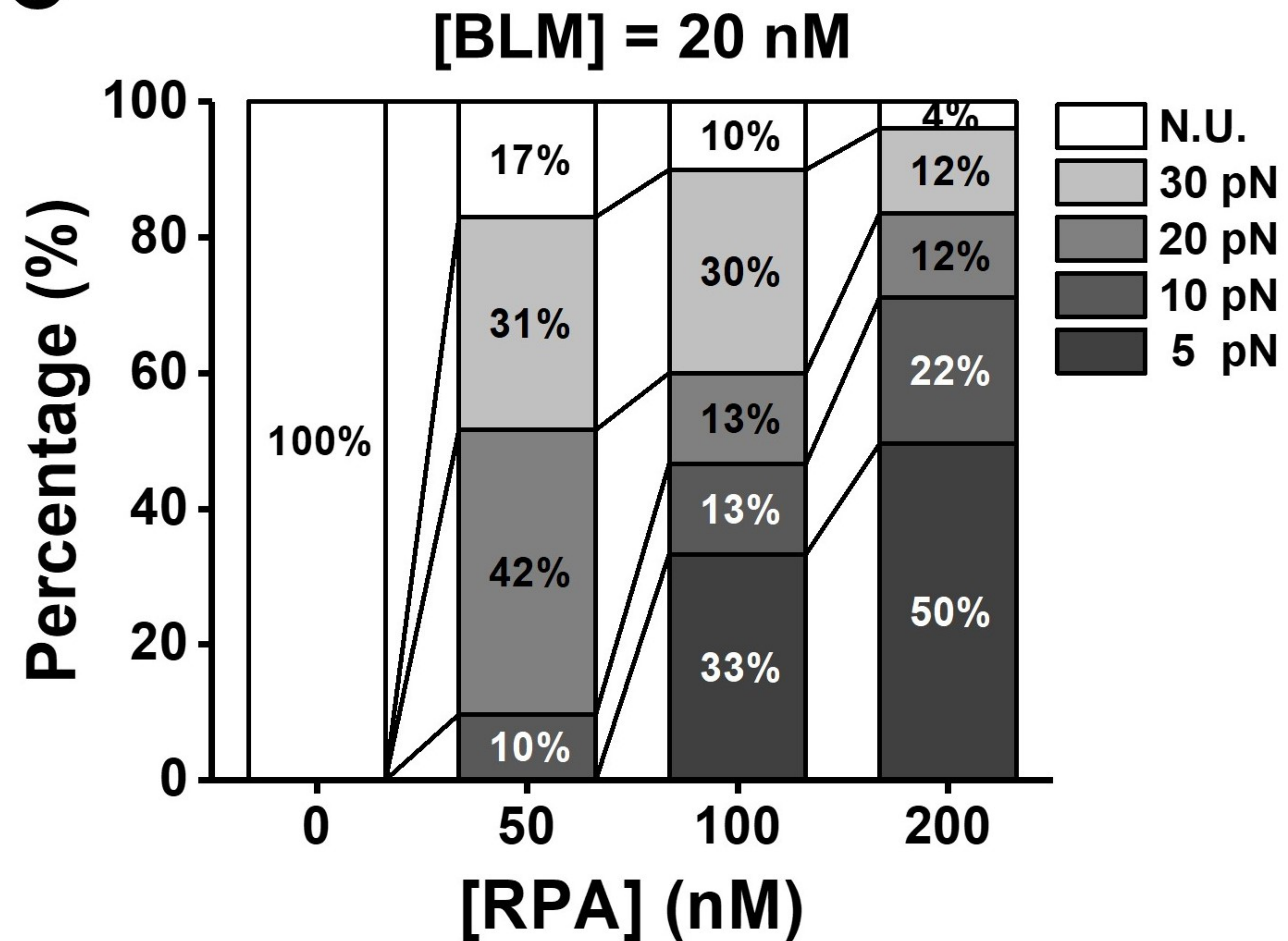
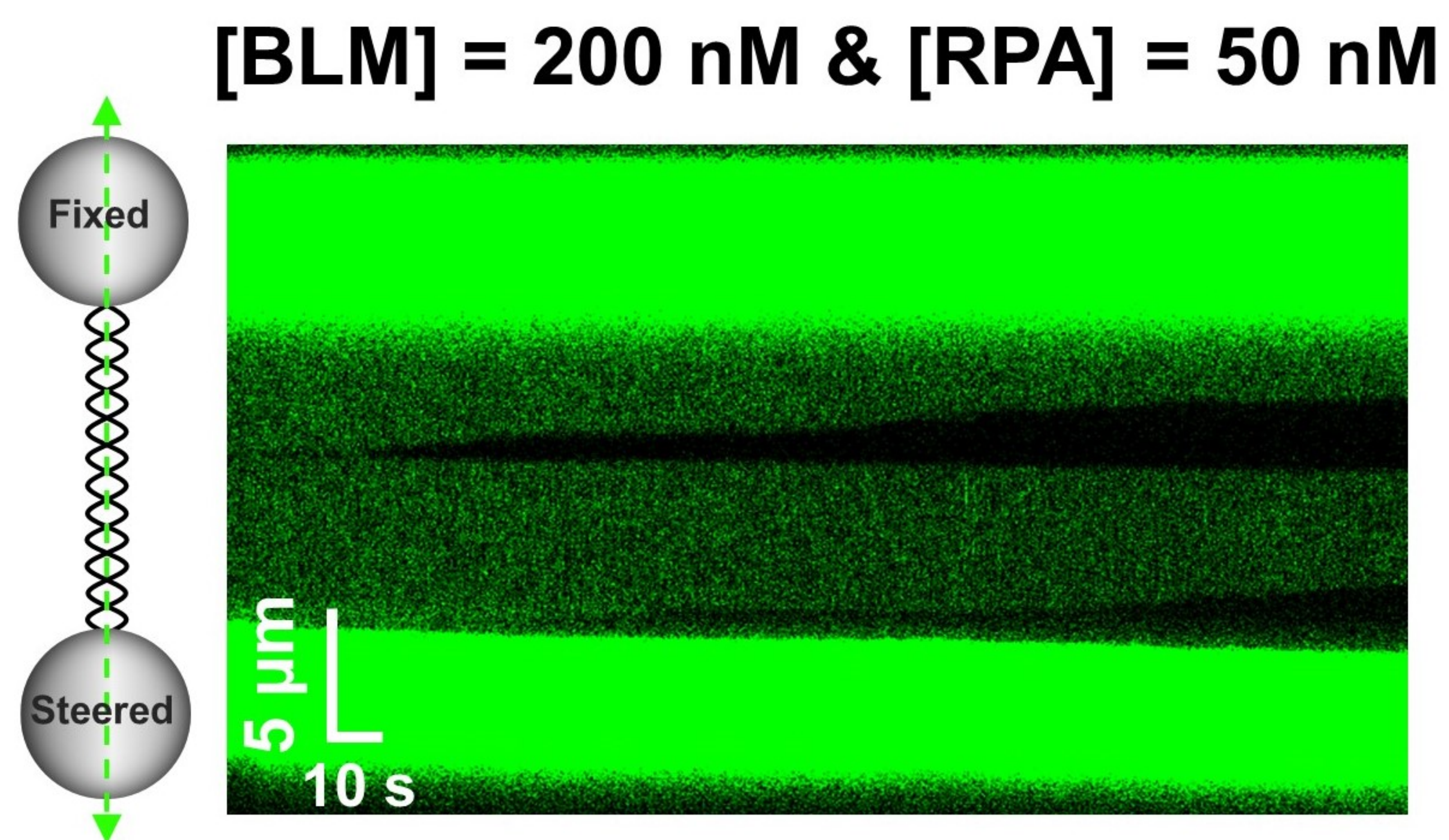
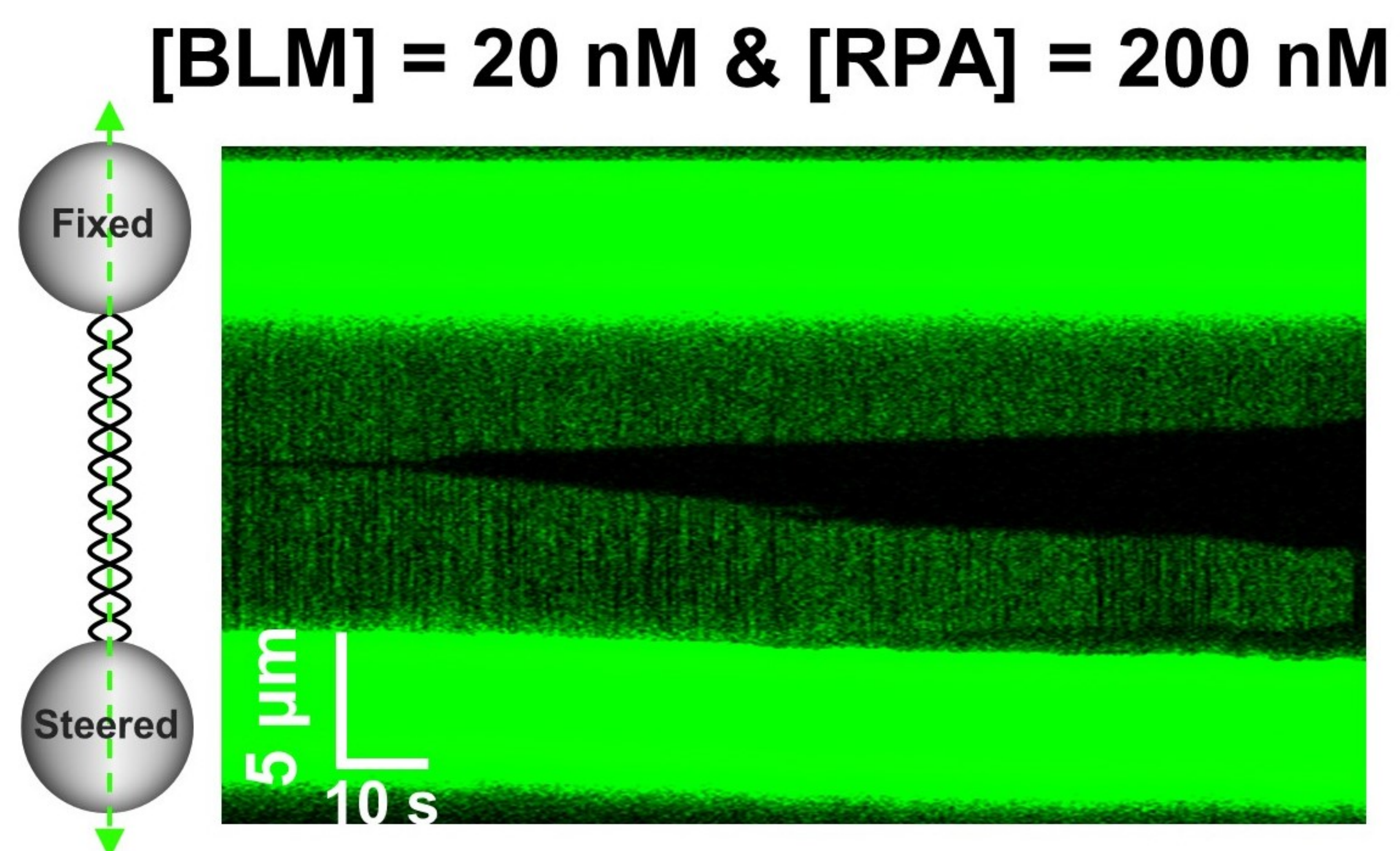
Figure 6-figure supplement 2. RPA cannot recruit BLM to the DNA unwinding fork. To examine whether RPA can recruit WT BLM to the unwinding fork, we conducted the experiments by first placing the tether in the channel containing 50 nM RPA without ATP under 50 pN where RPA spontaneously bound to and denatured dsDNA as indicated by both DNA length and fluorescence signals. After that, we moved the tethered DNA to a channel containing 20 nM BLM and 50 nM RPA and reduced the force to 35 pN. In this channel, up to 83% of the unwinding events showed no DNA unwinding (n = 33).

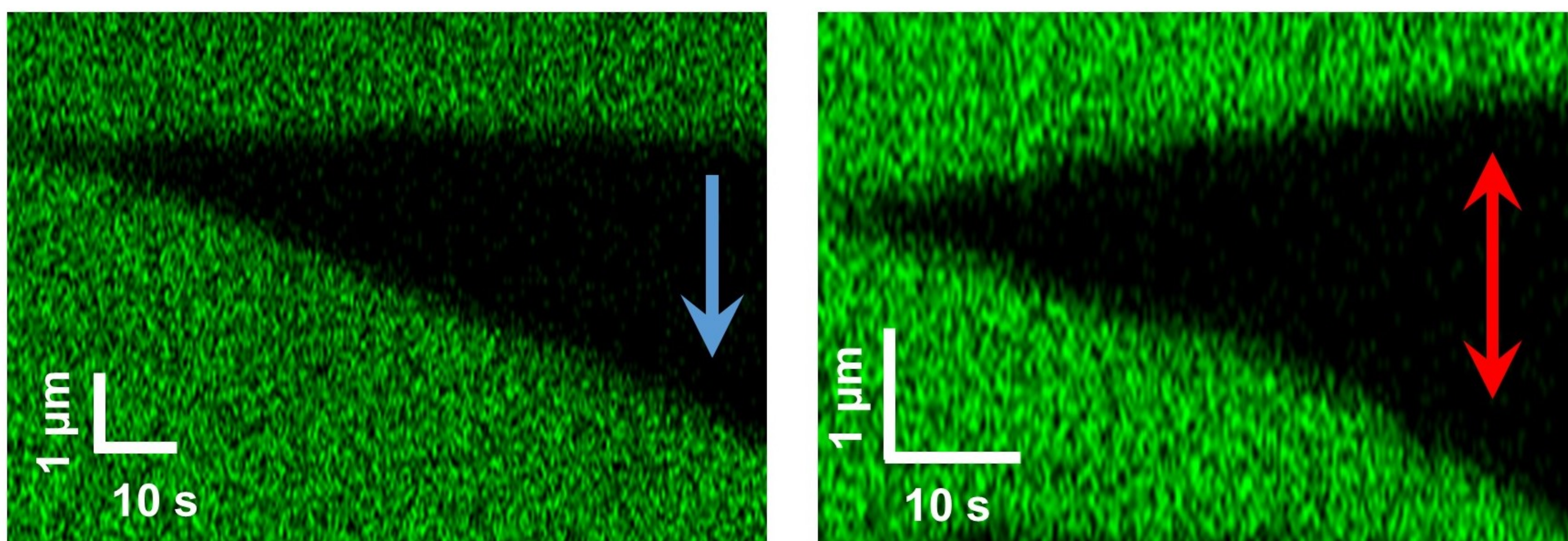
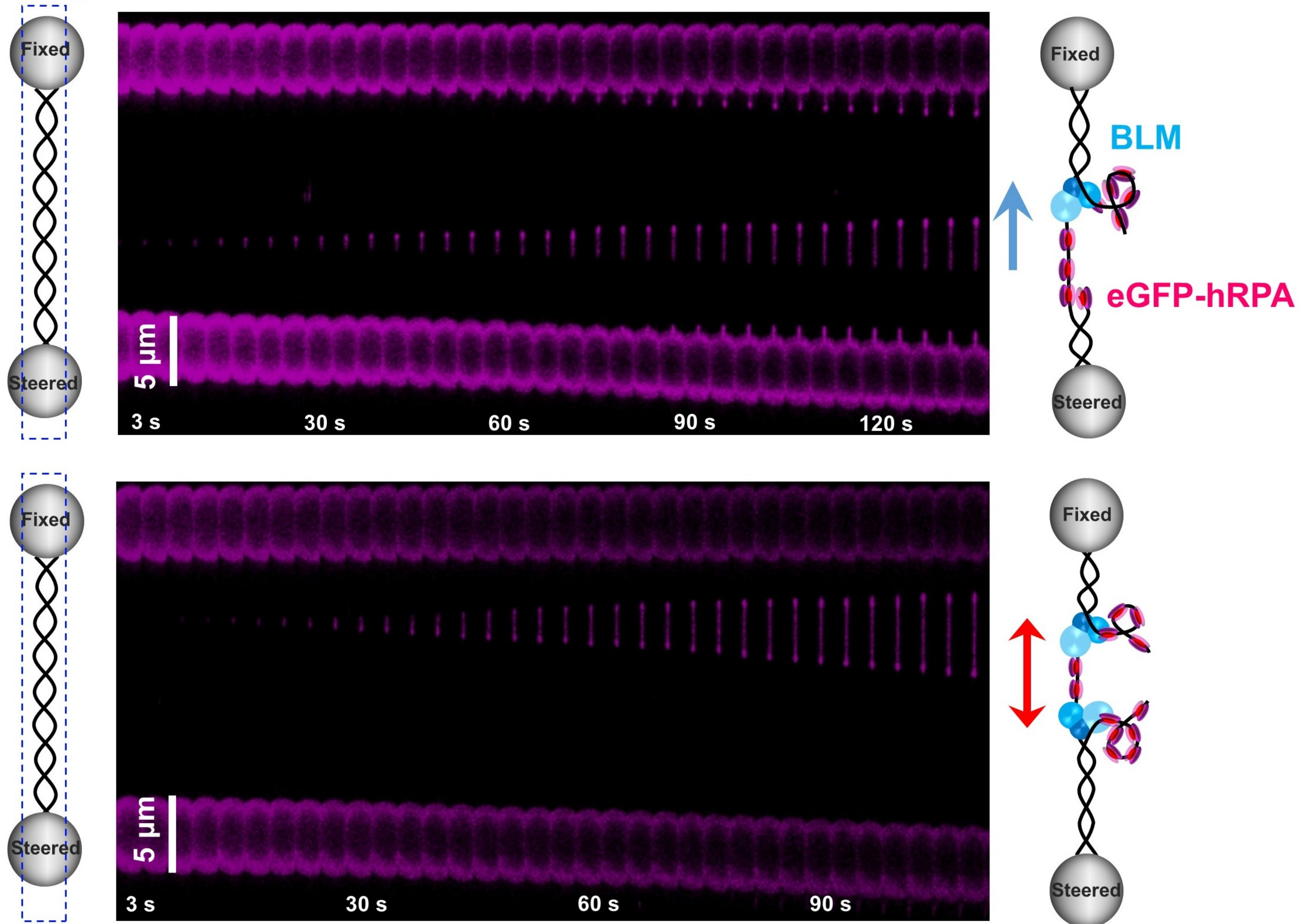
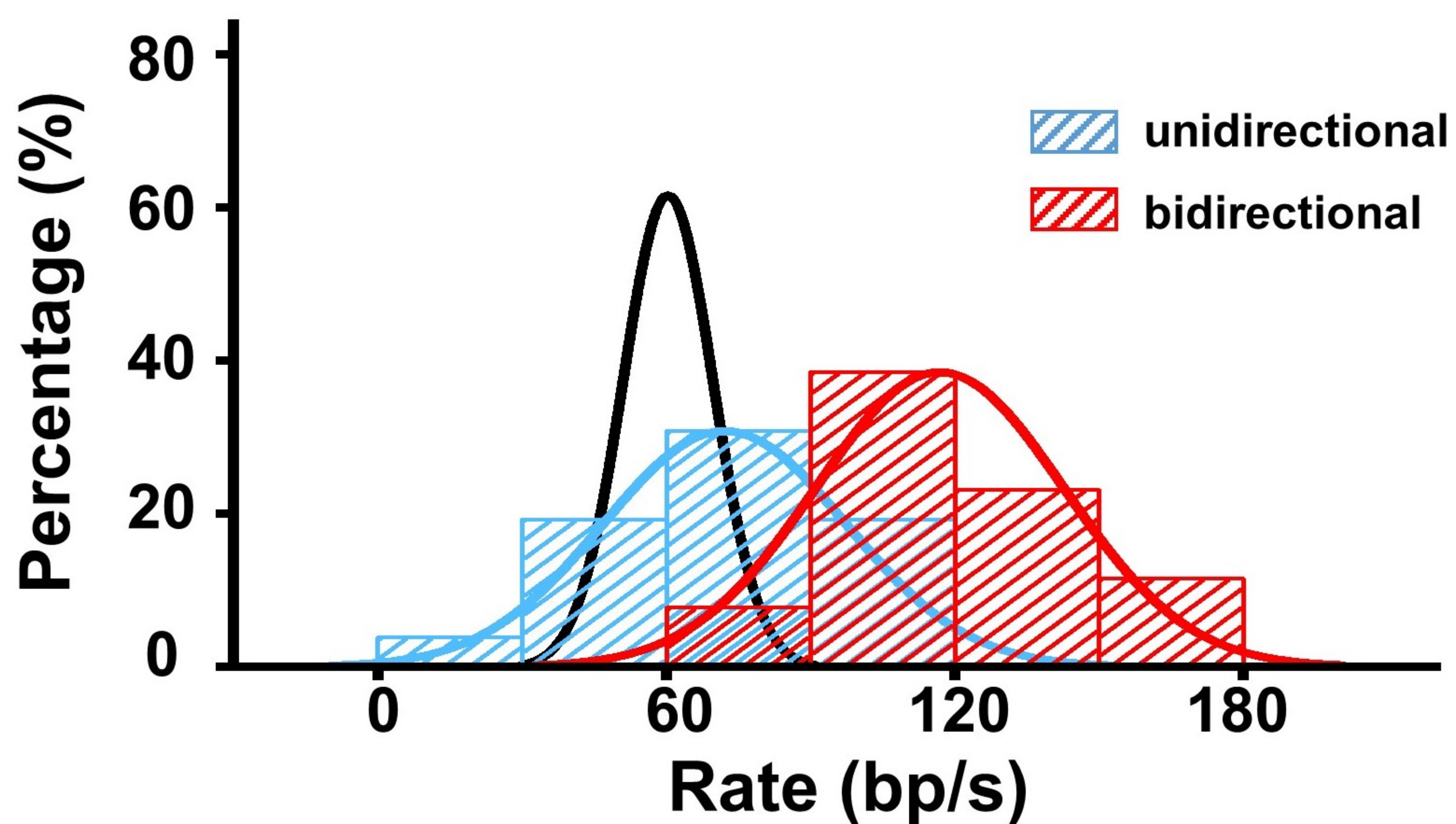
A**B****C****D****E**

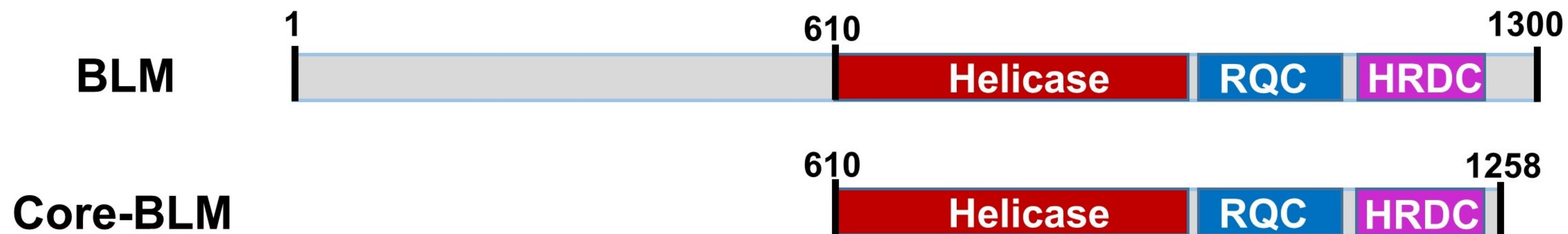
A**BLMs on relaxed ssDNA****BLMs on tensioned ssDNA**

or

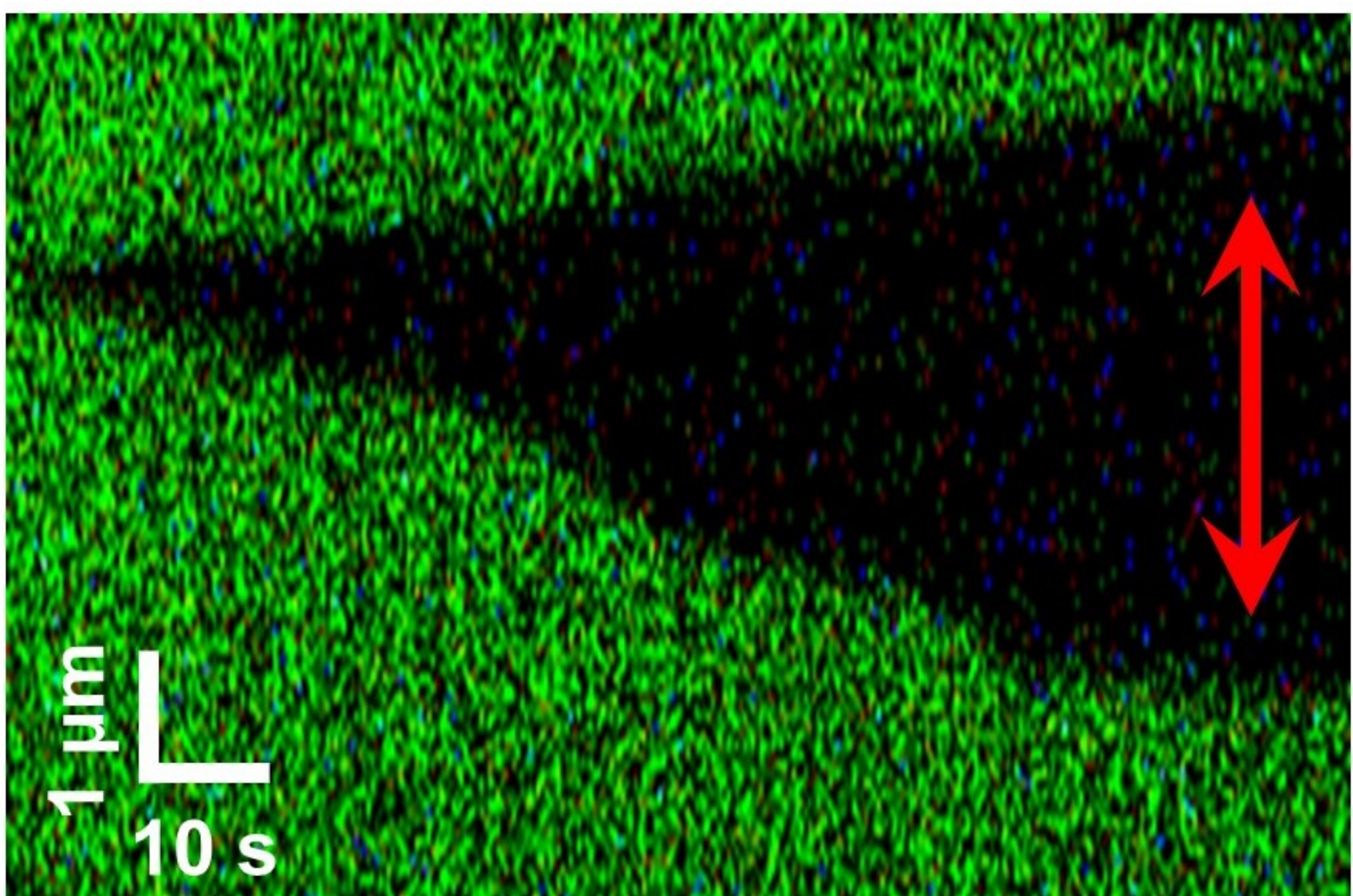
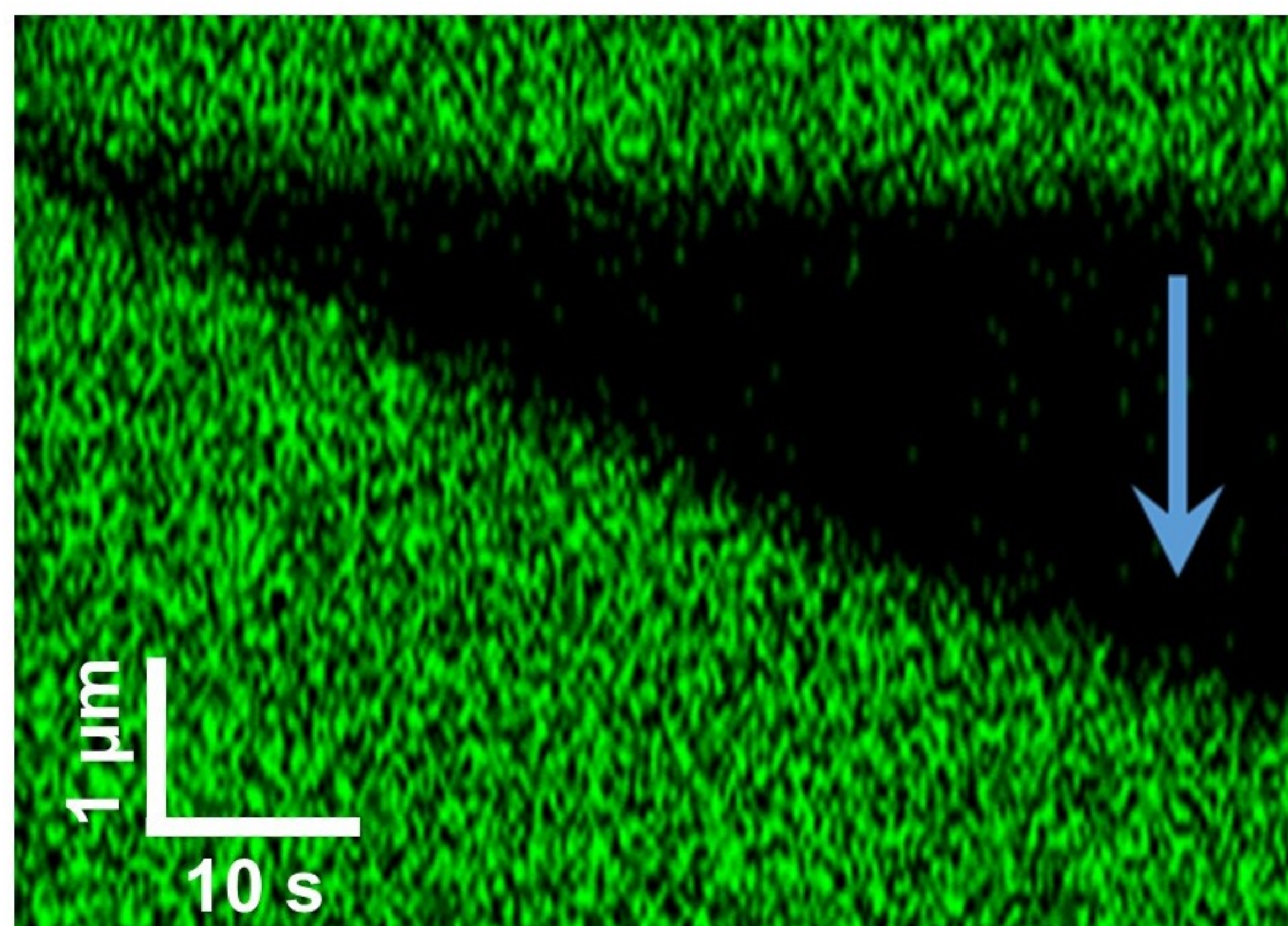
B

A**C****B****D**

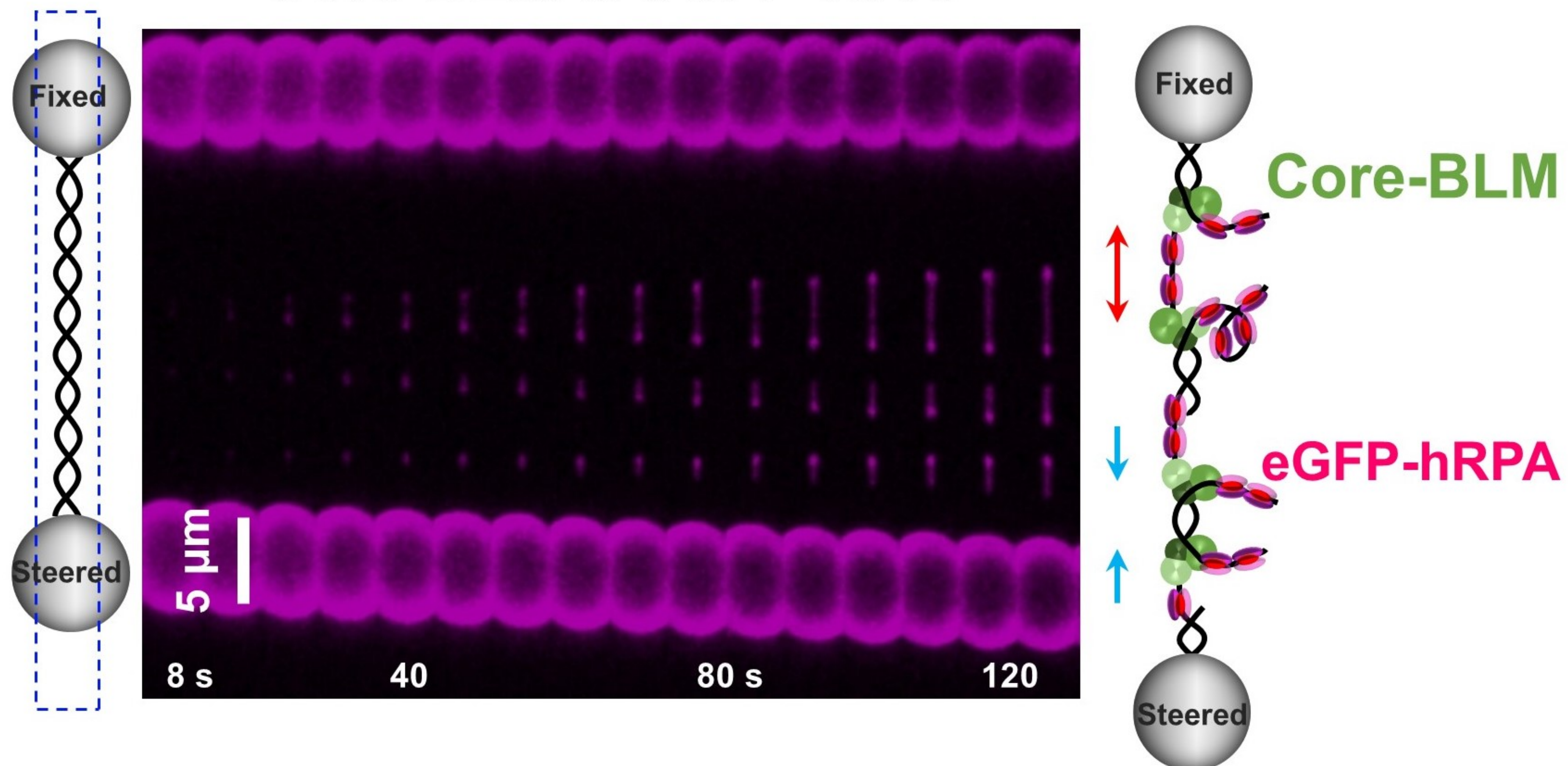
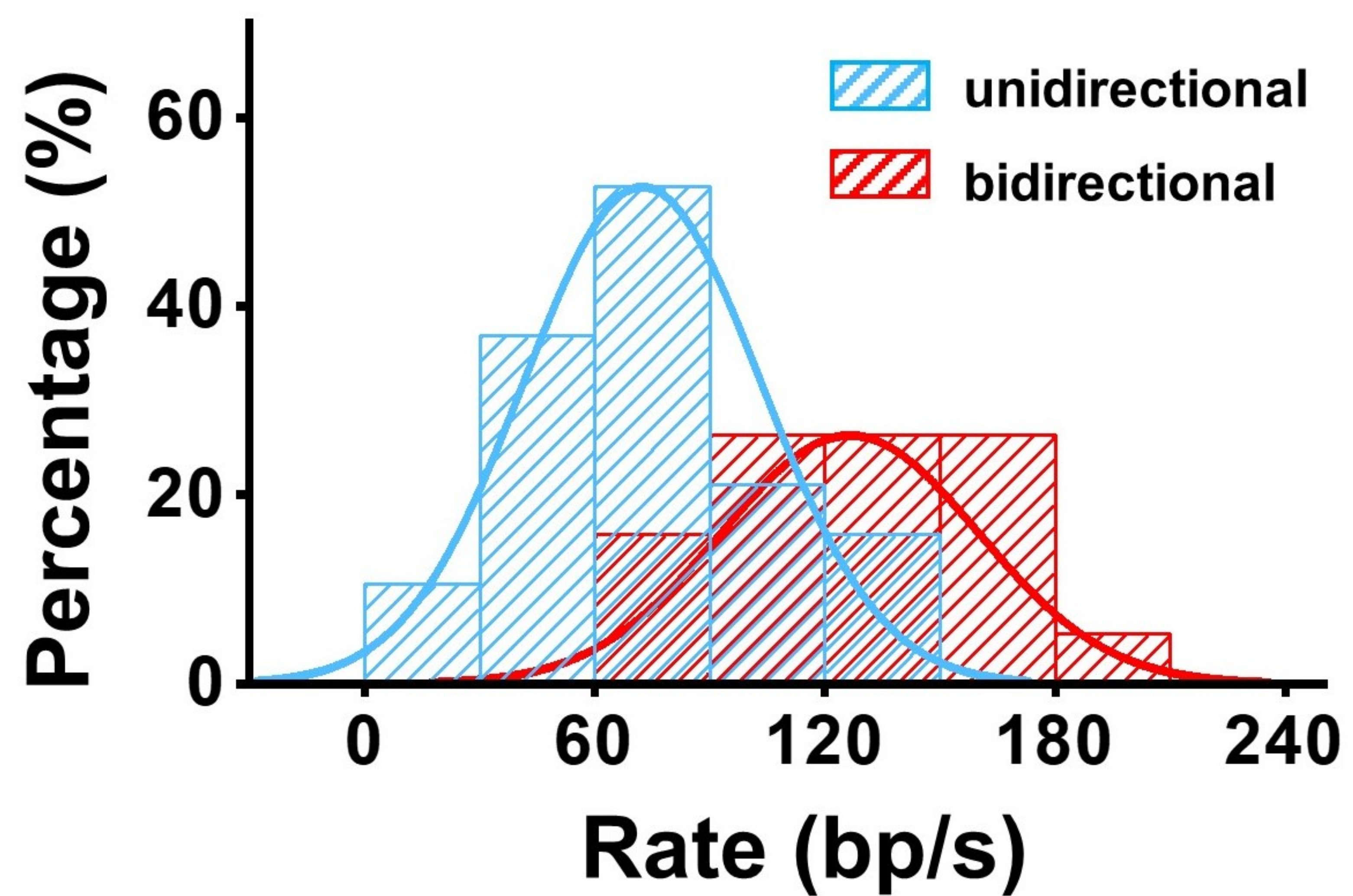
A**B****Scanning area****C**

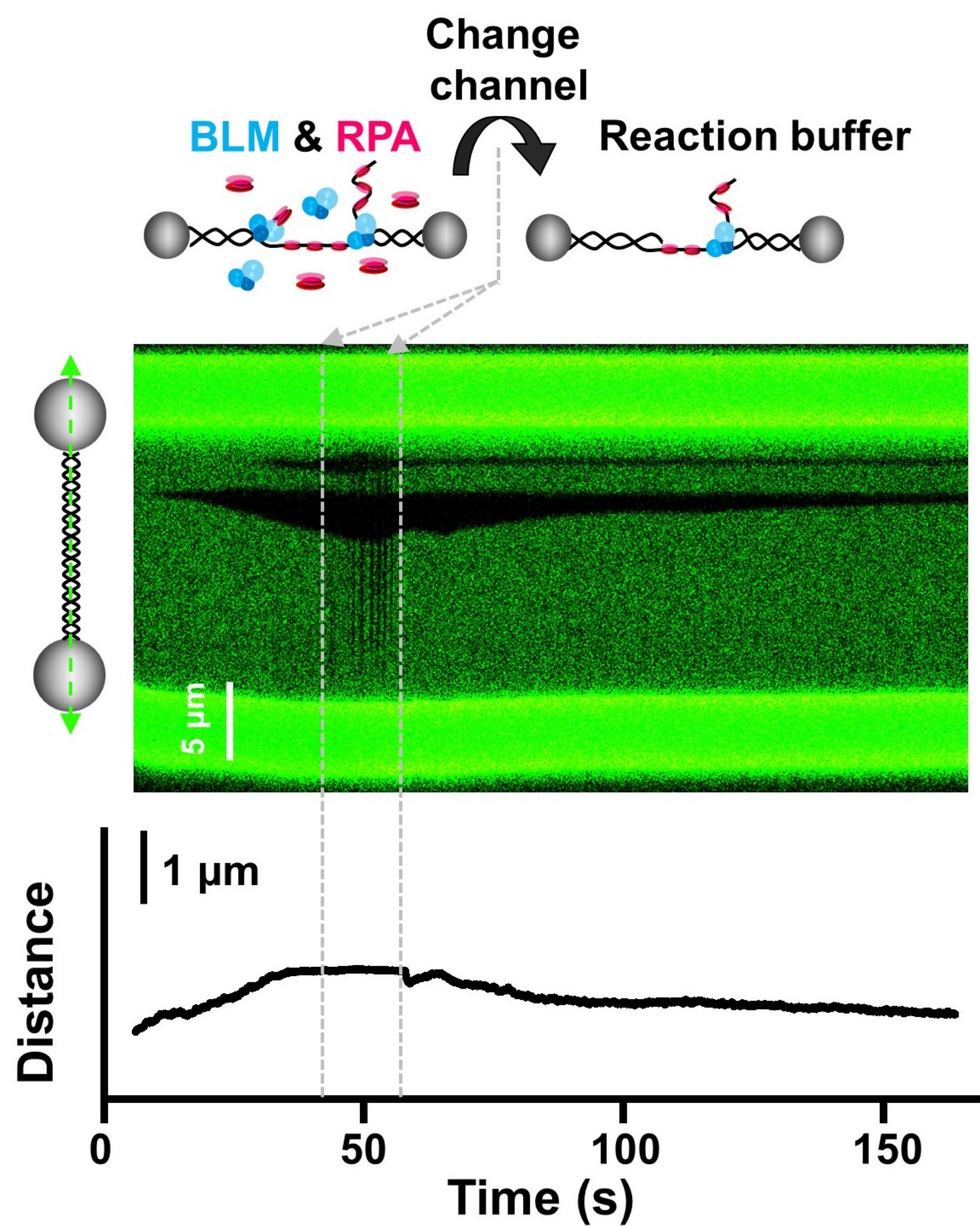
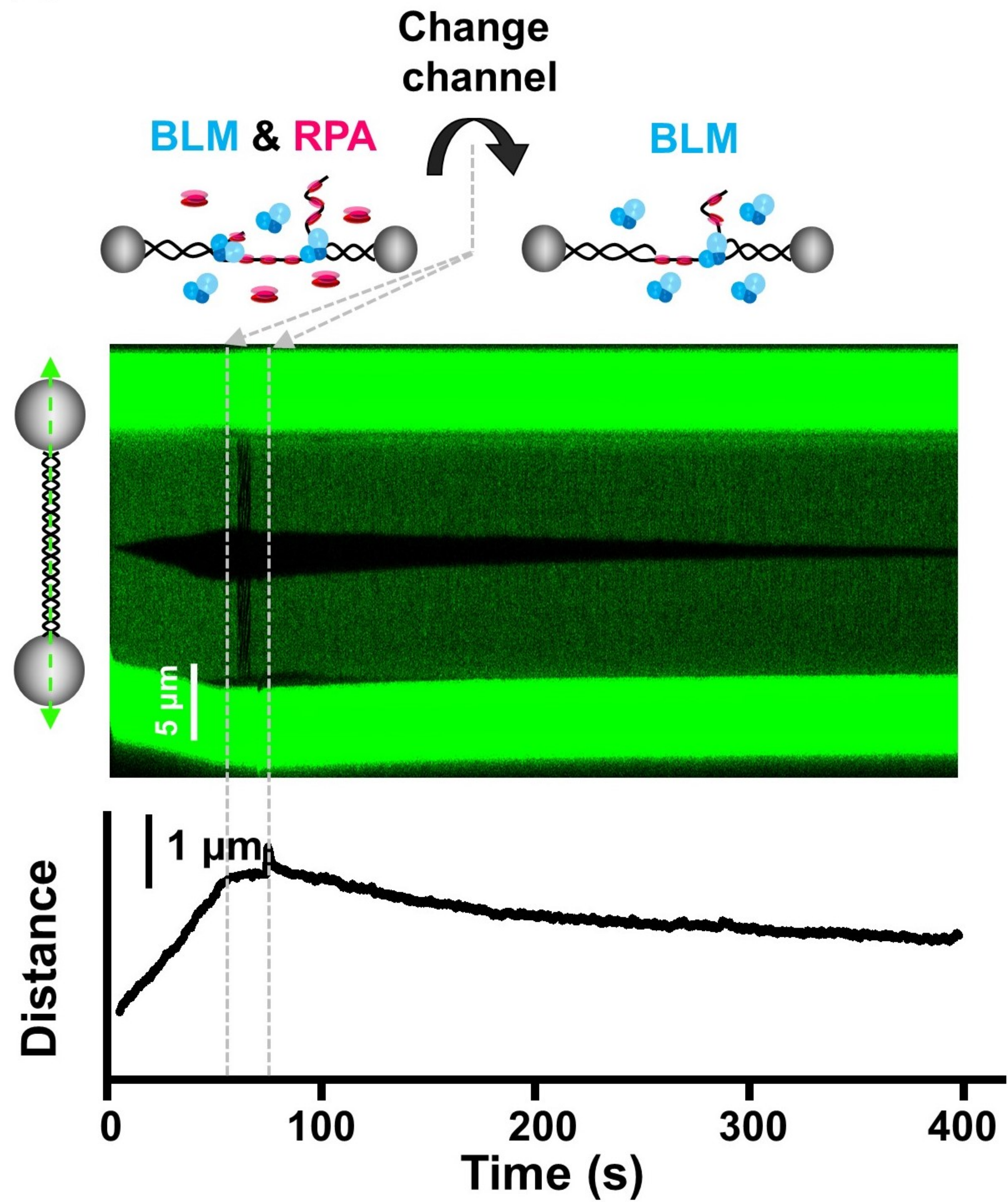
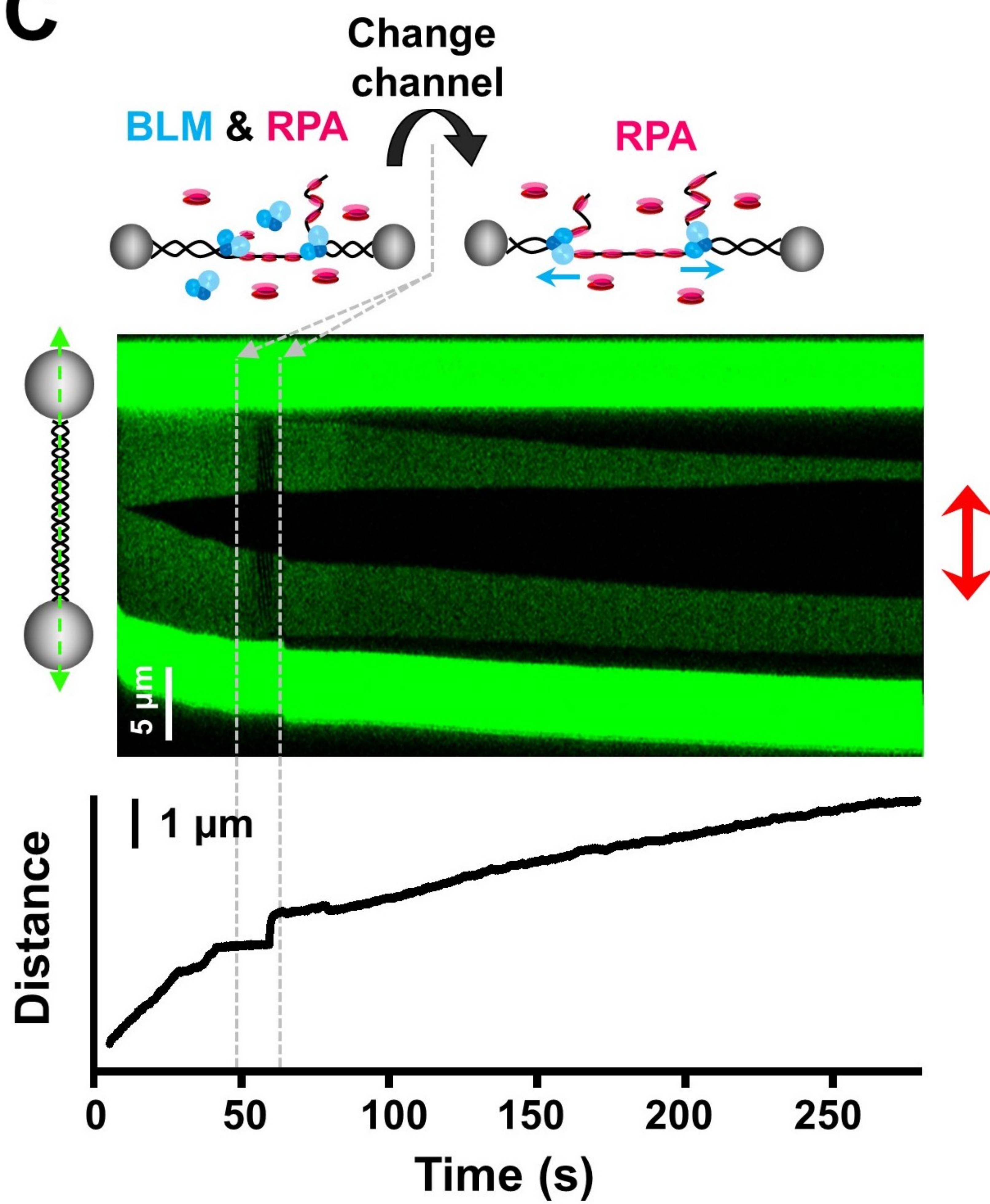
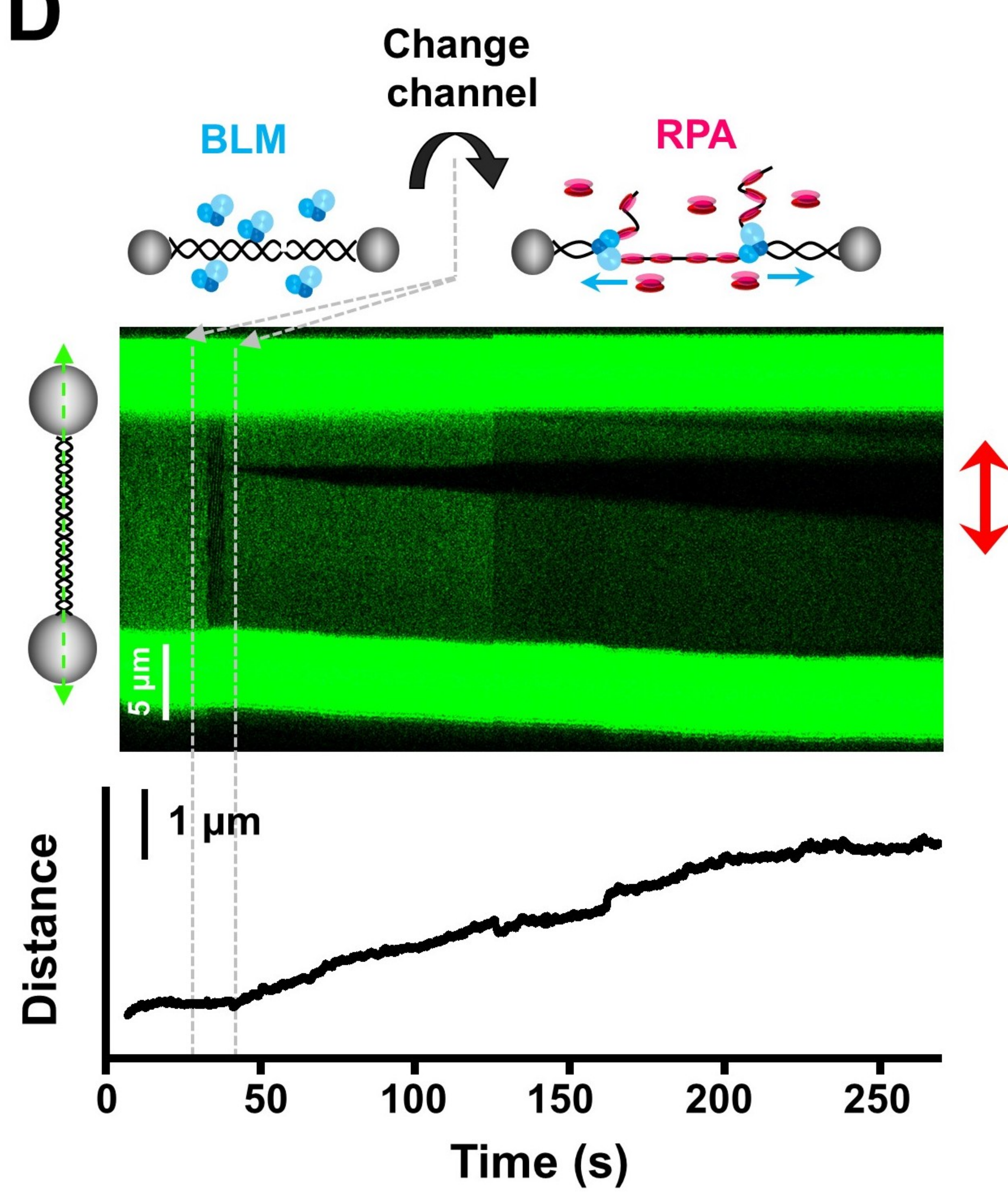
A**B**

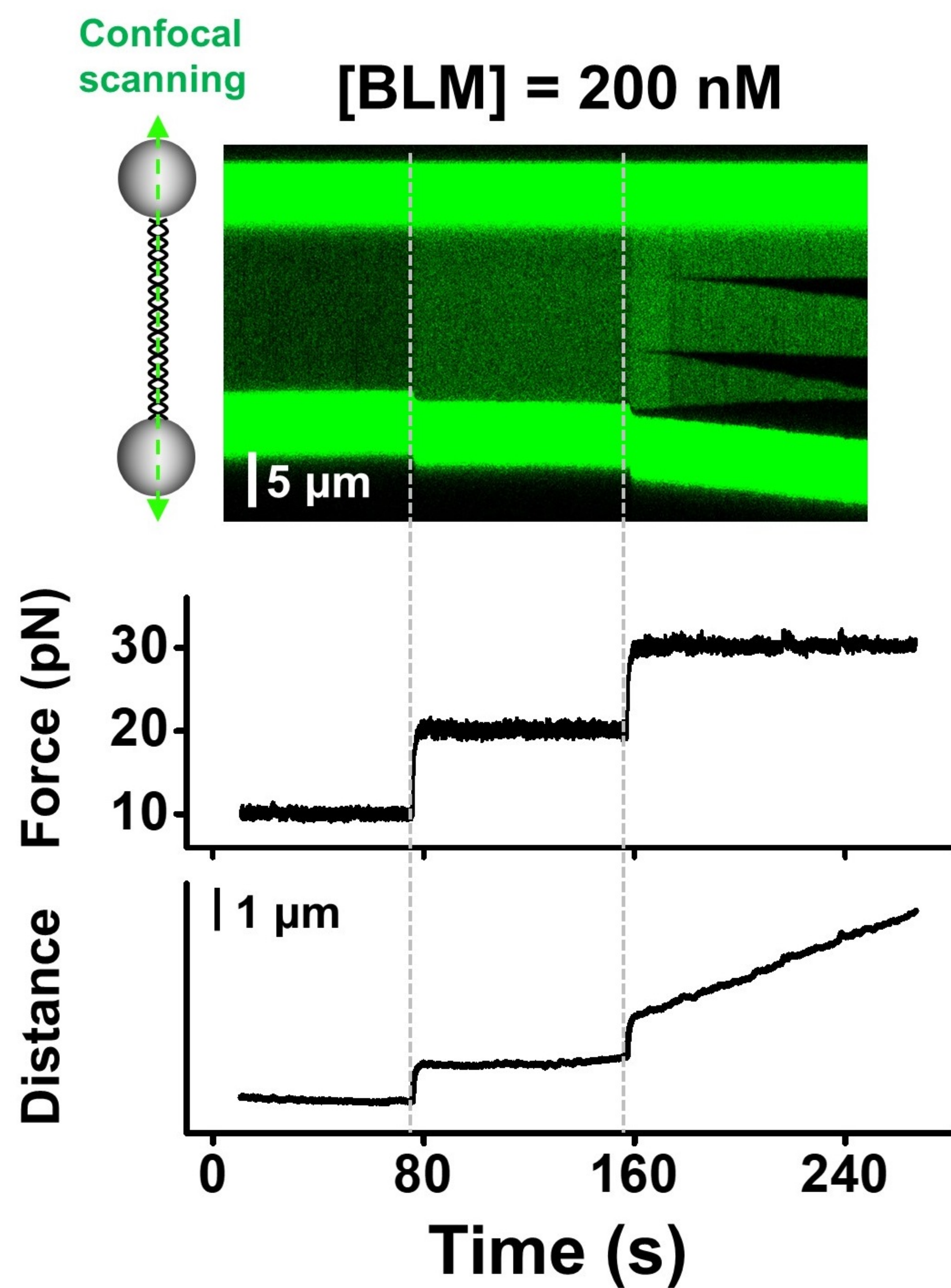
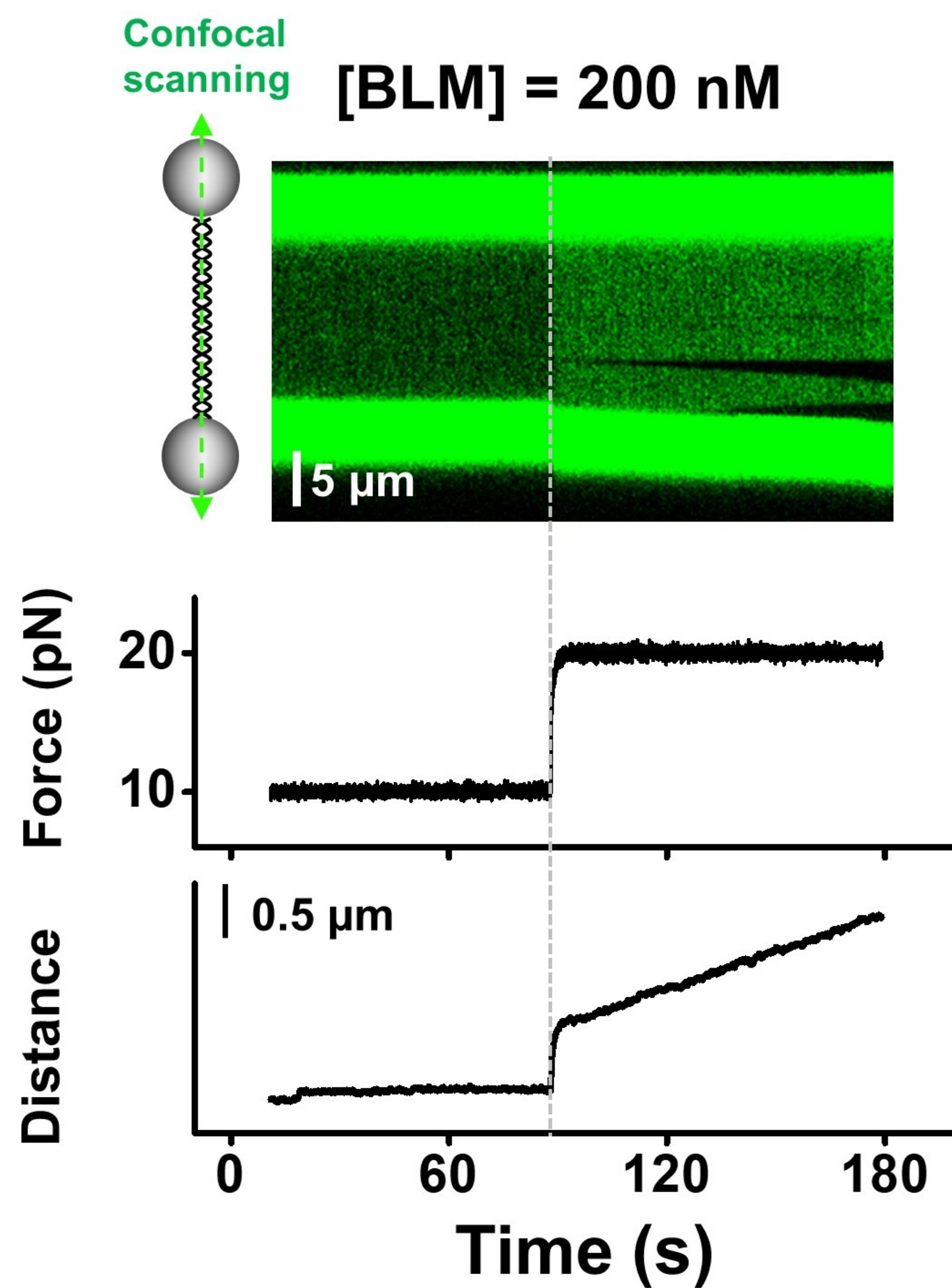
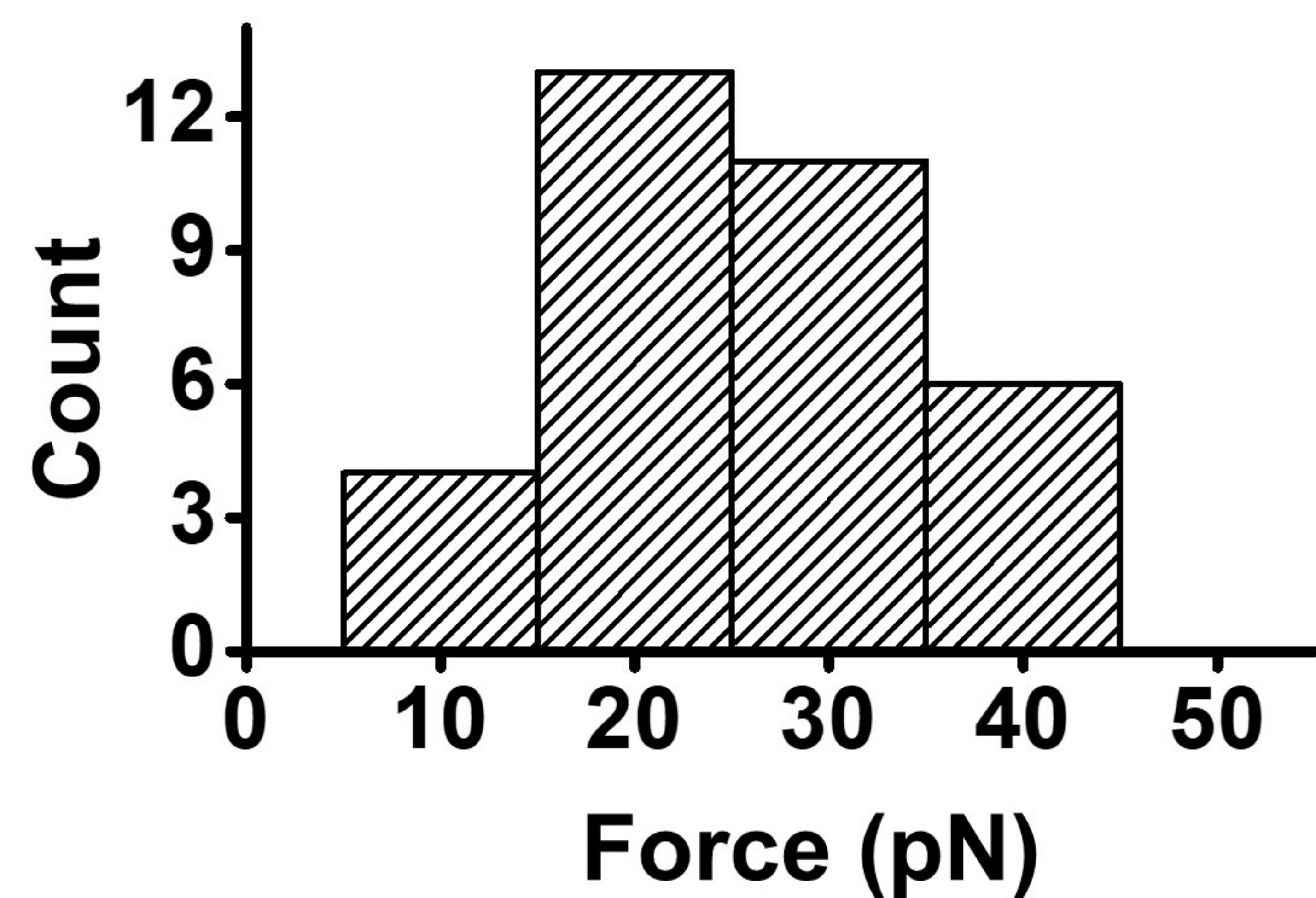
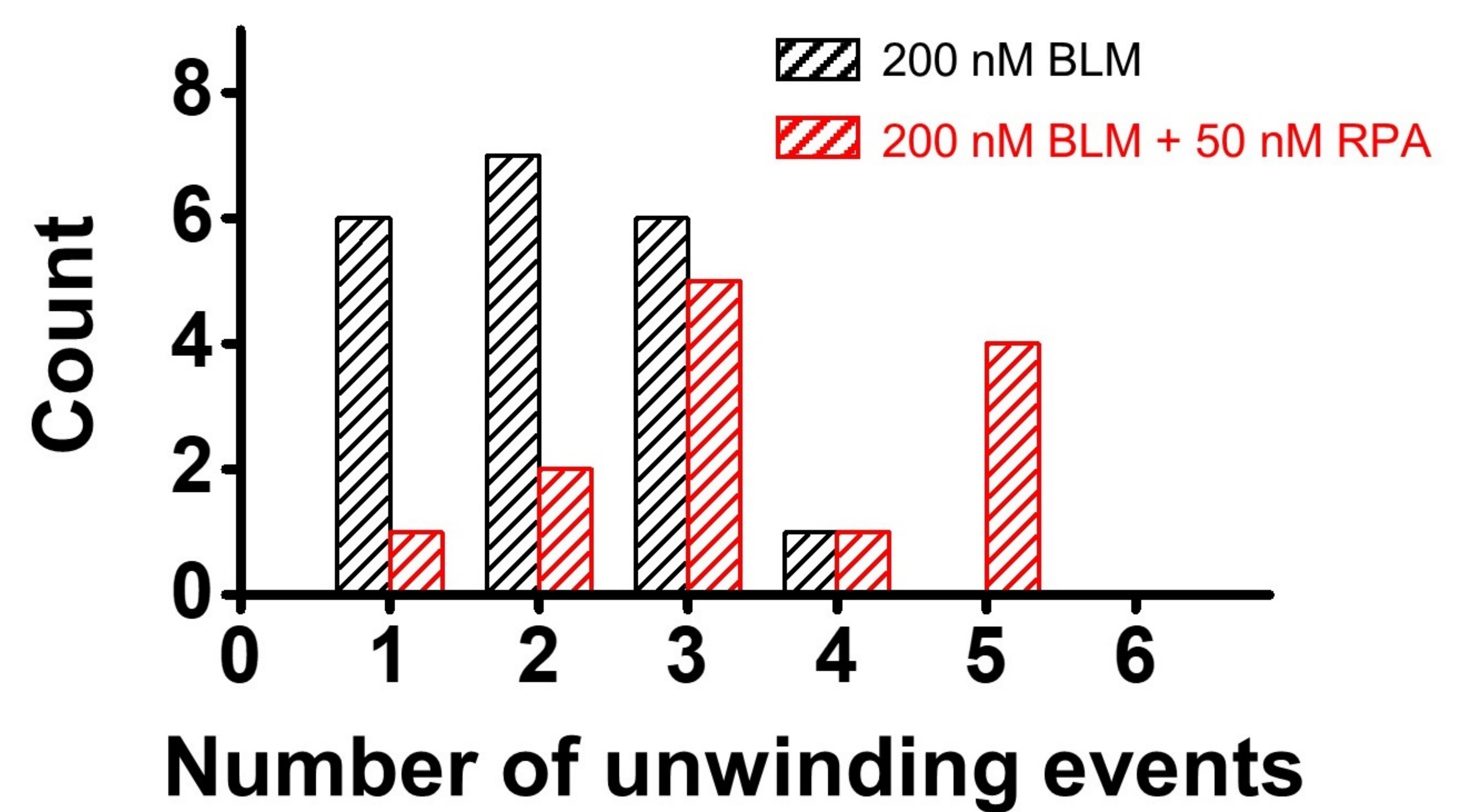
Core-BLM & RPA

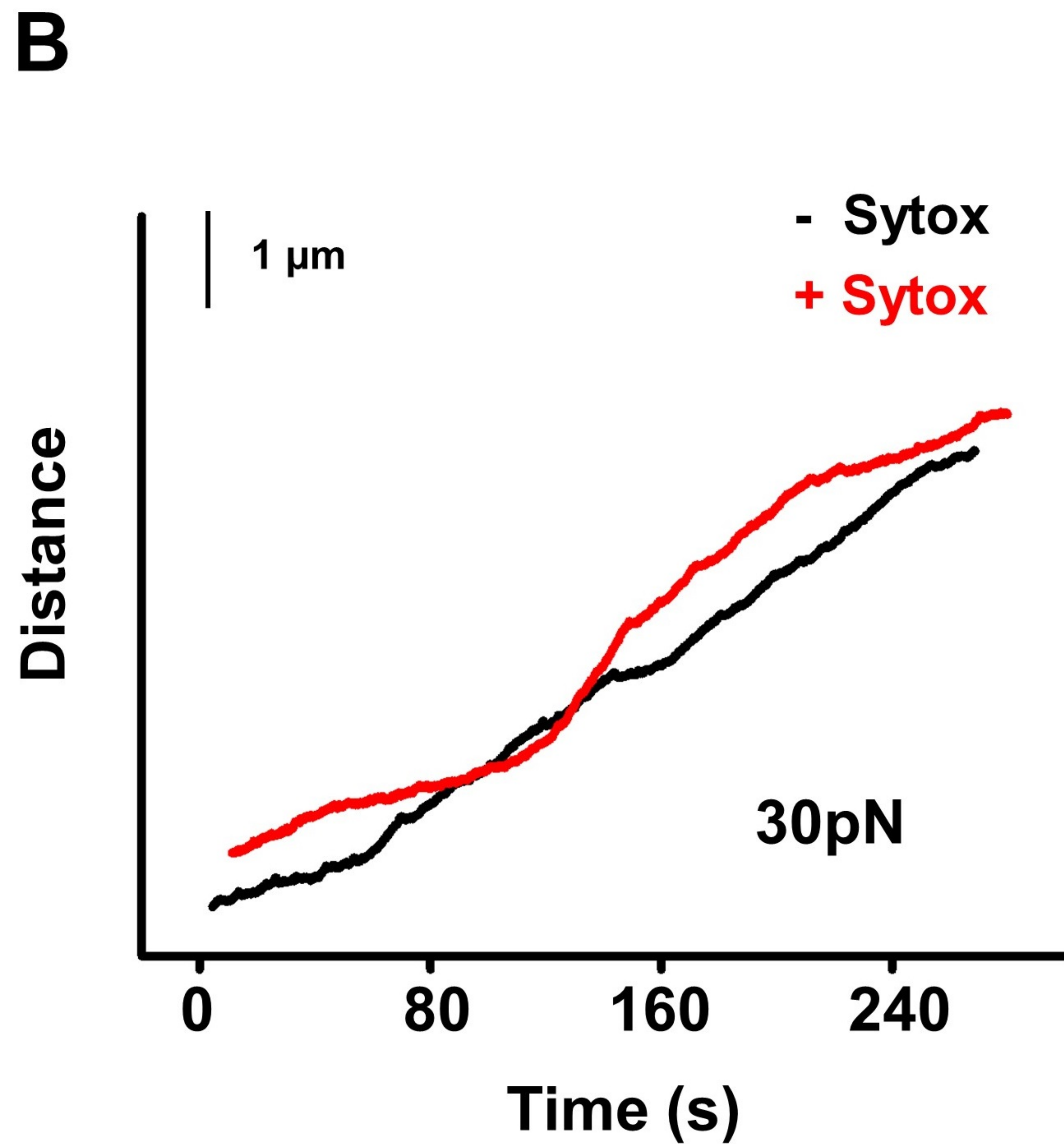
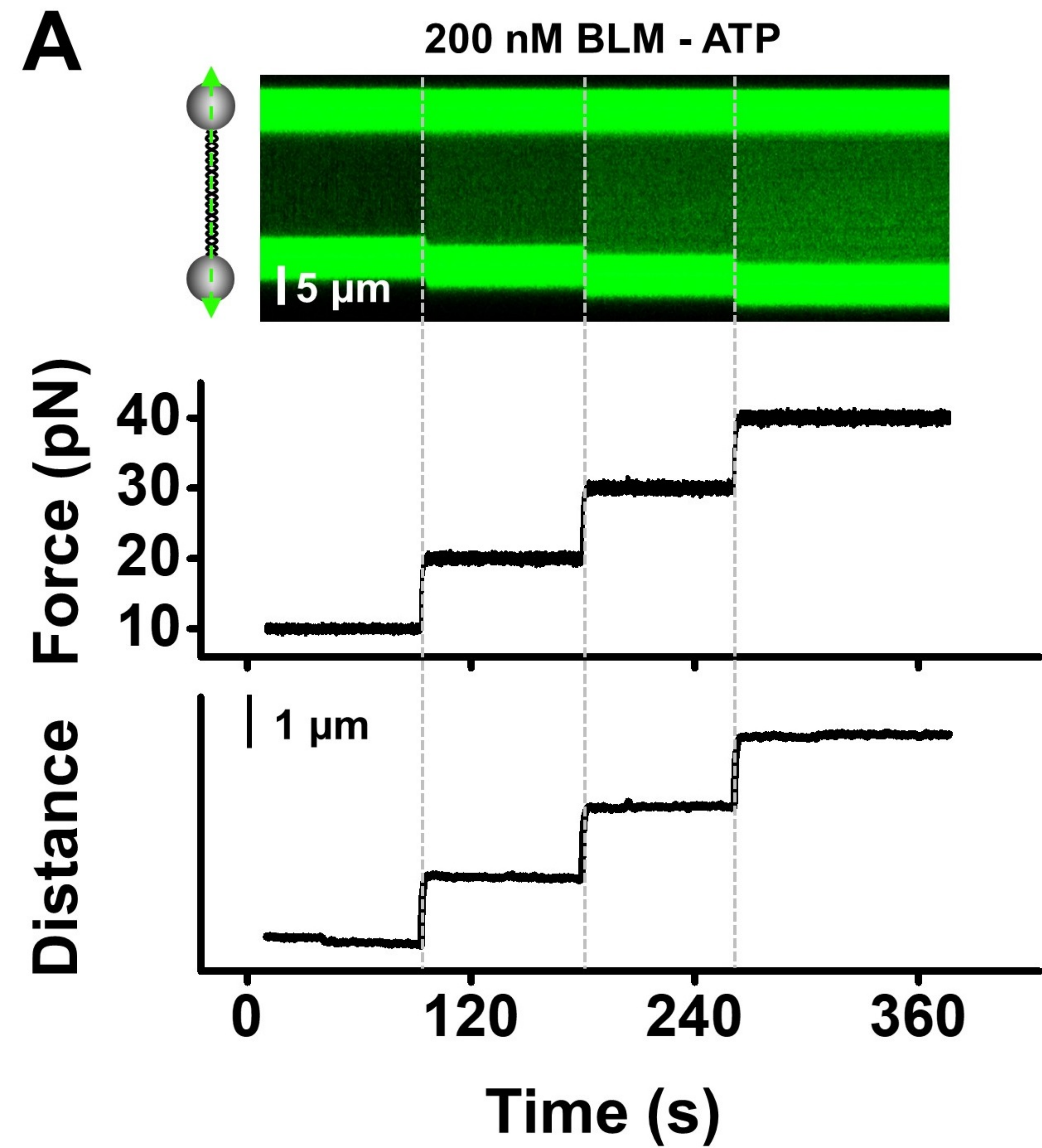
**C**

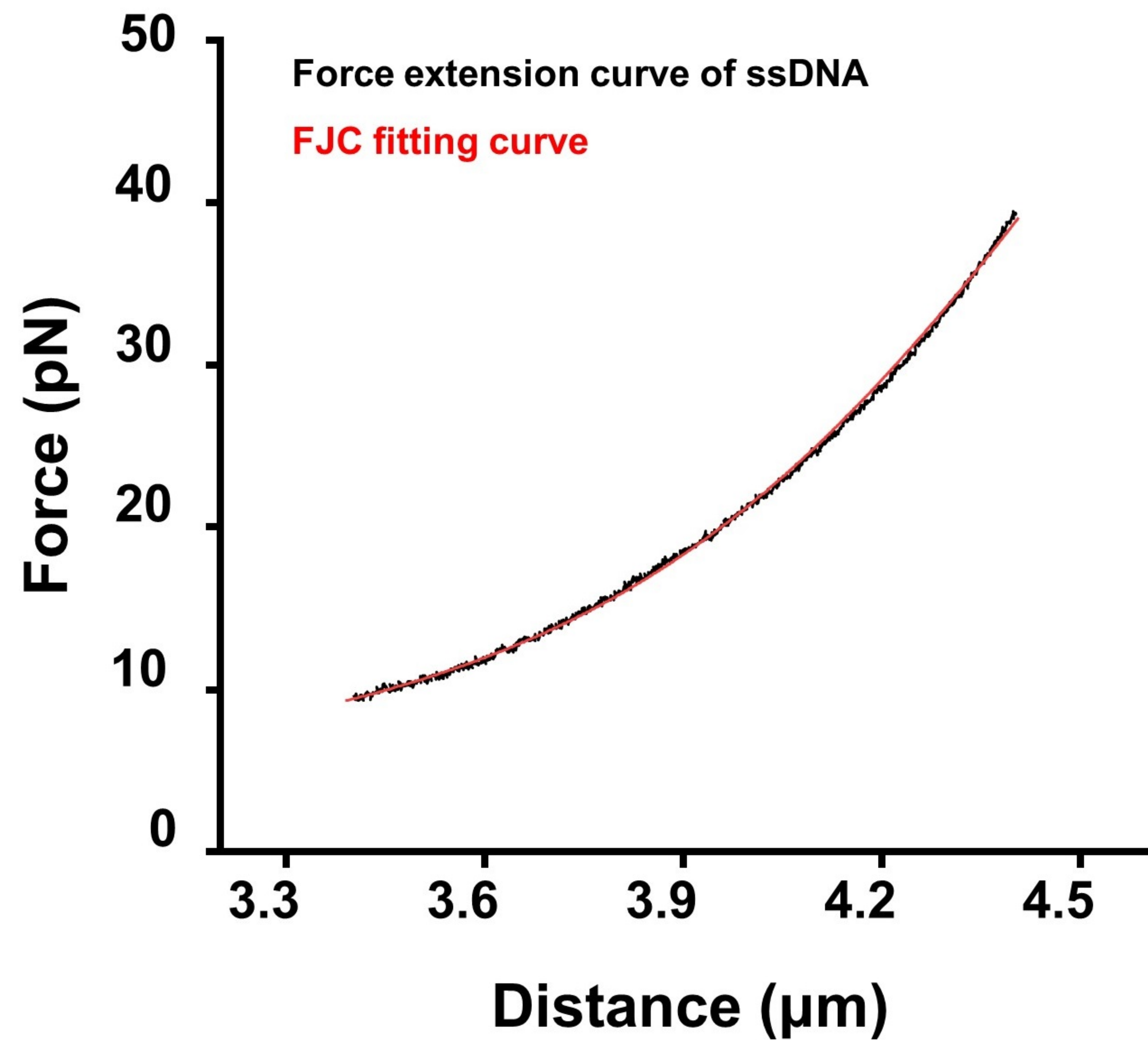
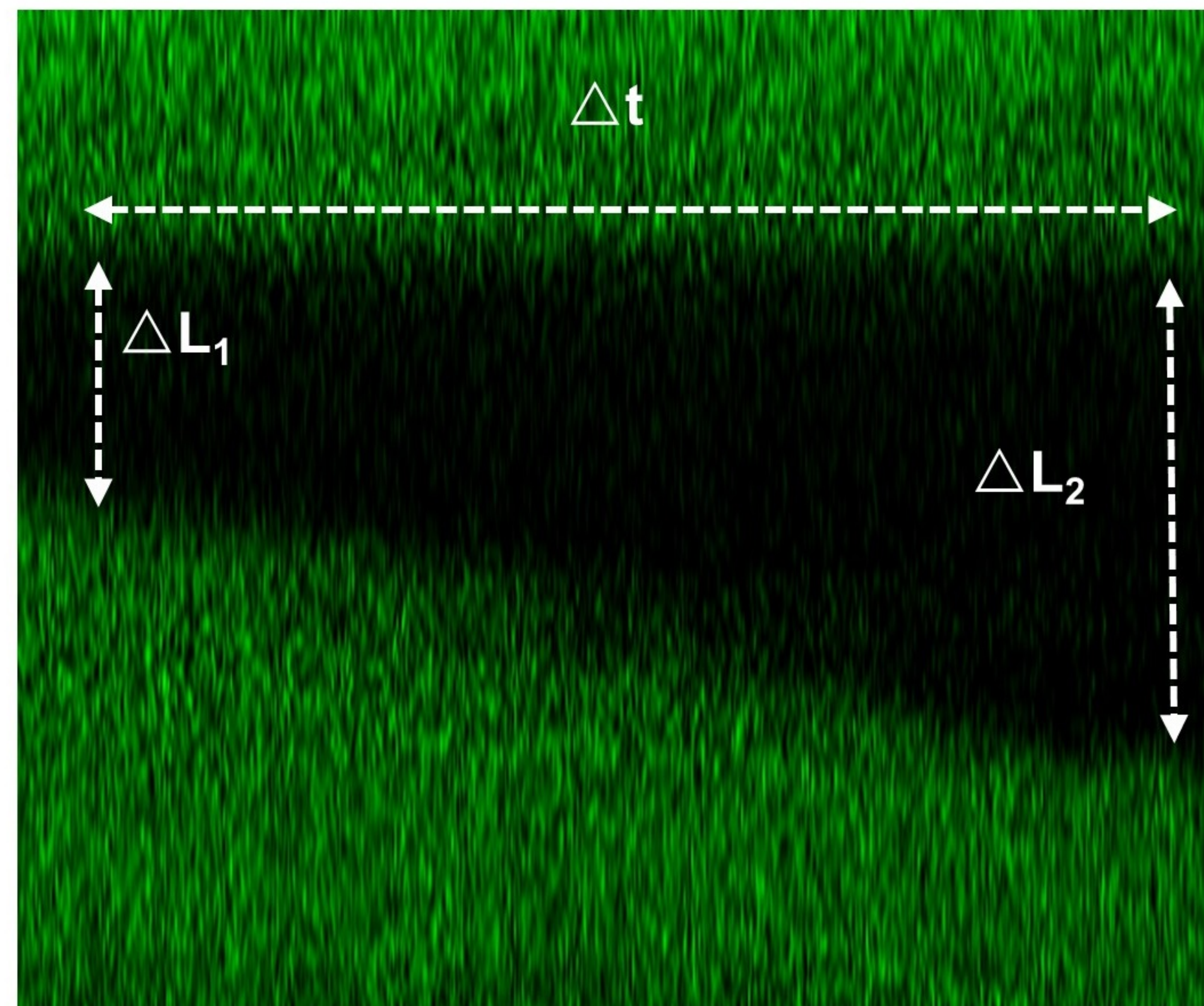
Core-BLM & eGFP-RPA

**D**

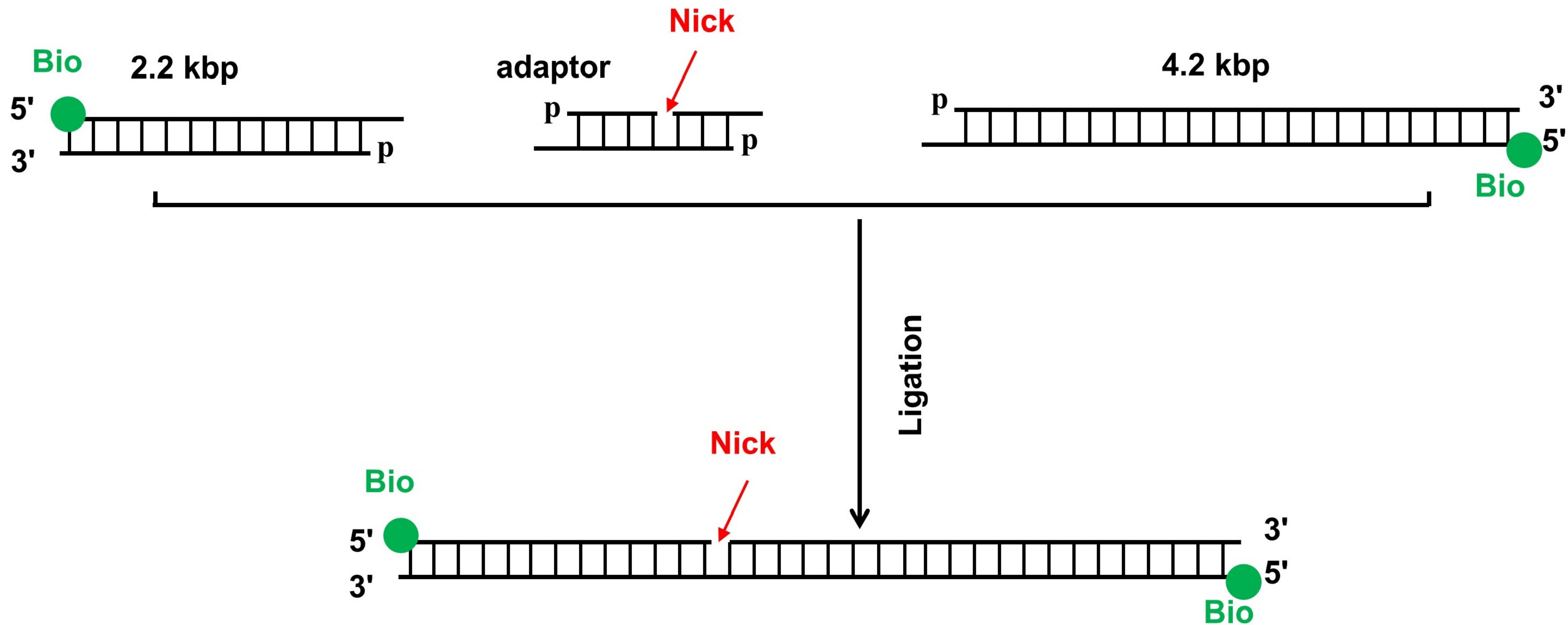
A**B****C****D**

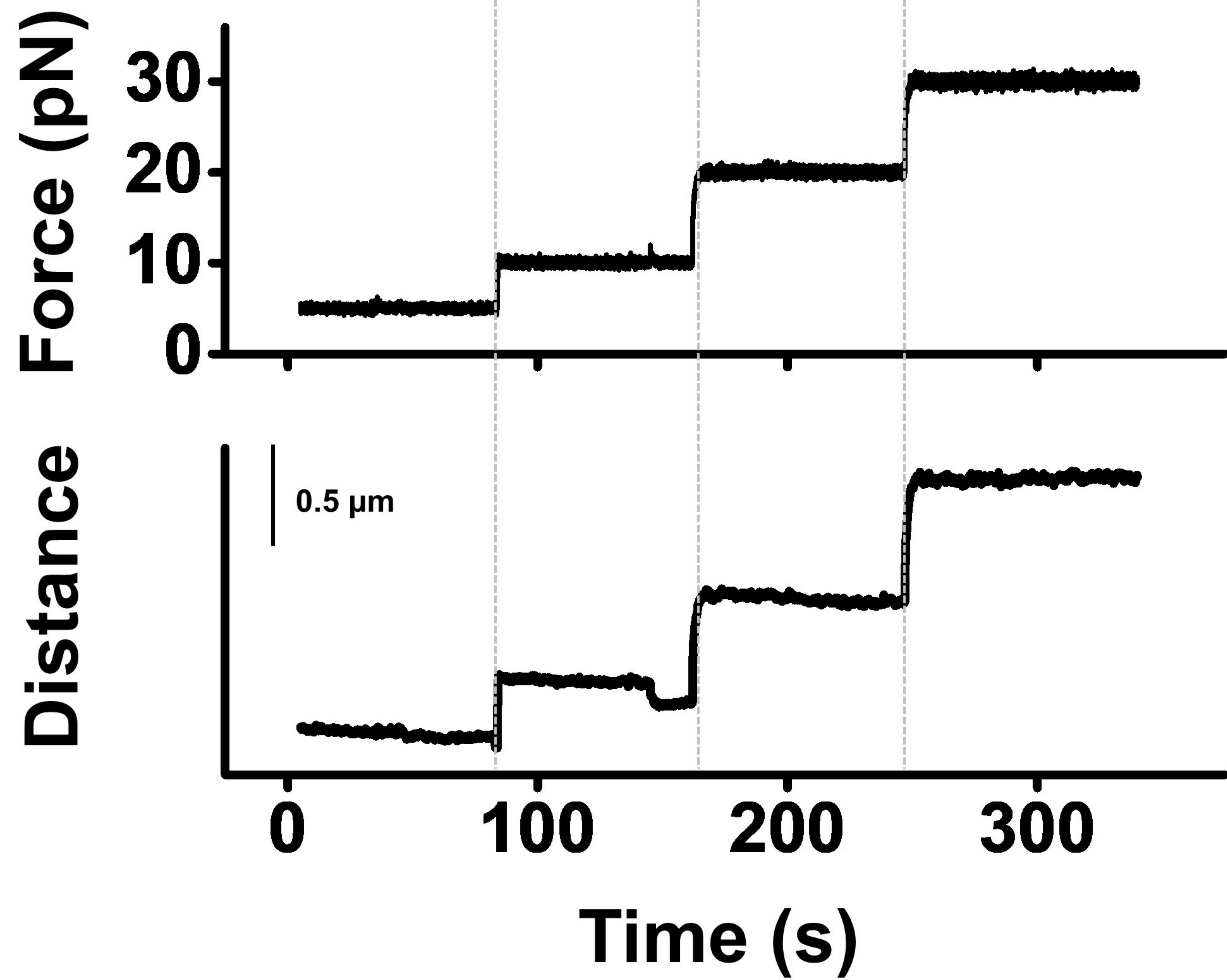
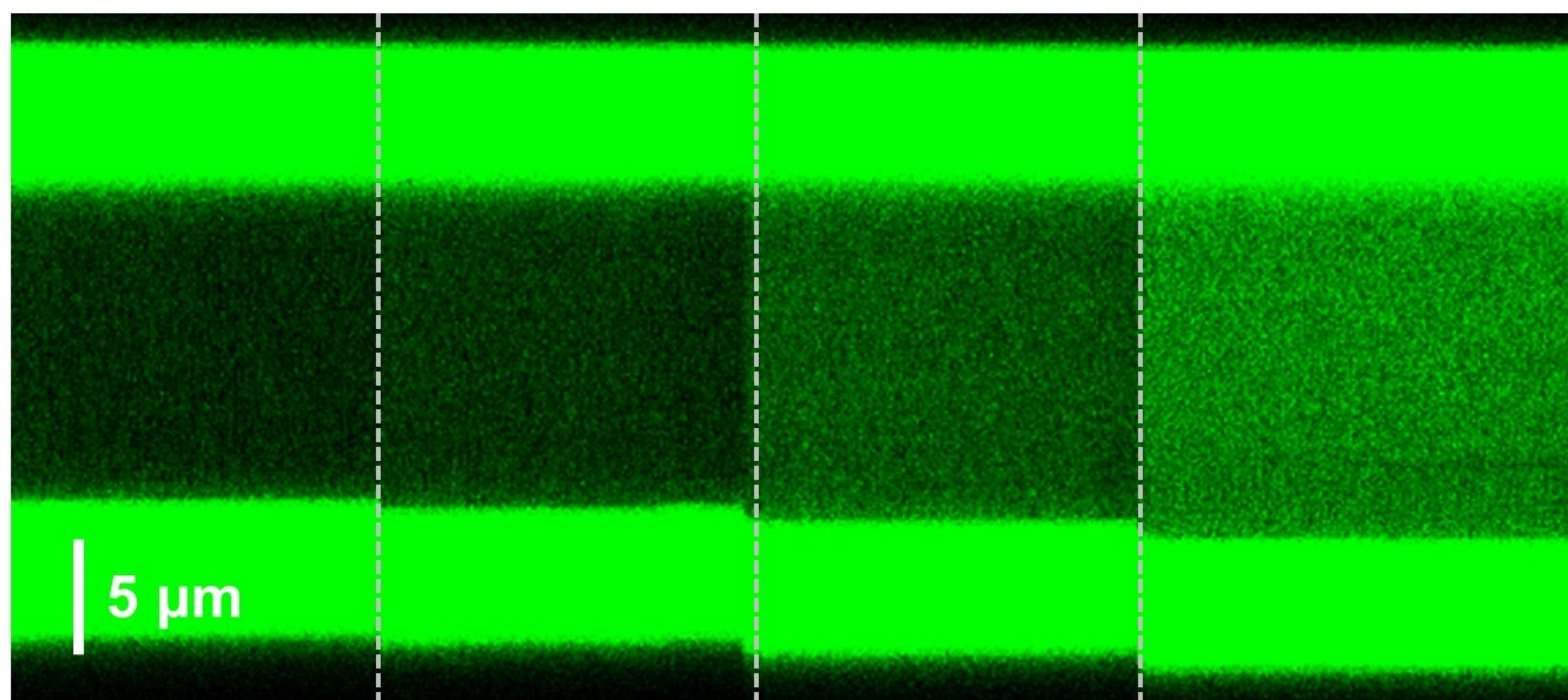
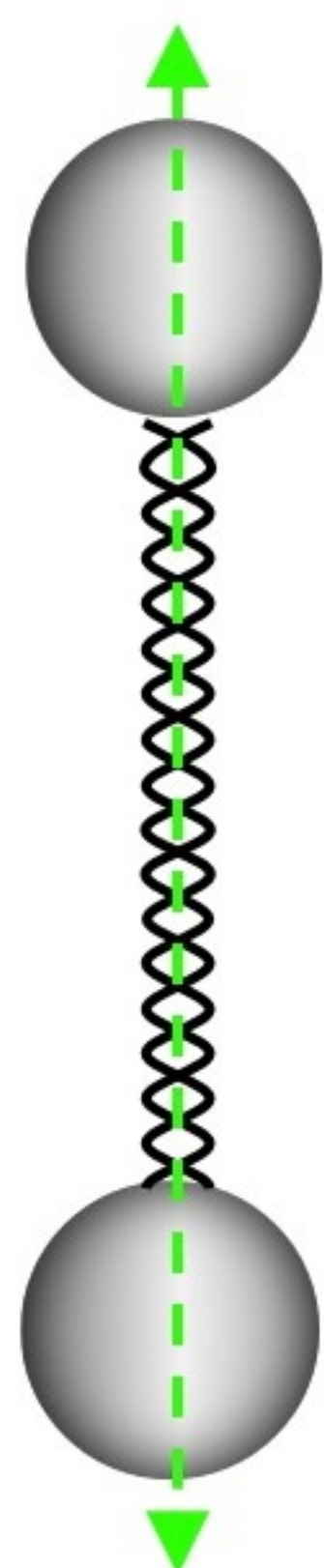
A**B****C****D**

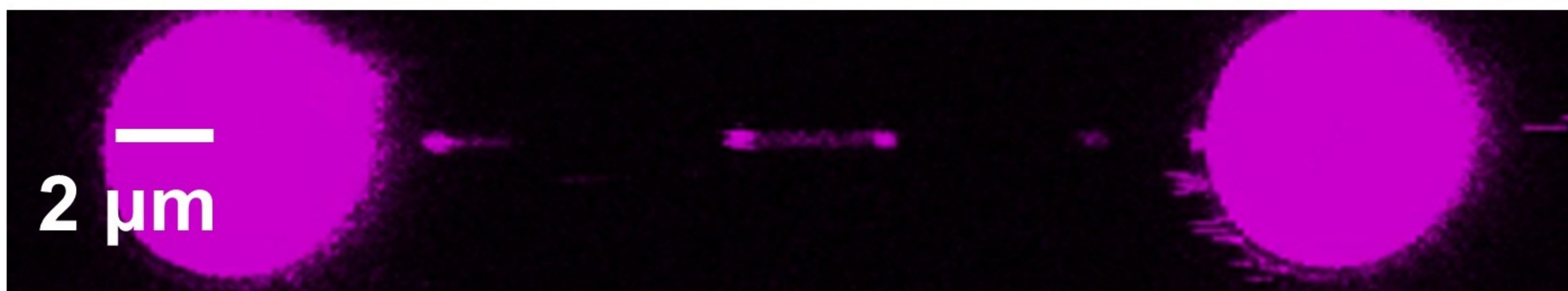
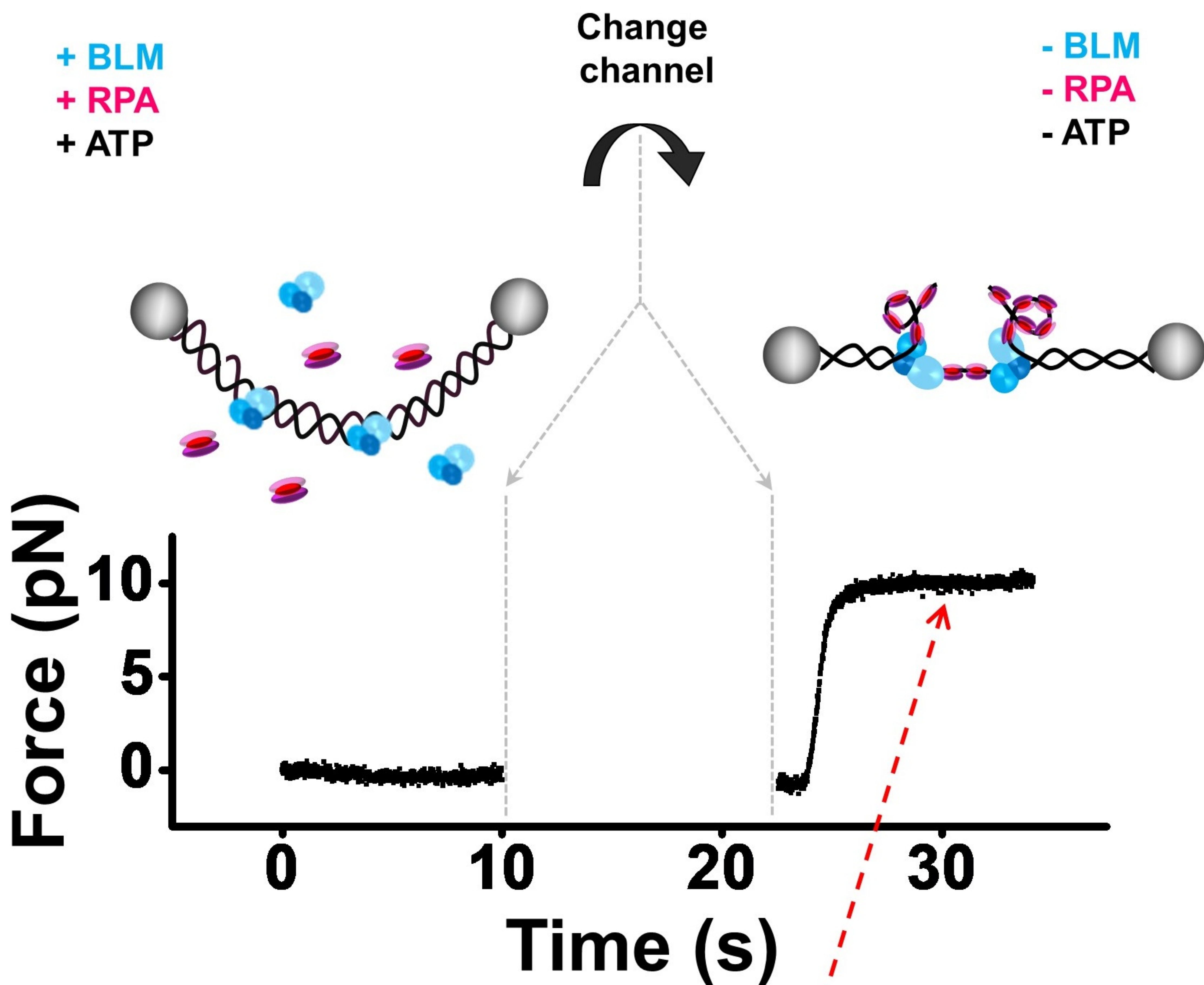


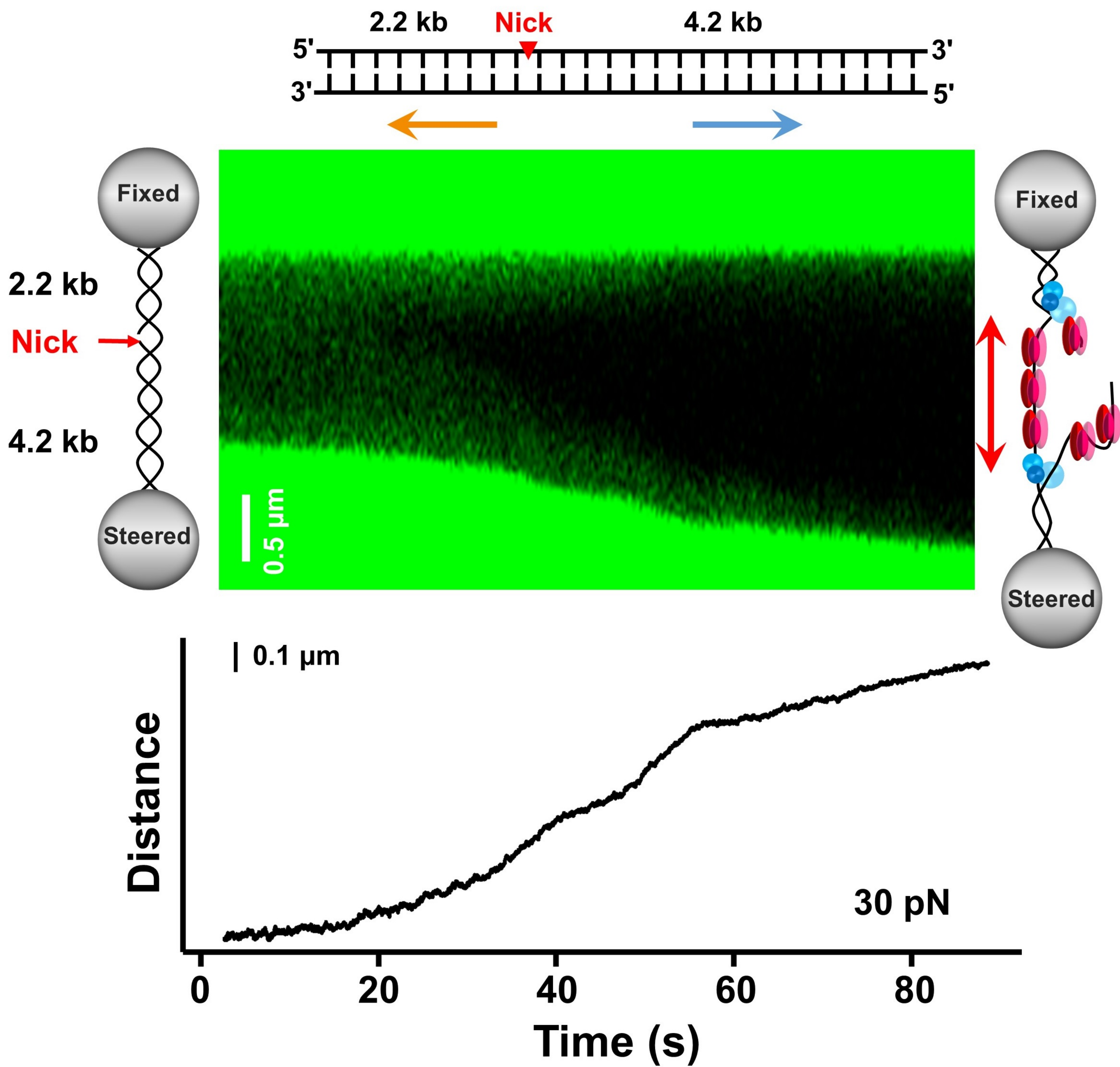
A**B**

$$V \text{ (nm/s)} = (\Delta L_2 - \Delta L_1) / \Delta t$$

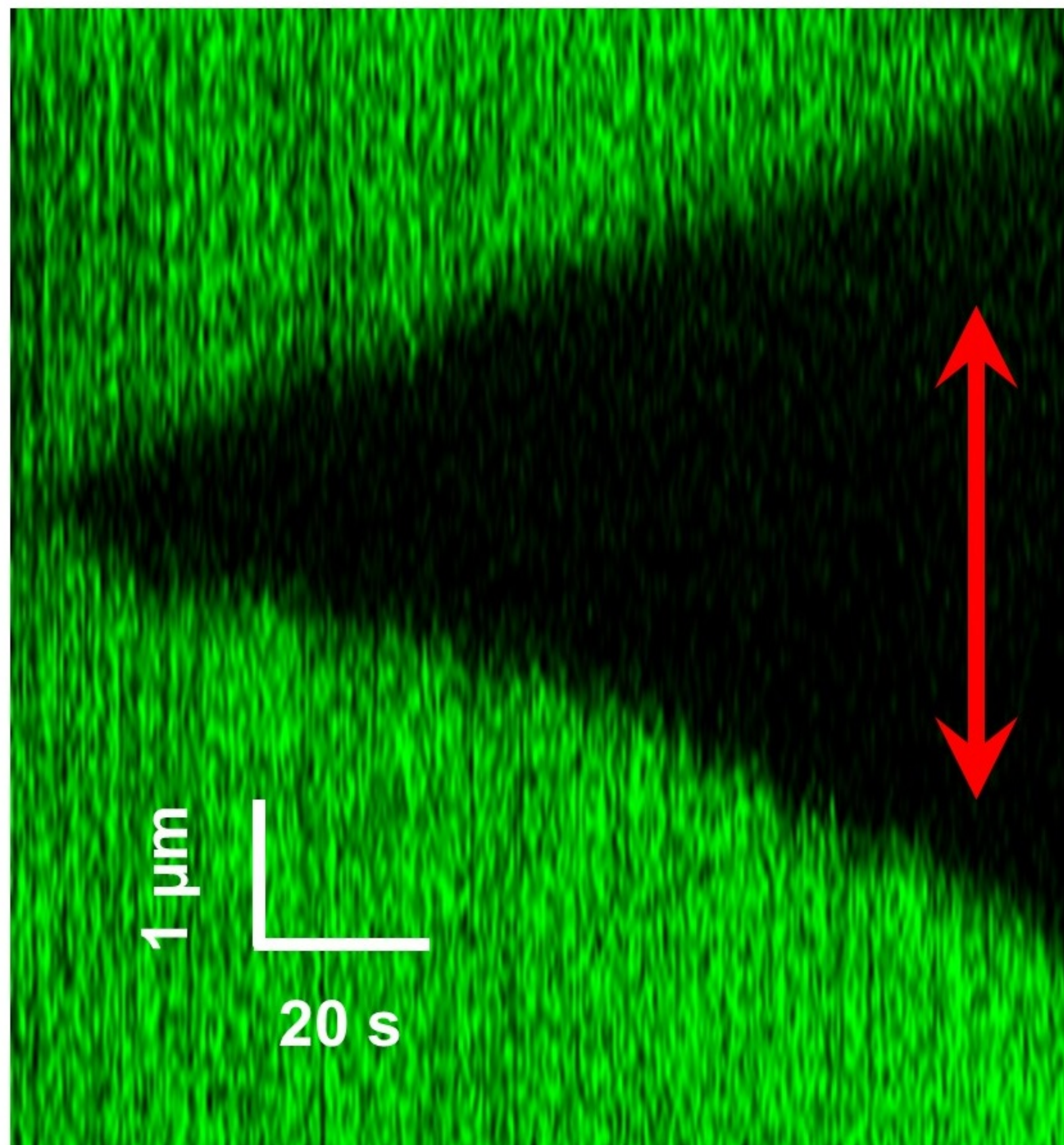




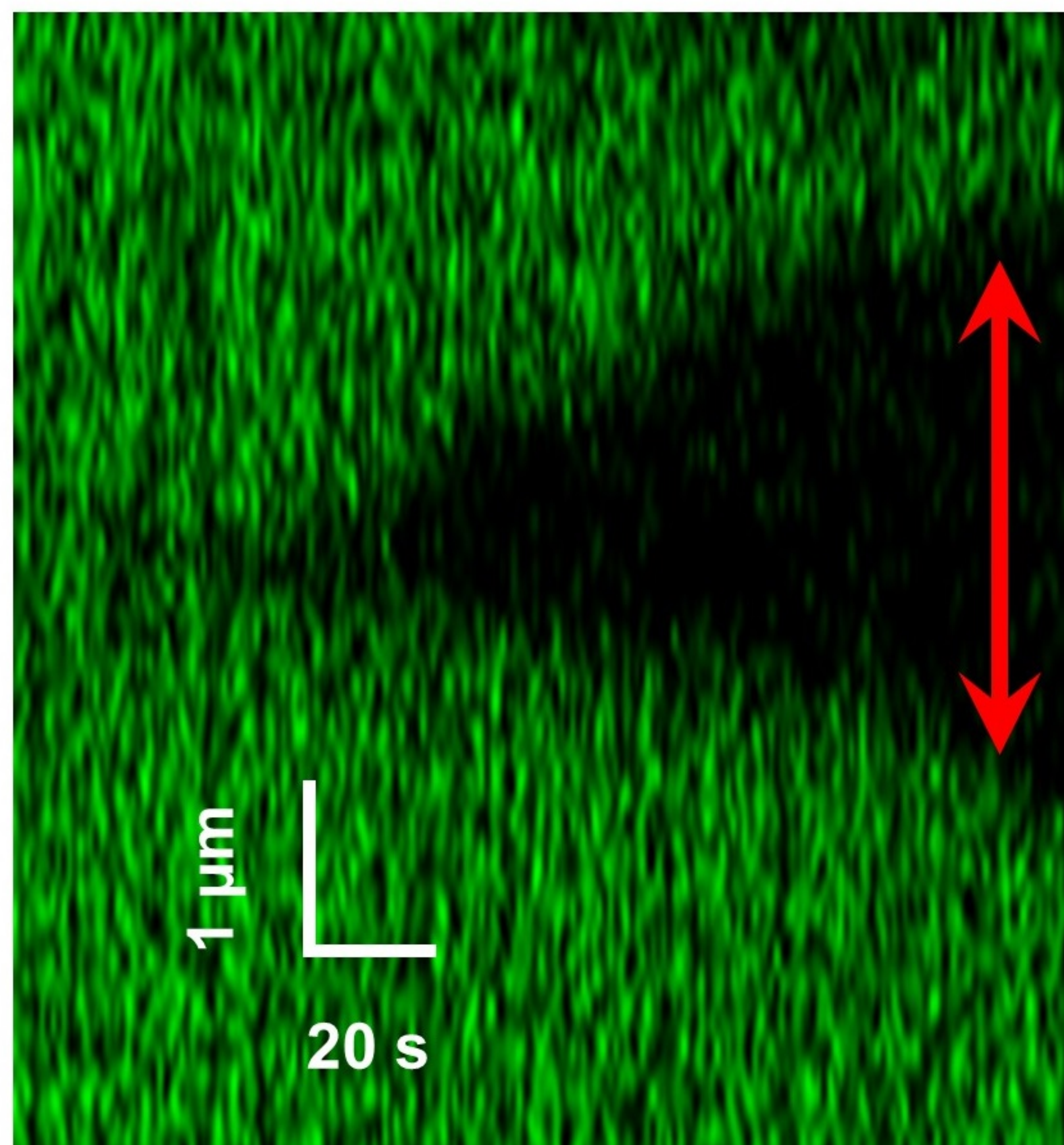




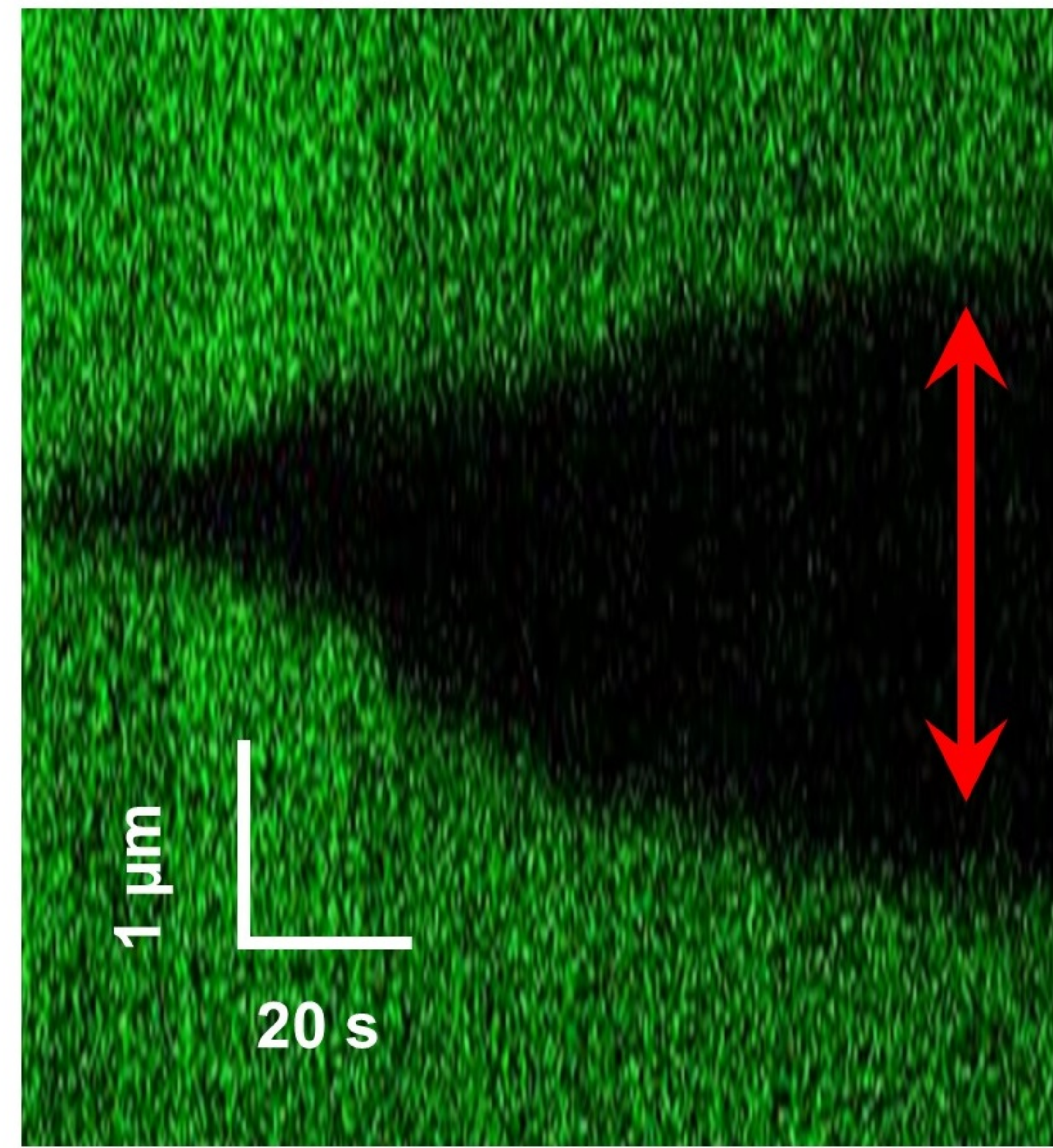
[BLM] = 200 nM
[RPA] = 50 nM

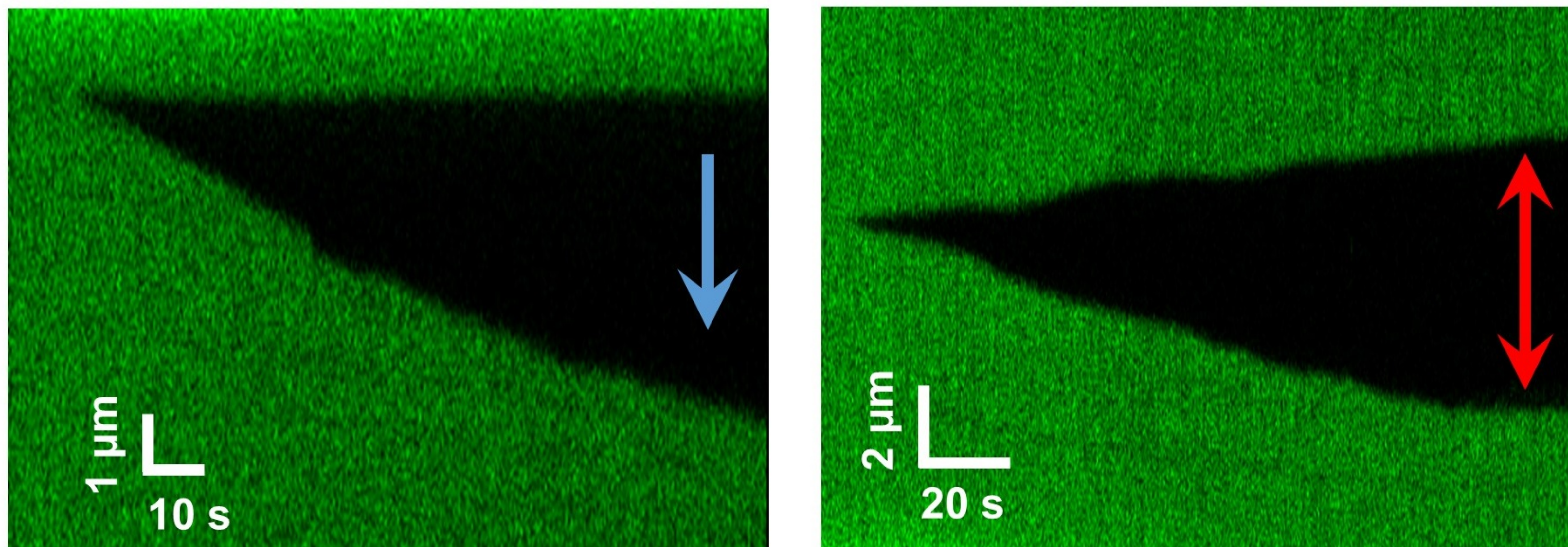
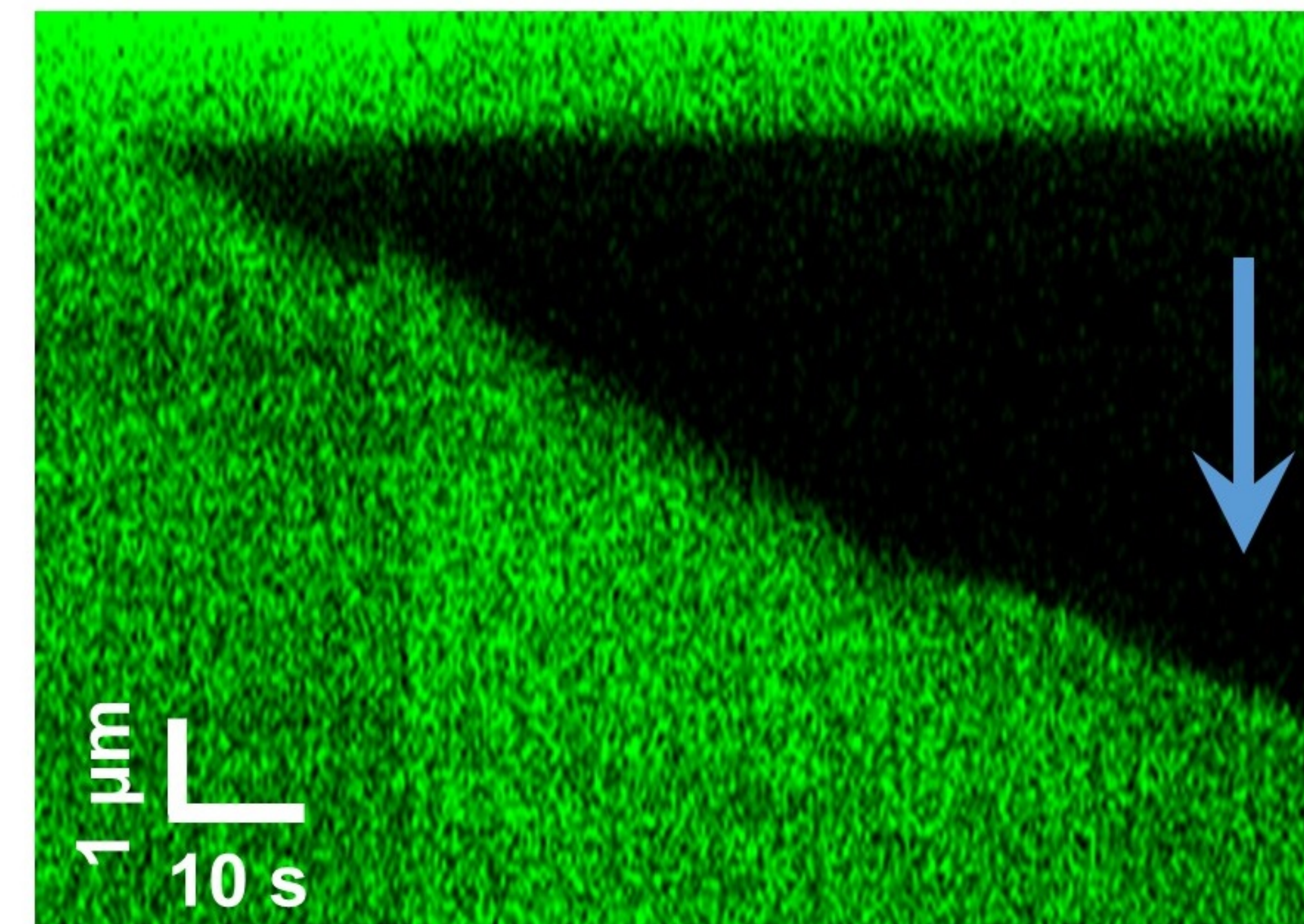
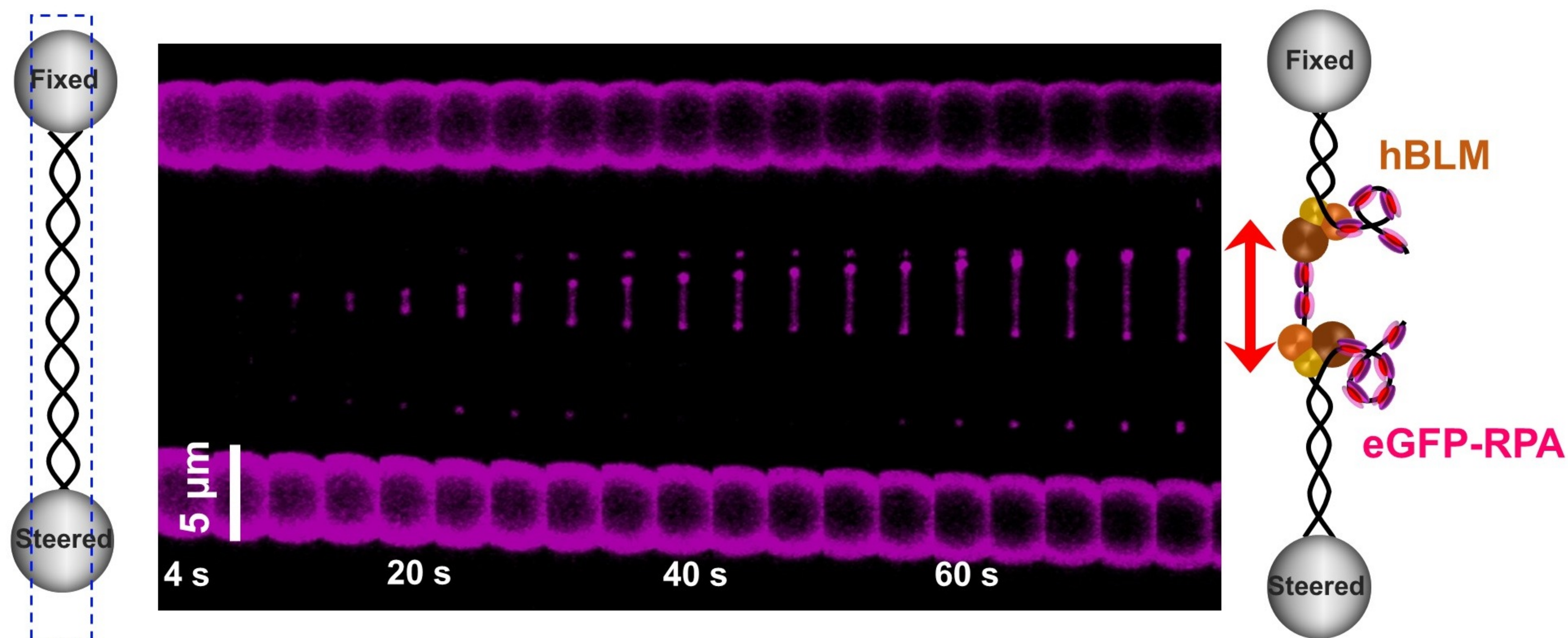
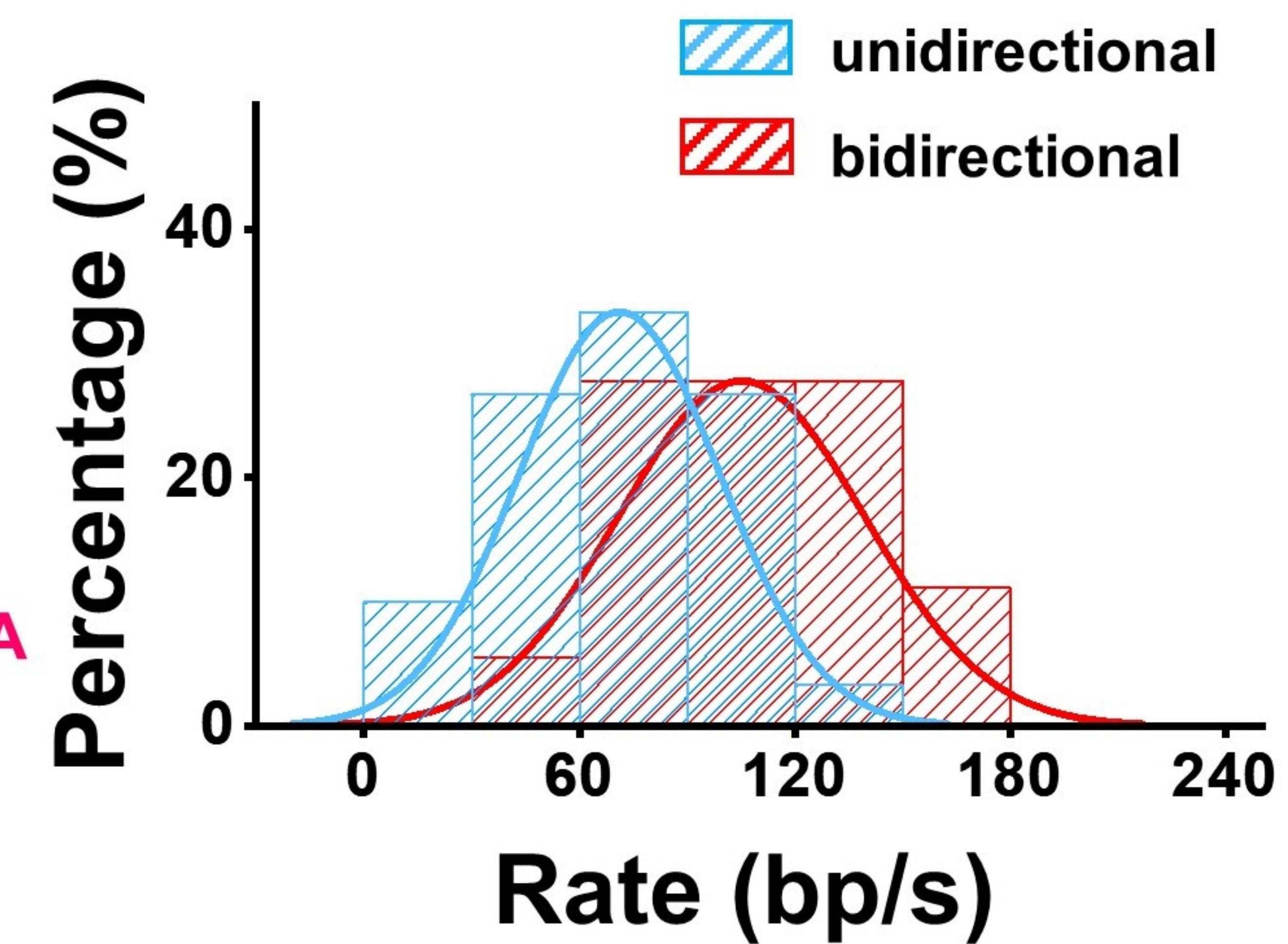


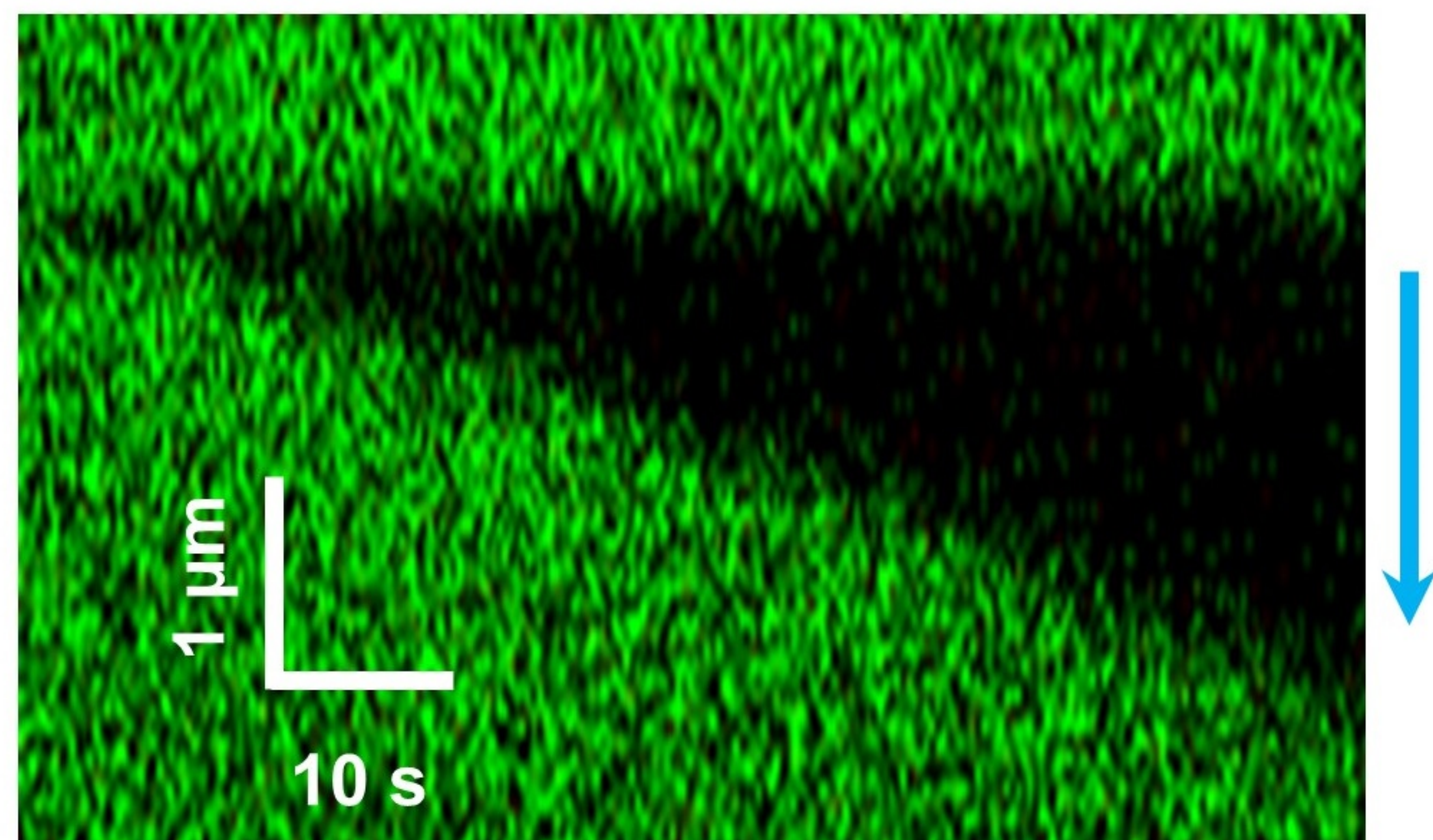
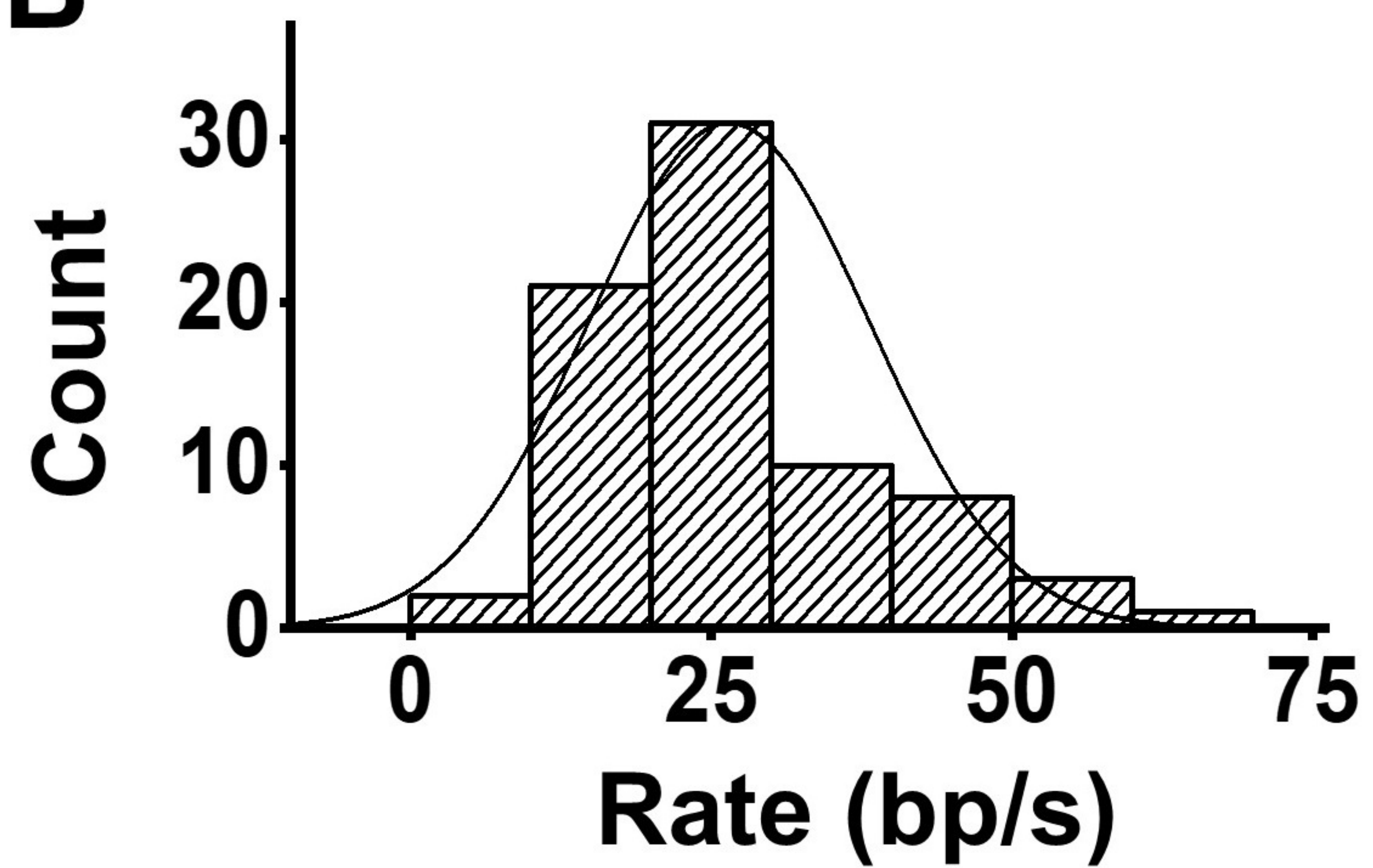
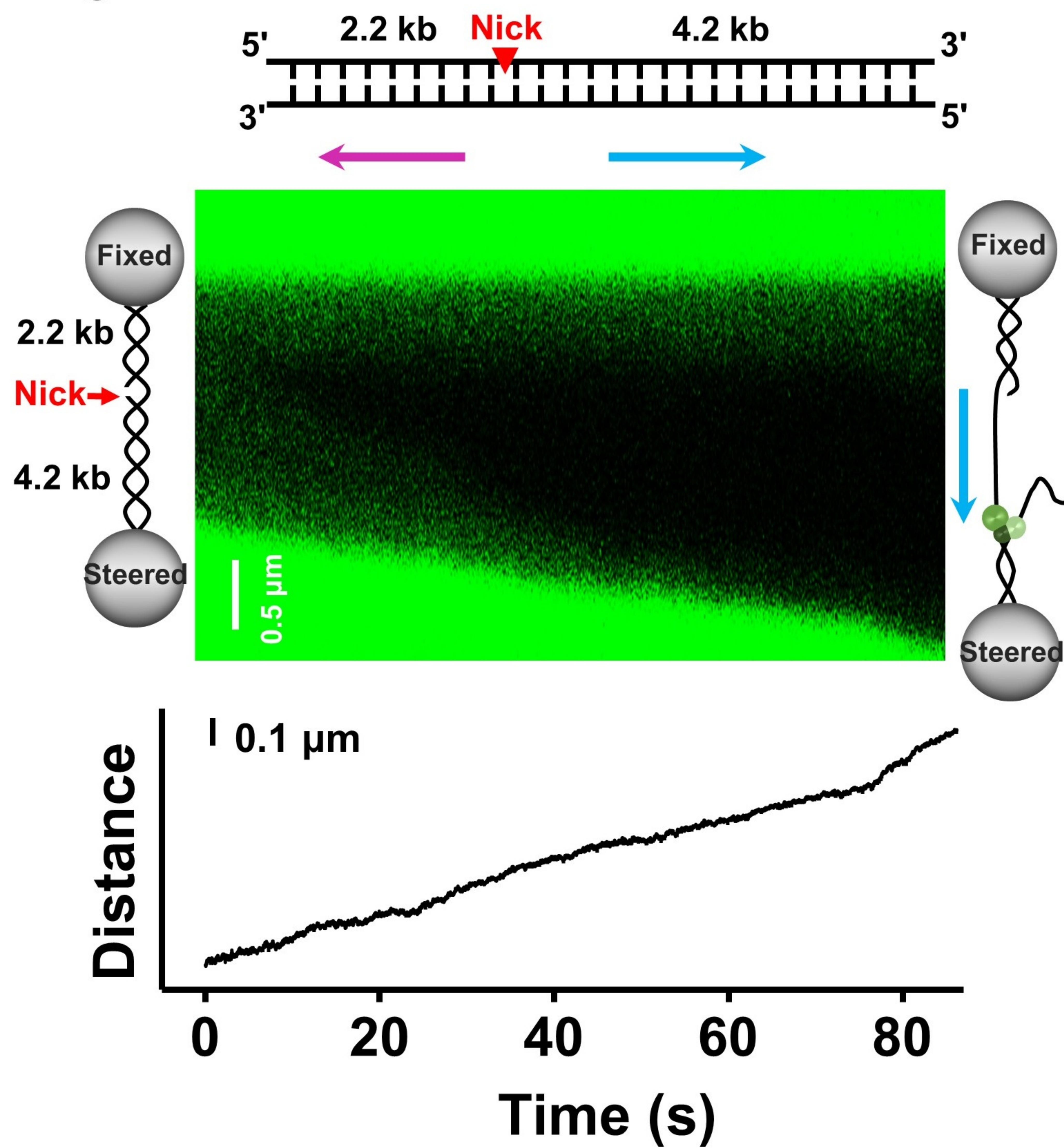
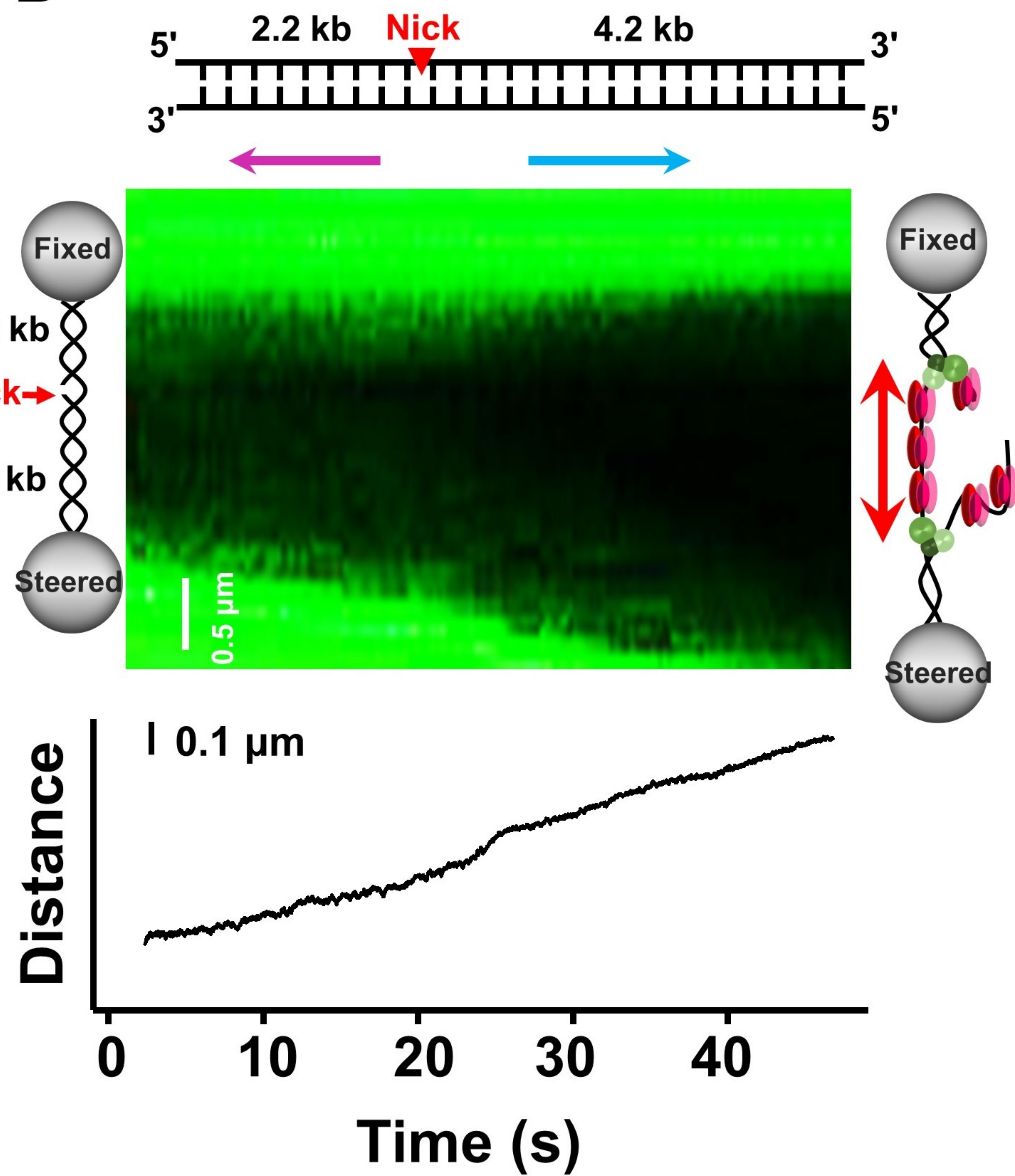
[BLM] = 200 nM
[RPA] = 100 nM

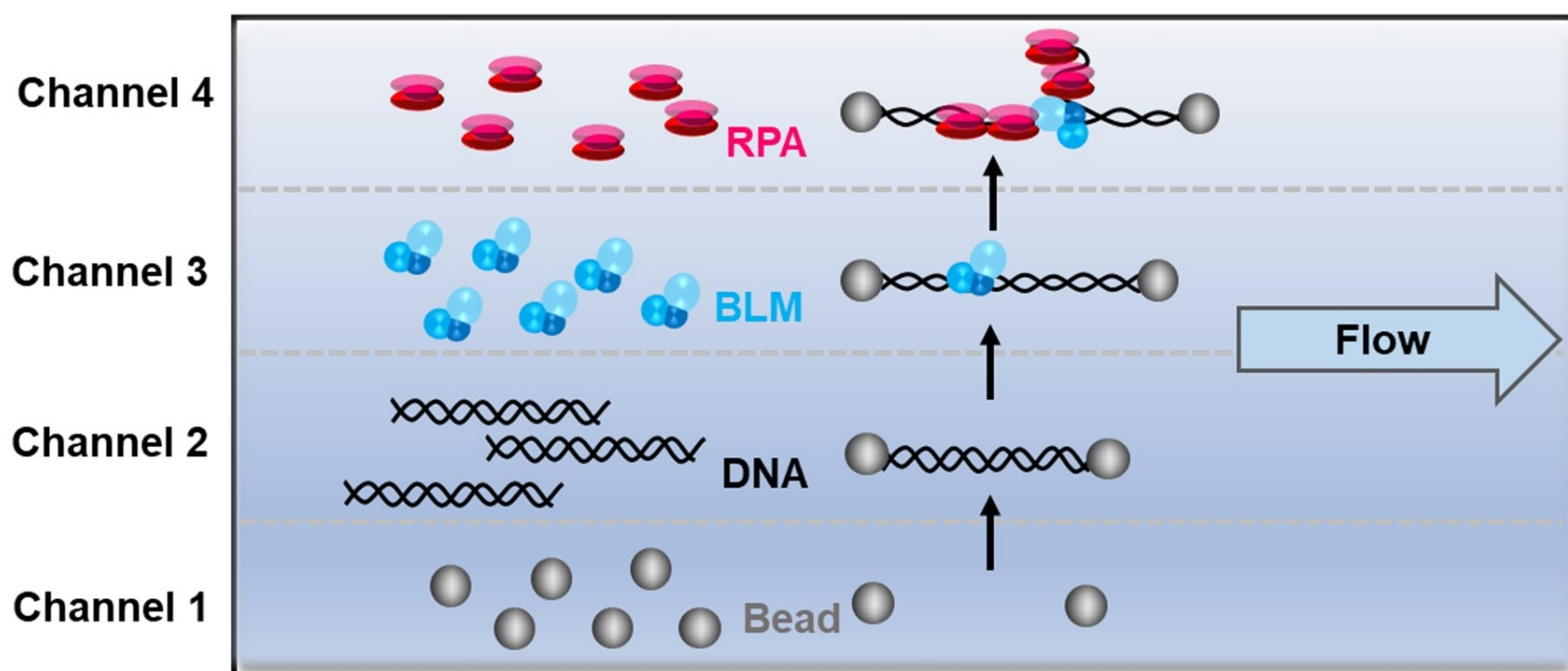


[BLM] = 20 nM
[RPA] = 100 nM



A**hBLM + hRPA****B****hBLM alone****C****hBLM + eGFP-hRPA****D**

A**B****C****D**

A**B**